

**Generation of Short Laser Pulses
by
Using Hollow Fibre and
Chirped Mirror Compressor System**

by
Yiming Cai
A thesis
presented to the University of Waterloo
in fulfilment of the
thesis requirement for the degree of
Master of Science
in
Physics

Waterloo, Ontario, Canada, 2017

©Yiming Cai 2017

Author's Declaration

I hereby declare that I am the sole author of this thesis. This is a true copy of the thesis, including any required final revisions, as accepted by my examiners.

I understand that my thesis may be made electronically available to the public.

Abstract

A FEMTOLASERS hollow core silicon fibre of length 1 m and 250 μ m inner diameter was set up in the lab in Waterloo with the purpose of generating sub 10fs pulses for Coulomb Explosion Imaging (CEI). The input laser was a new Ti: sapphire regenerative amplifier system providing energy of 1mJ per pulse at a duration of the 35fs with 1kHz repetition rate. Modifications to the initial setup were crucial in achieving the desired goal. A new, angled, incident window was made to eliminate reflective damage to the mirrors, and a new delivery beamline was built to minimize unwanted nonlinear effects. The pressure dependence of spectral broadening in argon gas was studied to find the best performance and found to be $p=0.43\text{atm}$. A chirped mirror system was set up to compensate the group delay dispersion in the beam line to the CEI experiment and compress the pulse, and MATLAB programs were written to carefully estimate how much material was necessary to minimise total dispersion of the system. The optimal input beam duration was determined by comparing the setting of the compressor with the output spectrum of the fibre and it was found that a spectrum capable of generating a 7.49fs laser pulse was produced if group delay dispersion and higher order dispersions were assumed to be zero. However, after calculating the higher order dispersion present in the system, which can not be compensated by the chirped mirrors, a laser pulse with a duration of 9.76fs is feasible with an average power of 0.45W. This result if verified by CEI will result in near equilibrium imaging of small molecules in the Waterloo lab for the first time.

Acknowledgements

I can not express enough thanks to my supervisor, Professor. Joseph Sanderson for his continued support and patience and encouragement.

I would also want to express thanks to my committee members, Professor Donna Strickland and Professor Wing-Ki. Liu for their guidance and advice.

I would also like to acknowledge all group members in the lab, especially Benji Wales and Reza Karimi for their help and advice.

I would like to thank my friend Wei, Du for his support of programming knowledge.

Dedication

This work is dedicated to my parents Cai, Qingshan and Ma, Haiyan.

Table of Contents

Author's Declaration.....	ii
Abstract.....	iii
Acknowledgements	iv
Dedication	v
Table of Contents	vi
List of Figures.....	viii
List of Tables	xii
1. Introduction.....	1
2. Review of The Nonlinear Effect	3
2.1 Optical Kerr Effect.	3
2.2 Self-Phase Modulation	4
2.3 The B-Integral	5
2.4 Critical Power for Self-Focusing	6
3. Dispersion Simulation	7
3.1 Dispersion	7
3.1.1 Group Delay Dispersion.	7
3.1.2 Group Velocity Dispersion.	8
3.2 Sellmeier Formula.	9
3.4 Dispersion Formula of Air and Argon gas	11
3.5 Dispersion Equation as a Function of Wavelength	11
4. Transverse Properties of a Laser Beam and Its Relevance to Hollow Fibre Propagation	15
4.1 Gaussian Beam.	15
4.2 Transverse Mode	16
4.3 Fundamental Mode	17
4.4 Fundamental Modes in an Optical Fibre	19
4.4.1 Single Mode and Multimode Fibre	19
5. Review of Progress in Generation of Few Cycle Pulses by Using The Hollow Fibre Technique	23
5.1 Achieving High Energy Pulses from a Hollow Fibre	29
5.2 Evaluating the Few Cycle Pulse Duration Using Coulomb Explosion Imaging (CEI)	
34	
6. The Laser System	37

6.1	Oscillator.....	37
6.3	Autocorrelator System.....	41
7.	Spectral Broadening by Hollow Fibre System.....	43
7.1	Experiment Setup of Hollow Fibre System.....	44
7.1.1	Beam Size After a Focus Lens.....	46
7.1.2	<i>Modification to The Incident Window.....</i>	<i>47</i>
7.1.3	<i>Preliminary Output Results and Modification to The Position of The Hollow Fibre</i> <i>48</i>	
7.1.4	<i>Germanium Plate Calibration.....</i>	<i>51</i>
7.2	Beam Polarization Control.....	55
7.3	Dispersion Estimation.....	55
7.3.1	<i>Calculation of Accumulated Total Group Delay Dispersion.....</i>	<i>56</i>
7.4	Impacts of Compressor setting on Generating Short Pulse.....	59
7.5	Experiment Result and Discussion.....	61
7.5.1	<i>Impacts of Pressure on Generating Short Pulse.....</i>	<i>61</i>
7.5.2	<i>Generation of the Shortest Laser Pulse.....</i>	<i>64</i>
8.	Conclusion.....	68
	Reference.....	71
	Appendix A: Future Improvement of Pressure Gradient Technique	76
	Appendix B: MATLAB fitting.m.....	77
	Appendix C: MATLAB Code GDDSum.m.....	79
	Appendix D: Instructions and MATLAB Code PluseSim.m.....	81
	Appendix E.....	89
1.	Instructions for Using Spectrum Correction Program.....	89
2.	Application of Spectrum Correction Program.....	90
	Appendix F: Hollow Fibre Alignment Steps.....	93
	Appendix G: Circuit Diagram of Electron Detector.....	97
	Appendix H: Circuit Diagram of Time of Flight.....	98
	Appendix I: Setup The Regenerative Amplifier.....	99

List of Figures

- Figure 1: Nonlinear refractive index measurement experiment setup based on Michelson interferometer..... 4
- Figure 2 : Sellmeier formula of refractive index versus wavelength in micrometre for fused silica. The minimal graph is picking wavelength range from 200nm to 2000nm. 10
- Figure 3 : Group velocity dispersion of fused silica at 0-1500nm. The GVD at 800nm is $36.09 \text{ fs}^2/\text{mm}$ 12
- Figure 4 : Third-order dispersion of fused silica at 0-1500nm. The TOD at 800nm is $27.43 \text{ fs}^3/\text{mm}$ 13
- Figure 5 : Fourth order dispersion of fused silica at 0-1500nm. The TOD at 800nm is $-11.44 \text{ fs}^4/\text{mm}$ 13
- Figure 6: Gaussian laser pulse size. Beam waist is at the $1/e^2$ intensity of laser beam. Pulse duration is expressed as full width at half maximum (FWHM). 16
- Figure 7 : (a) Calculated radiation patterns of a three-transverse-mode of vertical cavity surface emitting lasers (VCSEL); (b) spectrum of the VCSEL..... 18
- Figure 8 : (a) Four low order transverse cavity modes and their fields. (b) Intensity patterns in the modes of (a). 19
- Figure 9 : Transmission versus length of the fibre for the fundamental mode EH_{11} . 21
- Figure 10 : (a) Electric field distribution of the fundamental mode. (b) The intensity profile of fundamental mode, the lightest area, has the greatest intensity. (c)The real mode obtained in the Waterloo lab..... 22
- Figure 11 : (a) Spectral broadening in argon gas 4 atm pressure. (b) Pulse shape derived by taking the inverse Fourier transform of (a), pulse duration at FWHM is 18fs. The line with dots is the real autocorrelation trace of the pulses, and the solid line is the predicted autocorrelation trace by taking the inverse Fourier transform of (a) 24
- Figure 12 : Spectral broadening in krypton gas of 2 atm pressure. (b) Pulse shape derived by taking inverse Fourier transform of (a), pulse duration at FWHM is 10fs. The line with

dots is the real autocorrelation trace of the pulses, and the solid line is the predicted autocorrelation trace by taking the inverse Fourier transform of (a). 25

Figure 13 : Schematic of Nisoli’s experiment setup. L is an AR-coated lens of 30 cm focal length, M1 is a silver-coated mirror with 50 cm radius of curvature; M2, M5, and M6 are silver-coated plane mirrors and M3, M4 are chirped multilayer mirrors; P1–P4 are AR-coated multilayer 20° fused silica prisms. The beam reflected back by M4 is slightly separated from the incident beam to allow coupling by M6. PR provides polarization rotation using silver-coated mirrors. GP is a 1-mm-thick fused silica plate with AR-coated back side. BS is a broadband dielectric beam splitter on a fused silica substrate identical to GP. RM1 and RM2 are silver-coated roof mirror assemblies. 26

Figure 14 : Spectral broadening in argon (a) Spectral broadening in argon gas at the 4atm pressure and 140fs, 3.5GW peak power input laser. (b) Spectral broadening in argon gas at the 3.3atm pressure and 20fs, 4GW peak power input laser. The spectra of the input pulses are shown as dashed lines. 27

Figure 15 : Schematic of Eniko’s experiment setup. P1 is the YVO4 pump laser for the oscillator. P2 is the Nd:YLF pump laser for the chirp pulse amplification stage (CPA) Laser pump laser. SF57 is a 5cm glass block. Compressor contains AOPDF (DAZZLER system) and a set of Brewster angle fused silica prisms. 28

Figure 16 : (a) Laser pulses output spectral when hollow fibre is set in a constant pressure chamber. (b) Laser pulses output spectral when hollow fibre is placed in a pressure gradient chamber. 29

Figure 17 :Spectral broadening comparison between the statically filled chamber and the differentially pumped chamber. The grey dashed line represents the input resource pulse spectra. (Reprinted with permission from [43]) 30

Figure 18 : Spectral broadening in argon gas. (a)Spectrum of the input laser pulse, the energy of the input pulse is 8.5mJ. (b) Spectral broadening in argon gas, the pulse energy is 6.5mJ. 32

Figure 19 : Spectral broadening in neon gas, the pulse energy is 5.0mJ, and the pulse duration is 5fs by taking (a) into Fourier transform. 33

Figure 20 : Spectral broadening test results by the ultra broad band dispersion compensating mirror set (BBCOMP) manufacturer: FEMTOLASERS. 34

Figure 21: Deuteron molecule kinetic energy spectra obtained under 40fs (solid line) and 8.5fs (square) pulse. 35

Figure 22 : Layout of the Compact Laser Head and its real picture in the Waterloo lab. 38

Figure 23: Principle of the laser system. The seed laser is produced by the oscillator and then delivered to the Spitfire Ace-35F regenerative amplifier system.	40
Figure 24: Spitfire Ace Regenerative amplifier optical layout. The grey part is the Compressor part.	41
Figure 25: Optical layout of autocorrelation system.	42
Figure 26: Layout of Hollow fibre system.	44
Figure 27: Plot of group delay dispersion versus wavelength for chirped mirror compressor. The system provides negative 500 GDD.	46
Figure 28: Design of the incident window amount.	47
Figure 29 : Spectrum derived from a gas pressure $p=0.4\text{atm}$ and the calculated transform limited pulse duration 8.28fs. The light grey spectrum is the ideal spectral broadening test result provided by the manufacturer: FEMTOLASERS.	49
Figure 30: Configuration of the incident window and the comparison between old experimental setting and the new setting.	49
Figure 31 : Incident light propagates on a glass plate at Brewster's angle. The reflected light only has s-polarized wave and refracted light only has the p-polarized wave.	52
Figure 32 : Germanium window transmission versus wavelength. Transmission is zero if the wavelength below 1000nm.	52
Figure 33: Spectrum and transform limited pulse durations recorded after the hollow fibre filled with argon at a pressure of $p=0.43\text{ atm}$ and the input laser power of 1W, and output power after the Ge plate from (a) to (m) varied from 20mW to 280mW in steps of 20mW.	54
Figure 34: Optical layout of autocorrelation and hollow fibre system.	56
Figure 35: Group delay dispersion from the amplifier to the input of the hollow fibre versus wavelength. The dispersion at 800nm is 160.9 fs^2	57
Figure 36: Group delay dispersion from the amplifier to the last window of the hollow fibre chamber versus wavelength. The dispersion at 800nm is 233.1 fs^2	58
Figure 38: Group delay dispersion from the amplifier to autocorrelation BBO crystal versus wavelength. The dispersion at 800nm is 205.4 fs^2	58

Figure 38: Compaction of spectrum in different compressor setting and transform limited pulse duration. 60

Figure 39 : Spectra and transform limited pulse obtained by varying the gas pressure from a): 0.468atm, b) 0.434atm, c) 0.401atm, d) 0.368atm, e)0.334atm, f) 0.301atm . The frequency range for each plot is from 250THz to 500THz. Below shows the transform limited pulse duration versus gas pressure. There is a trend (dotted line) of increasing pulse duration as decreasing gas pressure. 62

Figure 40: Spectrum and transform limited pulse durations. The input pulse duration is $\tau_0=35\text{fs}$. Chirped pulse duration τ at FWHM is 7.49 fs. The argon gas pressure $p=0.43\text{atm}$, and the mode was observed as fundamental mode. Input laser power was 1.00W, and output power was 0.453W. The light grey is the ideal spectral broadening test results by the ultra broad band dispersion compensating mirror set (BBCOMP) manufacturer: FEMTOLASERS. 65

Figure 41: Original spectrum and pulse duration by taking spectrum into inverse Fourier Transform. Higher order dispersions $\text{TOD}=255.26\text{fs}^3$ and $\text{FOD}=-42.74\text{fs}^4$ were add to the PulseSim.m program to simulate the phase effect. The input pulse duration is $\tau_0=35\text{fs}$. Chirped pulse duration τ at FWHM is 9.76 fs. The argon gas pressure $p=0.43\text{atm}$, and the mode was observed as fundamental mode. Input laser power was 1.00W, and output power was 0.453W..... 67

Figure 42 : (2,2,2) Channel of CO_2 energy released as a percentage of that expected from Coulomb explosion at the equilibrium geometry as a function of the final charge states. 69

Figure 43: A design for the pressure gradient chamber..... 76

Figure 44 : (a) Original spectrum and pulse duration by taking the inverse Fourier Transform. Pulse duration at FWHM is 4.278fs. (b) Spectrum after background subtraction and pulse duration by taking the inverse Fourier Transform. Pulse duration at FWHM is 8.170fs. 91

Figure 45 : Real experimental setups of amplifier control boxes in the Waterloo lab. The top picture is the Spitfire Ace software ‘main’ control panel. The spectrum shows the build up when the current is 18.4 A, and timing setting: CH1: 83.25ns, CH2: 103.25ns, CH3:249.25ns. The output pulse has the duration of 35fs and power of 4.35W. 100

Figure 45 : Layout of connection between controllers of laser system. 102

Figure 46 : The beam path in the compressor..... 104

List of Tables

Table 1 : Second order nonlinear index for noble gas, air and fused silica.	4
Table 2 : Sellmeier coefficients for UV fused silica, calcium fluoride and silicon.	10
Table 3 : Sellmeier coefficients for argon gas and air.	11
Table 4 : Dispersion of components in hollow fibre and autocorrelation system.	14
Table 5 : Dispersion calculation of air and argon gas.	14
Table 7: Accumulated dispersion for autocorrelation and hollow fibre system and calibrated GVD for the hollow and chirped mirror compressor system.	59
Table 8 : Dispersion calculation for argon gas at different pressure.	63
Table 9 : Dispersion calculation from the hollow fibre chamber to the target chamber. The optical components include a 1mm hollow fibre output window, a 3mm window of the target chamber and a 1mm half-wave plate. The path length from the output window of the hollow fibre tube to the target chamber is 6454.60mm. The length of the argon filled hollow fibre tube is 1828.8mm. Chirped mirror system provides GDD of -500.	66

1. Introduction

Ultrafast laser technology has experienced a rapid development in the last thirty years attracting many researchers to the field of ultrashort pulse generation. Generation of progressively shorter laser pulses has been intensively studied because of its significance, and applicability to fields, such as medicine¹, information and communication technologies^{2,3} and imaging of molecular dynamics^{4,5} etc. Before the 1980s; scientists usually used the dye laser technique to generate the shortest laser pulses^{6,7}. However, the method could only achieve pulses in the nanojoule^{6,7}. In the 1980s, the development of Ti: sapphire with its huge bandwidth, greater than two hundred nanometers, was coupled with two new techniques, in Kerr lens mode-locking and chirped pulse amplification.⁸ Low power ultrashort pulses possible for instance 6 fs laser pulses at the average energy of 300mJ have been generated from a single oscillator, and multi mJ pulses with 21fs duration have been generated from regeneratively amplified Ti: sapphire laser seeded by a 10fs oscillator⁹. In 1996, the Nisoli's group used a Ti: sapphire regenerative laser system together with a hollow fibre filled with noble gases to generate pulses around the energy level of 100µJ and few-cycle duration less than 10fs^{38,39}. This method has been developed to become the most comprehensive way of generating high-energy laser pulses with short duration. In this thesis, firstly, some background of nonlinear optics will be introduced to explain the origin of the hollow fibre method. The influence of group delay dispersion for the laser and hollow fibre system will be carefully considered and simulated in chapter 3. In chapter 4, the theory of transverse modes will be discussed with reference to the

propagation of the laser through the hollow fibre. Previous work in the field of generating few-cycle laser pulses using the hollow fibre technique will be discussed in chapter 5. Chapter 6 presents the setup of the optical system that has been developed in the Waterloo lab, results, analysis and discussion are shown in chapter 7. Conclusions and suggestions for future work are discussed chapter 8.

2. Review of The Nonlinear Effect

2.1 Optical Kerr Effect

When an intense light field passes through a transparent material, the refractive index n depends on the intensity of the light by:

$$n = n_0 + n_2 I \quad (1)$$

where n_0 is the linear refractive index of the material, which at low intensity would be equivalent to n and, n_2 is called the second order nonlinear refractive index.

The amplitude of the laser electric field is quadratically related to the laser intensity, therefore, the refractive index of a medium depends quadratically on the electric field, this is called the Kerr effect. n_2 can be expressed as

$$n_2 = \frac{9\pi\chi_3}{n_0^2} \quad (2)$$

Experimental measurements of the nonlinear refractive index have been performed by various methods such as the wave mixing and Z-scan techniques and single shot interferometry.^{10,11} Ioan et al. (2013) used a Michelson interferometer setup as shown in Figure 1¹⁰, the refractive index of the sample will change along its thickness due to the intensity of the excitation laser. The fringe pattern on the beam analyser shifts indicating the change in optical path length nI (where I is the sample thickness) and hence the influence of n_2 . Therefore, they observe the phase change of the probe laser beam, after that, they fit these data with the theoretical function and obtain a nonlinear refractive index of the sample. Their results agree with those of the Z-scan technique¹²

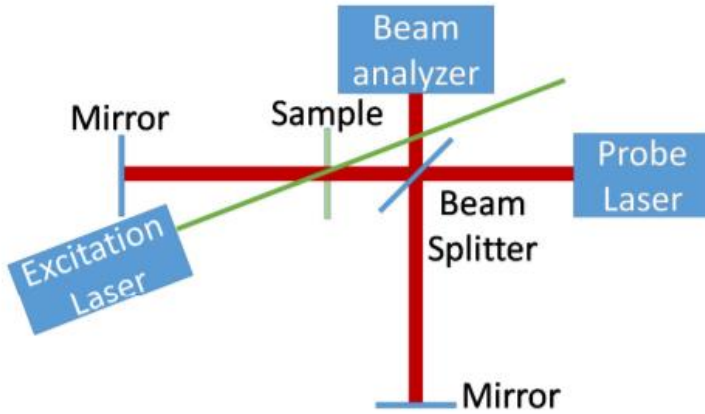


Figure 1: Nonlinear refractive index measurement experiment setup based on Michelson interferometer. (Reprinted with permission from [10])

The pressure dependent nonlinear refractive index n_2 at 800 nm for some materials is given below form.¹³

Material	n_2
SiO₂(fused silica)	$3.0 \times 10^{-20} m^2/W$
Air	$5.7 \times 10^{-23} m^2/W/atm$
Argon gas	$19.6 \times 10^{-23} m^2/W/atm$
N₂ gas	$6.7 \times 10^{-23} m^2/W/atm$
Ne gas	$1.8 \times 10^{-23} m^2/W/atm$

Table 1 : Second order nonlinear index for noble gas, air and fused silica.

2.2 Self-Phase Modulation

Self-phase modulation (SPM) is a phenomenon due to the Kerr Effect which always results in the broadening of the bandwidth of an intense laser beam. When an ultrafast laser pulse propagates through media, the varying index of refraction, which depends on the laser intensity, will induce the phase shift of the laser pulse. For a Gaussian pulse, the light wave moves more slowly when the intensity is high

(as n_2 is high) at the peak of the pulse and faster at the back and front of the pulse where I is low. This means that the back of the pulse (low intensity) will catch up the middle (high intensity), and the front will move away. This means that a wave will be compressed at the back and stretched at the front introducing two new wavelengths from the original light wave. When the laser passes through a nonlinear medium, such as a silica fibre, a phase shift is observed as¹⁴

$$\Delta\varphi = \frac{4\pi n_2 LP}{\lambda A_{eff}} \quad (3)$$

where L is the fibre length and P is the laser power, A_{eff} is the effective fibre core area or if the beam radius is smaller than the fibre radius, then A_{eff} represents the beam radius.

2.3 The B-Integral

The accumulated phase shift over the nonlinear optical systems can be expressed by calculating the B-integral value. Equation of the B-integral is given by¹⁵

$$B(\tau) \equiv \frac{2\pi}{\lambda} \int_0^L n_2 \cdot I(\tau, z) dz \quad (4)$$

where I is the intensity of the laser beam, L is the propagation distance along the z -direction and n_2 is the nonlinear refractive index.

In a conventional chirped pulse amplification (CPA) system, a low energy mode-locked laser pulse is stretched, amplified and then compressed. The detail will be discussed in Chapter 5. In the regenerative amplifier system, the cumulative B- integral value is expected to be kept low, around 1~2;^{16,17} otherwise, the effect will be to cause self-focusing of the laser beam. Self-focusing of the

laser beam will reduce the beam radius increasing the intensity. This lensing effect, which is crucial in Kerr lens mode locking, may result in damage to the gain medium. Researchers have used a semiconductor material with a negative nonlinear refractive index to neutralise the accumulated positive B-integral value, but it is not commonly incorporated in practical laser systems.¹⁸

In this thesis, the hollow fibre sits inside a transparent vacuum tube, and B-integral on the optical elements such as input window of the vacuum tube will be calculated in Chapter 7.

2.4 Critical Power for Self-Focusing

Self-focusing of the laser beam in bulk media may cause damage; therefore, it is significant to investigate the power for self-focusing and its limitation.^{19 20} In the experiment, the peak power of the ultrafast laser is expected to be lower than the critical power of self-focusing. Researchers have found the expression of peak power of a Gaussian pulse and the critical power for self-focusing to be²¹

$$P = 0.94 \frac{E_p}{\tau_p} < P_{cr} = \frac{3.79\lambda_0^2}{8\pi n_0 n_2} \quad (5)$$

where E_p is the pulse energy and τ_p is the pulse duration obtained from the full width at half maximum (FWHM). λ_0 is the wavelength of the laser beam and n_0 and n_2 , as mentioned above, are the linear and nonlinear refractive index respectively.

3. Dispersion Simulation

3.1 Dispersion

To generate a pulse of short duration by using a hollow fibre and chirped mirror compressor system, an understanding of how to control the dispersion throughout the laser system is critical. Dispersion is described as the phenomenon by which the phase velocity of a wave depends on the frequency of the wave as it passes through a medium.

3.1.1 Group Delay Dispersion

The dependence of the Group delay time τ_g , on wavelength within the pulse is called group delay dispersion(GDD). For a femtosecond laser pulse where the bandwidth is large, the effect of GDD cannot be ignored.

Consider an ultrafast laser signal is given by²²

$$\tilde{E}(\omega) = E(\omega - \omega_0)e^{-i\varphi(\omega - \omega_0)} \quad (6)$$

where ω_0 is central frequency. $\varphi(\omega - \omega_0)$ is the phase of the laser pulse. To understand spectral phase and obtain the effect of dispersion, it is convenient to expand the spectral phase of the pulse as a Taylor series

$$\varphi(\omega) = \varphi(\omega_0) + \varphi'(\omega_0)(\omega - \omega_0) + \frac{1}{2}\varphi''(\omega_0)(\omega - \omega_0)^2 + \frac{1}{6}\varphi'''(\omega_0)(\omega - \omega_0)^3 + \dots \quad (7)$$

In the above equation, $\varphi(\omega_0)$ is the spectral phase of the central frequency.

$\varphi'(\omega_0) = \frac{d\varphi}{d\omega}$ is defined as the group delay and $\varphi''(\omega_0) = \frac{d^2\varphi}{d\omega^2}$ is the group delay dispersion (GDD).

3.1.2 Group Velocity Dispersion

The group delay dispersion per unit length of the material is called the group velocity dispersion (GVD).

$$GVD = \frac{GDD}{L} \quad (8)$$

The phase due to a medium of length L is

$$\varphi(\omega) = k(\omega)L \quad (9)$$

where $k = 2\pi/\lambda$ is the frequency dependent wave number. Similarly, we can expand phase in Taylor series

$$\dots \quad k(\omega)L = k(\omega_0)L + k'(\omega_0)(\omega - \omega_0)L + \frac{1}{2}k''(\omega_0)(\omega - \omega_0)^2 L + \frac{1}{6}k'''(\omega_0)(\omega - \omega_0)^3 L + \dots \quad (10)$$

In the above equation, $k(\omega_0)$ is the spectral phase of the central frequency of the optical medium. $k'(\omega_0) = \frac{dk}{d\omega}$ is defined as group velocity and $k''(\omega_0) = \frac{d^2k}{d\omega^2}$ is group velocity dispersion (GVD). The higher order terms of $k'''(\omega_0)$, $k''''(\omega_0)$ are third order dispersion (TOD) and fourth order dispersion (FOD) respectively and so on. When the $k''(\omega_0) = \frac{d^2k}{d\omega^2}$ and all higher order dispersions are zero, it represents all the spectral components travel in a same group velocity. Normally material has positive GVD which means the longer wavelength components travel faster than the shorter wavelength. For material with a negative GVD, by contrast, the shorter wavelength components travel faster than the longer wavelength components.

The group velocity distribution in optical fibres can be written as a function of wavelength²³

$$GVD = -\frac{2\pi c}{\lambda^2} \frac{d^2k}{d\omega^2} \quad (11)$$

3.2 Sellmeier Formula

The theoretical simulation function for the dependence of refractive index on wavelength is given by the Sellmeier dispersion formula ²⁴:

$$n(\lambda) = \sqrt{1 + \sum_j \frac{A_j \lambda^2}{\lambda^2 - B_j}} \quad (12)$$

λ unit is in micrometres, A_j and B_j are the constant value which should be determined by fitting to experimental data. Researchers have found that j value up to 3 are enough to simulate accurately the wavelength dependence on refractive index.²⁵ Therefore, it is convenient to expand the above formula to a three-term equation:

$$n(\lambda) = \sqrt{a + \frac{b\lambda^2}{\lambda^2 - c'^2} + \frac{d\lambda^2}{\lambda^2 - e^2} + \frac{f\lambda^2}{\lambda^2 - g^2}} \quad (13)$$

c' is one of the Sellmeier coefficients, to distinguish it from light speed c .

3.3 Dispersion Formula of Glass Material

For fused silica, the three-term refractive index fitting equation can be expressed as²⁶:

$$n(\lambda) = \sqrt{1 + \frac{0.6961663\lambda^2}{\lambda^2 - (0.0684043)^2} + \frac{0.4079426\lambda^2}{\lambda^2 - (0.1162414)^2} + \frac{0.8974794\lambda^2}{\lambda^2 - (9.896161)^2}} \quad (14)$$

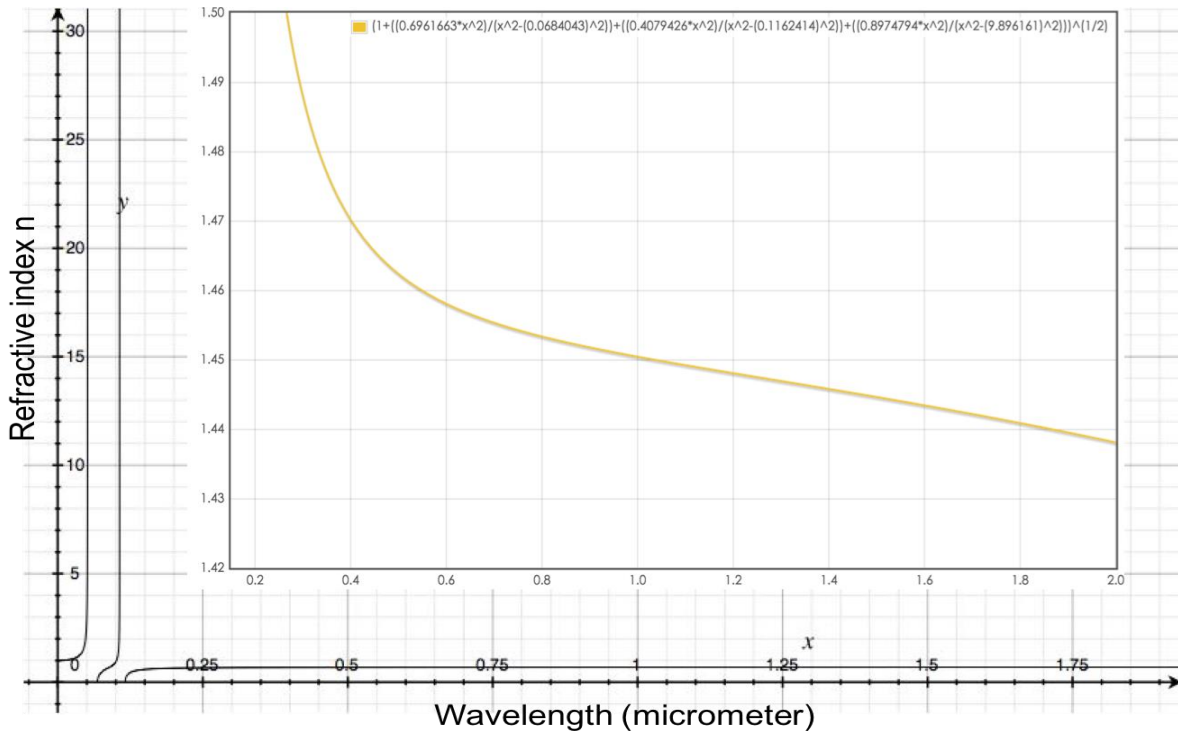


Figure 2 : Sellmeier formula of refractive index versus wavelength in micrometre for fused silica. The minimal graph is picking wavelength range from 200nm to 2000nm.

The Sellmeier Coefficients for glass materials^{27,28,29} used in this thesis are shown as below table:

Coefficient	UV Fused Silica	CalciumFluoride (CaF2)	Silicon	MgF2
a	1	1	1	1
b	0.6961663	0.443749998	10.6684293	0.48755108
c	0.0684043	0.001780279	0.301516485	0.04338408
d	0.4079426	0.444930066	0.003043475	0.39875031
e	0.1162414	0.007885361	1.13475115	0.09461442
f	0.8974794	0.150133991	1.54133408	2.3120353
g	9.89661	0.012411949	1104	23.793604

Table 2 : Sellmeier coefficients for UV fused silica, calcium fluoride and silicon.

3.4 Dispersion Formula of Air and Argon gas

Reference³⁰ shows the dispersion equation for argon gas at room temperature is

$$n - 1 = 6.432135 \times 10^{-5} + \frac{2.8606021 \times 10^{-2}}{144 - \lambda^{-2}} \quad (15)$$

The above equation is in the form:

$$n(\lambda) = 1 + \sum_j \frac{A_j}{B_j - \lambda^{-2}} \quad (16)$$

Then, expanding the formula to a two-term equation gives

$$n(\lambda) - 1 = a + \frac{b}{c' - \lambda^{-2}} + \frac{d}{e - \lambda^{-2}} \quad (17)$$

The Sellmeier Coefficients for argon gas and air ³¹are shown in the table below:

Coefficient	Argon	Air
a	0.00006432135	0.0000806051
b	0.028606021	0.0248099
c	144	132.274
d	0	0.000174557
e	0	39.32957

Table 3 : Sellmeier coefficients for argon gas and air.

3.5 Dispersion Equation as a Function of Wavelength

Bourquin et al. (1998) gives the equation of GVD, TOD and FOD of any optical components with the thickness of L_m as a function of wavelength³²

$$GVD = \frac{d^2 \phi_m(\omega)}{d\omega^2} = \frac{\lambda^3 L_m}{2\pi c^2} \frac{d^2 n(\lambda)}{d\lambda^2} \quad (18)$$

$$TOD = \frac{d^3 \phi_m(\omega)}{d\omega^3} = -\frac{\lambda^4 L_m}{4\pi^2 c^3} \left(3 \frac{d^2 n(\lambda)}{d\lambda^2} + \frac{\lambda d^3 n(\lambda)}{d\lambda^3} \right) \quad (19)$$

$$FOD = \frac{d^4 \phi_m(\omega)}{d\omega^4} = \frac{\lambda^5 L_m}{8\pi^3 c^4} \left(12 \frac{d^2 n(\lambda)}{d\lambda^2} + \frac{8\lambda d^3 n(\lambda)}{d\lambda^3} + \frac{\lambda^2 d^4 n(\lambda)}{d\lambda^4} \right) \quad (20)$$

where $L_m=1\text{mm}$ is used to plot the dispersion figures to get the unit dispersion.

$$\frac{dn}{d\lambda} = -\frac{1}{n\lambda^3} \left[\frac{bc'^2}{\left(1-\frac{c'^2}{\lambda^2}\right)^2} + \frac{de^2}{\left(1-\frac{e^2}{\lambda^2}\right)^2} + \frac{fg^2}{\left(1-\frac{g^2}{\lambda^2}\right)^2} \right] \quad (21)$$

According to the above equations and Sellmeier equation, a MatLab program 'fitting.m' is written to calculate GVD, TOD and FOD of materials in this thesis. Figure [3], [4] and [5] show the GVD, TOD and FOD of fused silica

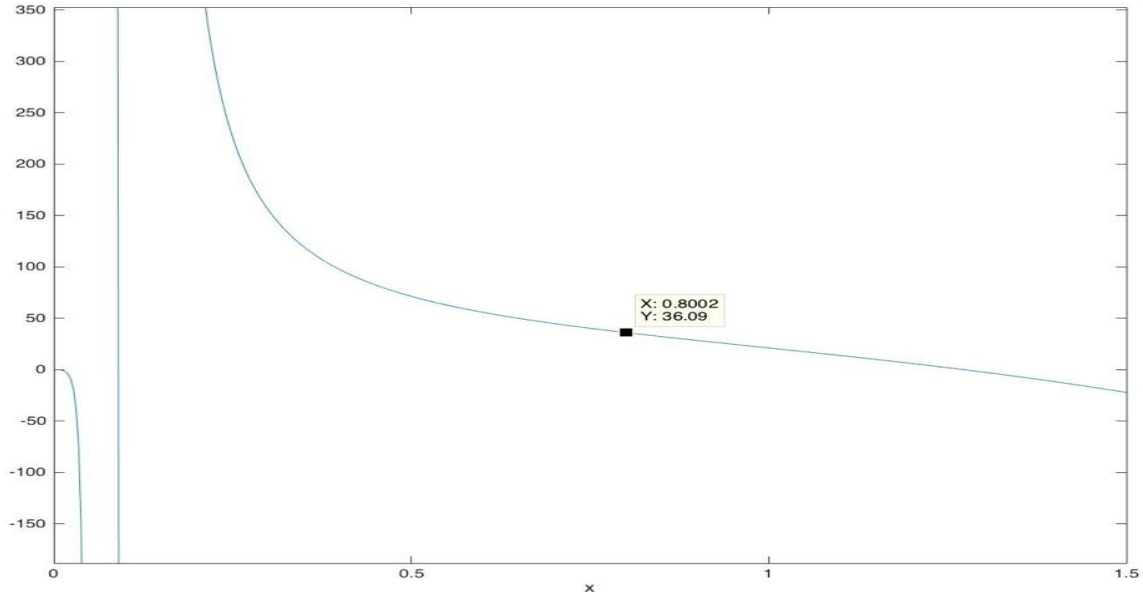


Figure 3 : Group velocity dispersion of fused silica at 0-1500nm. The GVD at 800nm is 36.09 fs^2/mm

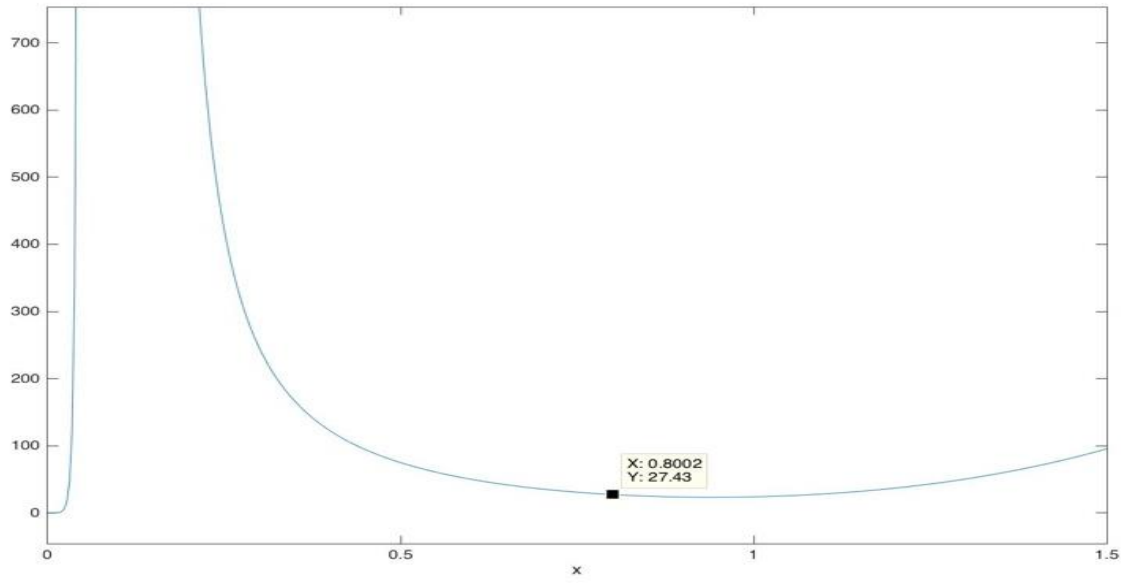


Figure 4 : Third-order dispersion of fused silica at 0-1500nm. The TOD at 800nm is 27.43 fs³/mm

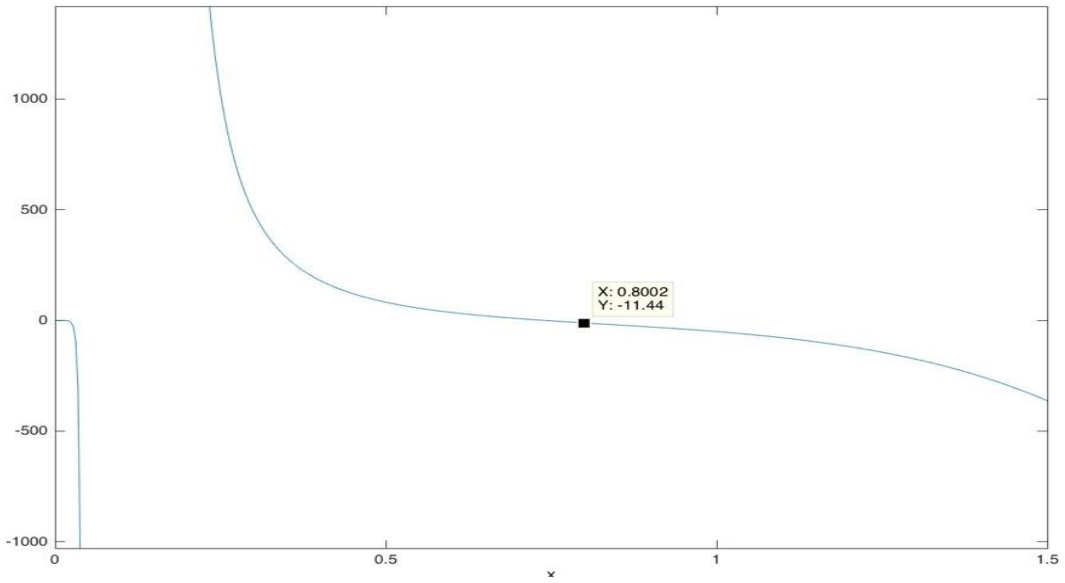


Figure 5 : Fourth order dispersion of fused silica at 0-1500nm. The TOD at 800nm is -11.44 fs⁴/mm.

The group velocity dispersion, third order dispersion, fourth order dispersion and group delay dispersion at 800nm of each optical component in hollow fibre system and autocorrelation system are summarised in below table. It is worth to mention that BBO crystal in autocorrelation system has only 0.02mm of thickness; therefore, the dispersion of BBO crystal is ignored.

Components	Material	Thickness (mm)	Number	GVD (fs ² /mm)	TOD (fs ³ /mm)	FOD (fs ⁴ /mm)	GDD (fs ²)
Hollow Fibre Window	UVFS	1	2	36.09	27.43	-11.44	72.22
Half-Wave Plate	MgF2	1	2	19.75	13.71	-5.030	39.50
Focus Lens	UVFS	3	1	36.09	27.43	-11.44	108.33
Beam Splitter (A.C.)	UVFS	1	1	36.09	27.43	-11.44	36.09
Round Continuously Filter (A.C.)	UVFS	0.25	1	36.09	27.43	-11.44	9.03

Table 4 : Dispersion of components in hollow fibre and autocorrelation system.

Gas	GVD (fs ² /mm)	TOD (fs ³ /mm)	FOD (fs ⁴ /mm)
Air	0.0213	0.00989	0.001153
Argon	0.01897	0.008641	0.000772

Table 5 : Dispersion calculation of air and argon gas.

4. Transverse Properties of a Laser Beam and Its Relevance to Hollow Fibre Propagation

During the few cycle pulse generation experiment, it is necessary that the laser beam is accurately aligned and delivered to the core of the hollow fibre. In order to achieve this, the method is to adjust the control clamp knobs of the x and y translation stage to slightly adjust the position of the hollow fibre to see a “best” mode after the laser propagating through the fibre. The “best” mode is described as the foundation mode E_{11} , which has the lowest energy loss. In this chapter, I will briefly introduce the optic theory of transverse modes.

4.1 Gaussian Beam

It is well known that Gaussian laser beam is a radially symmetrical distribution electromagnetic energy. Assuming the laser propagates along z direction, the electric field of the beam can be described by Gaussian function

$$E(r, z) = E_0(r, z) \text{EXP} \left(-\frac{r^2}{\omega_0^2} \right) \quad (22)$$

The above equation describes how the fundamental Gaussian beam propagate with a Gaussian profile of the lowest order transverses electromagnetic mode (TEM_{00}). The transvers mode, describes the intensity distribution of the cross section of laser beam. The function of laser intensity is defined by

$$I(r, z) = I_0(r, z) \exp \left(-\frac{2r^2}{\omega_0^2} \right) \quad (23)$$

For equation (23) and (24), r is the radius of the laser beam, ω_0 is called beam the waist, at which the intensity of the laser is $1/e^2$ of the total intensity.

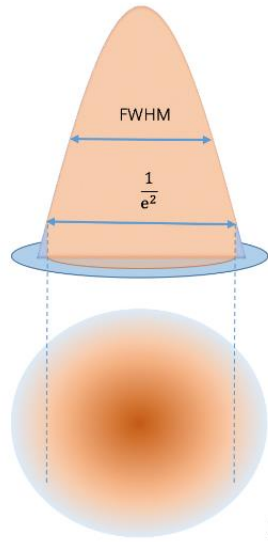


Figure 6: Gaussian laser pulse size. Beam waist is at the $1/e^2$ intensity of laser beam. Pulse duration is expressed as full width at half maximum (FWHM).

In the lab, the radius of the laser beam can be approximately measured by using an iris. First place the iris in the beam and open the iris so all of the power goes through the power meter. Then carefully adjust the knob to reduce the iris diameter until $1/e^2$ of the total laser beam energy passes through it. The inner diameter of the iris is exactly the same as the laser beam waist.

4.2 Transverse Mode

Laser beams can have different and higher order modes. There are many types of transverse mode such as transverse electromagnetic mode (TEM), transverse magnetic mode (TM), transverse electric mode (TE), Hybrid mode(EH) and linear polarisation mode (LP).

- Transverse electromagnetic mode (TEM): Both directions of an electric field or magnetic field is perpendicular to the direction of laser propagation.

- Transverse magnetic mode (TM): Only magnetic field is perpendicular to the direction of laser propagation; the electric field is along the laser propagation direction.
- Transverse electric mode (TE): Only electric field is perpendicular to the direction of laser propagation; the magnetic field is along the laser propagation direction.
- Hybrid mode(EH): Both directions of an electric field or magnetic field is along the direction of laser propagation.
- Linear polarisation mode (LP): In the fibre which refractive index of the core is in proximity to the refractive index of the cladding. It is called weakly guided fibre and lead to the construct of linear polarisation. Linear polarisation mode is a superposition of several modes when the laser pulse propagates through the fibre.

4.3 Fundamental Mode

Gholami et al. (2009) show the theoretical radiation calculation for the linear polarisation mode ³³. It is observed that the fundamental mode LP₀₁, has the highest radiation power at the centre; however, for the higher order mode, the peak radiation intensity is farther from the centre. Those different modes exist for various wavelengths, as shown in figure 7(b).

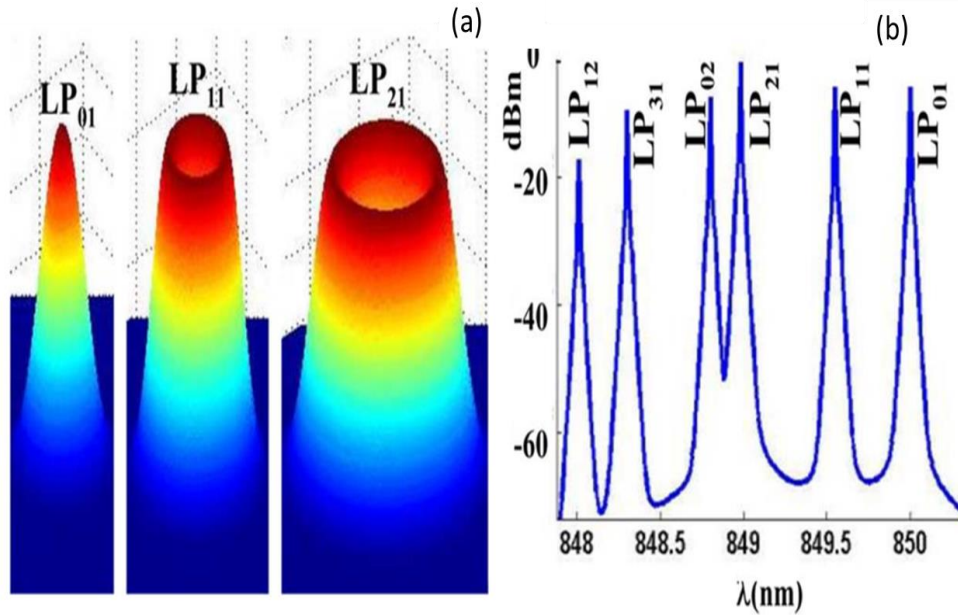


Figure 7 : (a) Calculated radiation patterns of a three-transverse-mode of vertical cavity surface emitting lasers (VCSEL); (b) spectrum of the VCSEL. (Reprinted with permission from [33])

As mentioned above, the propagation characteristics of our laser beam can be assumed to be, that the intensity is always greatest at the centre and tails off at the both edges, which means the laser beam has an ideal Gaussian profile and progresses produce as a fundamental Transverse mode, which can be expressed as $TEM_{00}=LP_{01}=EH_{11}$. It is possible to influence the order of the transverse mode of a laser beam by adjusting the distribution in the laser gain medium³⁴. Reference³⁵ shows the electric field distribution of electromagnetic transverse modes in Figure 8.

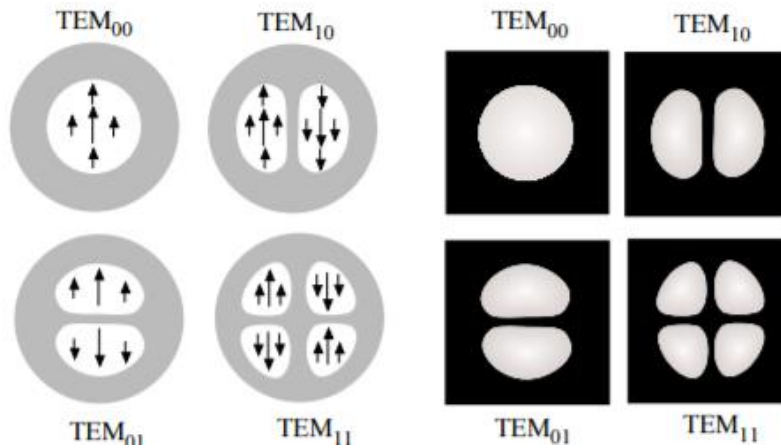


Figure 8 : (a) Four low order transverse cavity modes and their fields. (b) Intensity patterns in the modes of (a). (Reprinted with permission from [35])

For the short pulse application Coulomb Explosion Imaging, it is important to maximise the intensity by keeping the peak intensity of the laser at the centre, this is also important when coupling into a hollow fibre which will be discussed in the next section about the fundamental mode in fibres.

4.4 Fundamental Modes in an Optical Fibre

4.4.1 Single Mode and Multimode Fibre

For fused silica fibres, the lowest energy loss mode is fundamental mode EH₁₁. Marcatili et al. (1964) showed their research on the modes of the hollow dielectric fibres.³⁶ Consider a hollow fibre with inner radius a . Dielectric constant in core is ϵ_0 and in cladding is ϵ_1 and magnetic permeability is μ_0 for both core and cladding area. k is the propagation constant of the core area. To determine figure out the field components of the normal modes and their propagation constants, for the fundamental mode E₁₁, they assuming that

$$ka = \frac{2\pi a}{\lambda} \gg |v|\mu_{11} \quad (24)$$

and

$$\left| \frac{\gamma}{k} - 1 \right| \ll 1 \quad (25)$$

where $k = \omega \sqrt{\epsilon_0 \mu_0}$ is the propagation constant in the core space. μ_{11} is the first root of the Bessel function J_0 , $v = \sqrt{\epsilon_1 / \epsilon_0}$ is the ratio of the dielectric constants, also equals the ratio of the refractive index between the core and the cladding material.

They obtained the propagation constant of the mode γ which can be expressed as

$$\gamma \approx k \left[1 - \frac{1}{2} \left(\frac{u_{11} \lambda}{2\pi a} \right)^2 \left(1 - \frac{iv_1 \lambda}{\pi a} \right) \right] \quad (26)$$

We can separate the complex function into a real term β and an imaginary term $\frac{\alpha}{2}$:

$$\beta = \frac{2\pi}{\lambda} \left[1 - \frac{1}{2} \left(\frac{2.405\lambda}{2\pi a} \right)^2 \right] \quad (27)$$

$$\alpha = \left(\frac{2.405}{2\pi} \right)^2 \frac{\lambda^2}{2a^3} \frac{v^2 + 1}{\sqrt{v^2 - 1}} \quad (28)$$

The real term β represents the phase constant and the imaginary term $\frac{\alpha}{2}$ represents the field attenuation constant, the unit for α is decibels per meter. If the input power for hollow fibre is P_1 and output power is P_2 , then the power transmission function of the fundamental mode is³⁷

$$T = e^{-2\alpha L}$$

The transmission loss of the optical fibre that was used in this project is calculated as 0.3791dB/m. Figure 10 shows the transmission versus the fibre length at 0.4 atm argon gas

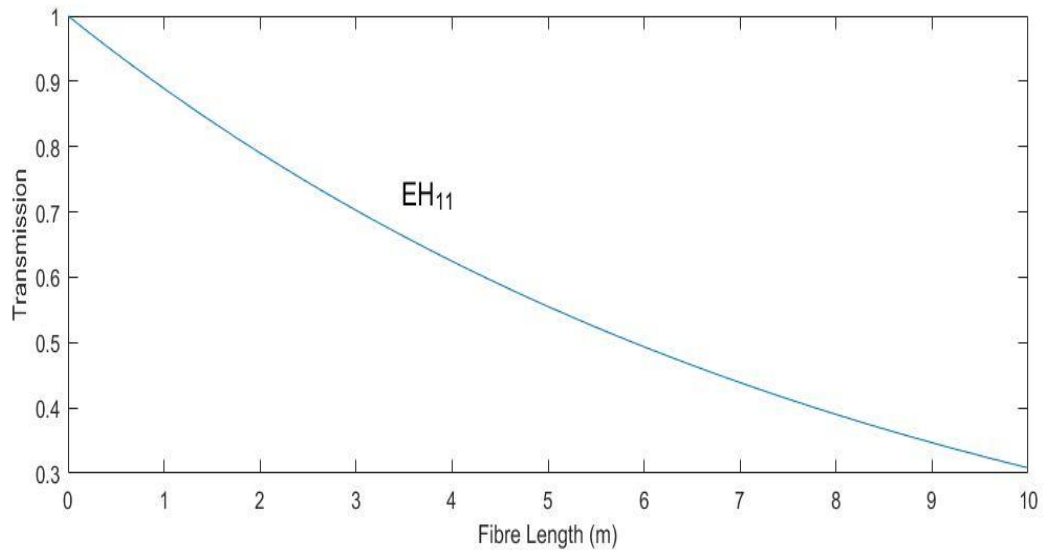


Figure 9 : Transmission versus length of the fibre for the fundamental mode EH_{11} .

Marcatili also showed the intensity profile as a function of distance r is expressed as

$$I(r) = I_0 J_0^2\left(\frac{2.405r}{a}\right) \quad (29)$$

The largest beam intensity is at the centre of the mode and gradually attenuated along the radius.

The electric field components and intensity distribution of the fundamental mode E_{11} are shown in below Figure 10.³⁵

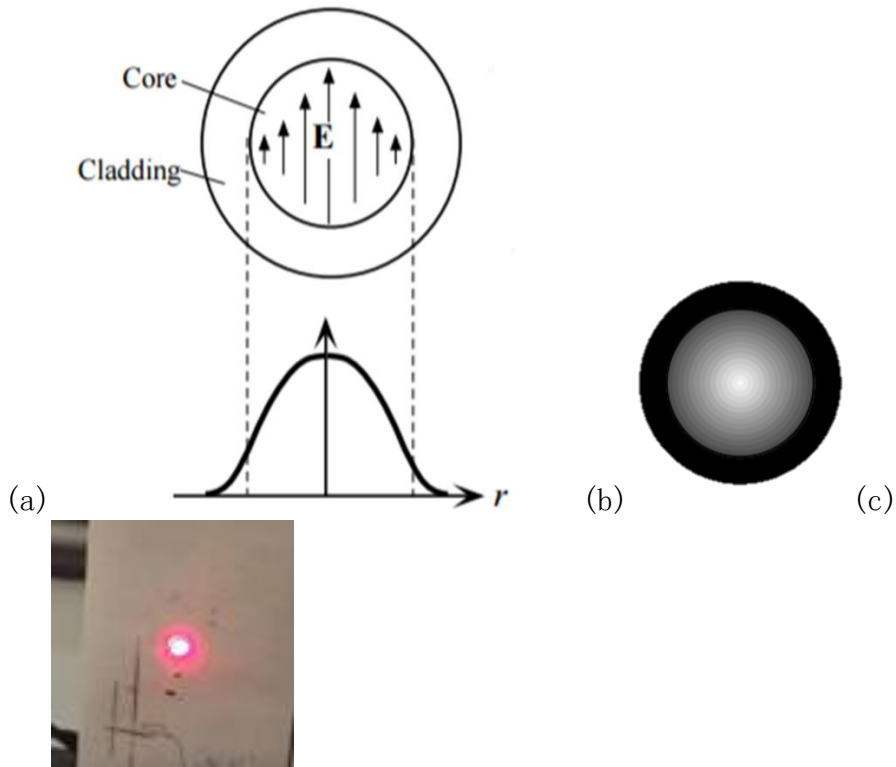


Figure 10 : (a) Electric field distribution of the fundamental mode. (b) The intensity profile of fundamental mode, the lightest area, has the greatest intensity. (Reprinted with permission from [35]) (c)The real mode obtained in the Waterloo lab.

5. Review of Progress in Generation of Few Cycle Pulses by Using the Hollow Fibre Technique

In 1996, Nisoli and his co-workers used a hollow core silica fibre filled with argon or krypton gas at high-pressure $p=4\text{atm}$ to achieve spectral broadening through self-phase modulation³⁸. They used a 70cm long hollow core fibre with $140\mu\text{m}$ inner diameter. A 1kHz, $660\mu\text{J}$, 140fs duration, 780nm wavelength input pulse to the hollow fibre chamber was provided by a Ti: sapphire laser with a chirped-pulse amplification system. Figure 11 shows the spectrally broadened output for $p=4\text{ atm}$ of argon gas, with the input peak pulse power at 3.5GW. The transform limited pulse duration was calculated to be 18fs. Experimental results for krypton gas showed a larger spectral broadening, and consequently, a shorter possible pulse duration down to 10fs. The reason for this difference is that krypton gas has a larger nonlinear refractive index.

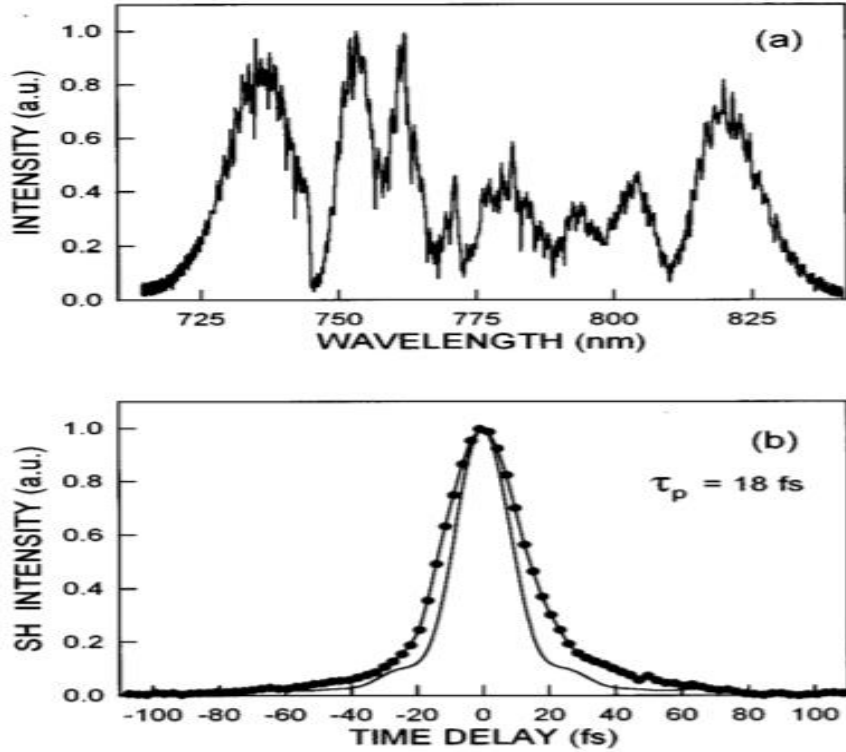


Figure 11 : (a) Spectral broadening in argon gas 4 atm pressure. (b) Pulse shape derived by taking the inverse Fourier transform of (a), pulse duration at FWHM is 18fs. The line with dots is the real autocorrelation trace of the pulses, and the solid line is the predicted autocorrelation trace by taking the inverse Fourier transform of (a) (Reprinted with permission from [38])

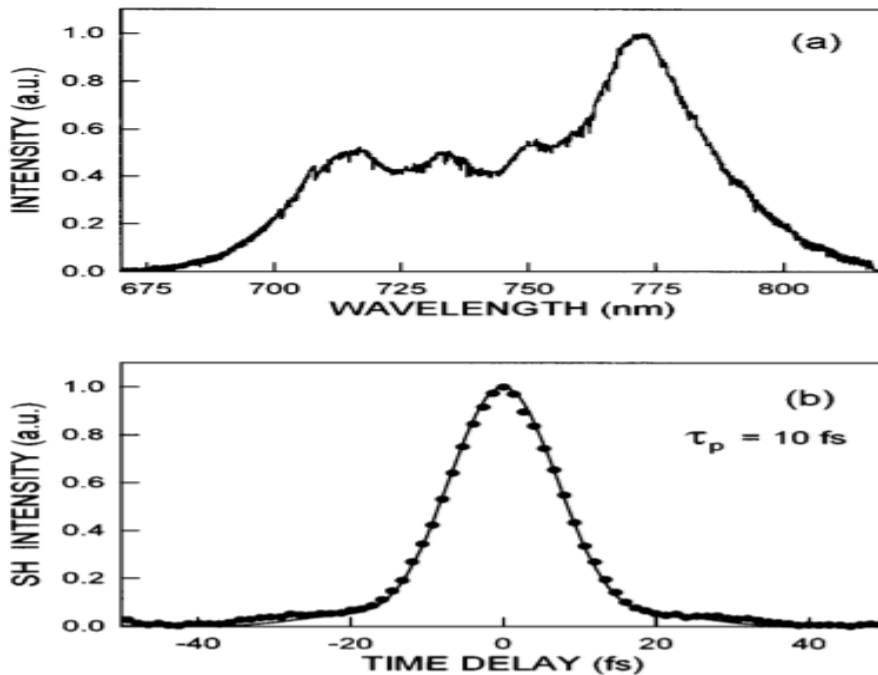


Figure 12 : Spectral broadening in krypton gas of 2 atm pressure. (b) Pulse shape derived by taking inverse Fourier transform of (a), pulse duration at FWHM is 10fs. The line with dots is the real autocorrelation trace of the pulses, and the solid line is the predicted autocorrelation trace by taking the inverse Fourier transform of (a). (Reprinted with permission from [38])

Nisoli et al. followed up their work after 1997, by changing the input laser source and using hollow fibres with different length and diameter.³⁹ They changed from a 70cm length, 140 μ m inner diameter fibre to various 60-70cm length, 70-80 μ m inner diameter fibres. One of their laser sources was Ti: sapphire laser system; with pulse duration of the 140fs, in addition to this, they also used another source producing a centre wavelength of 780nm and duration of the 20fs. A schematic of their experimental setup is shown in Figure 13. The dispersive compressor was used to compensate the dispersion from the optical components. The Autocorrelation was recorded by using an interferometric autocorrelator. Figure 14 shows the spectral broadening in argon gas but with different input pulses. The dashed line represents

the input laser spectrum. Figure 14 (a) is the spectrum that they published in 1996, (Figure 11 (a) for an input pulse of 140fs), the broadening range was from 710nm to 880nm. Figure 14(b) shows the spectrum produced with a 20fs input pulse, and the broadening range is from 610nm to 1080nm. It is observed from the Figure 14(b) that the input laser of has a wider spectrum when the duration of the laser pulse is shorter(as expected from the fourier transform relation between pulse duration and spectrum), giving spectral broadening a greater influence for a shorter input laser pulse.

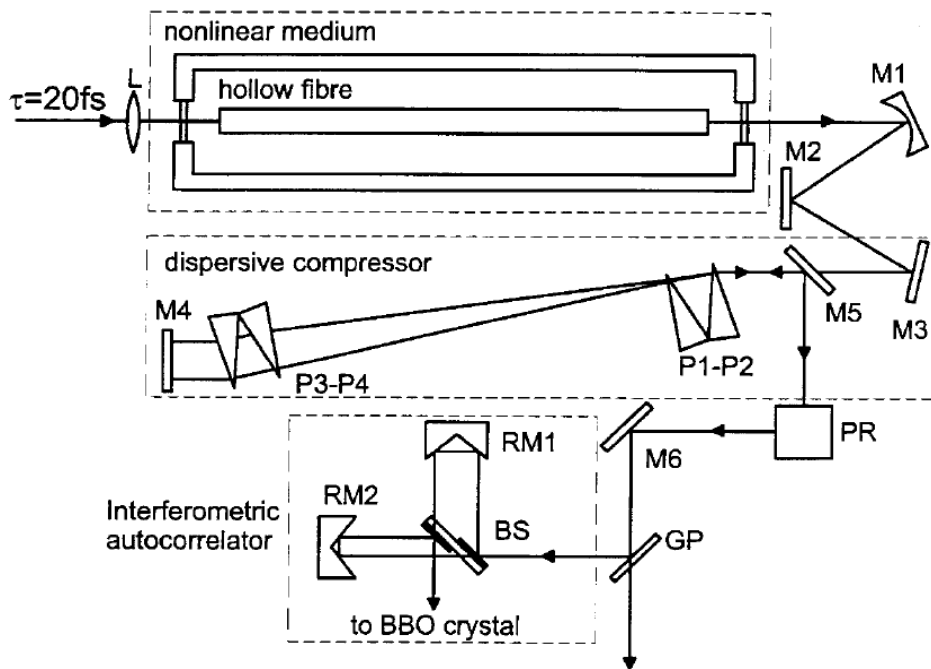


Figure 13 : Schematic of Nisoli's experiment setup. L is an AR-coated lens of 30 cm focal length, M1 is a silver-coated mirror with 50 cm radius of curvature; M2, M5, and M6 are silver-coated plane mirrors and M3, M4 are chirped multilayer mirrors; P1–P4 are AR-coated multilayer 20° fused silica prisms. The beam reflected back by M4 is slightly separated from the incident beam to allow coupling by M6. PR provides polarization rotation using silver-coated mirrors. GP is a 1-mm-thick fused silica plate with AR-coated back side. BS is a

broadband dielectric beam splitter on a fused silica substrate identical to GP. RM1 and RM2 are silver-coated roof mirror assemblies. (Reprinted with permission from [39])

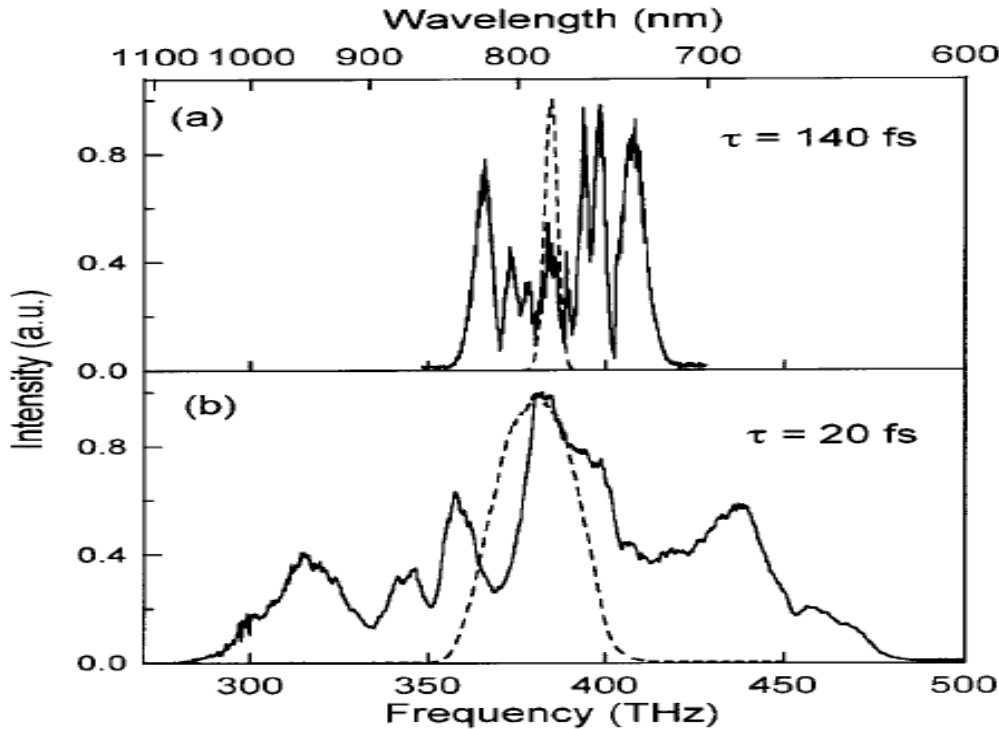


Figure 14 : Spectral broadening in argon (a) Spectral broadening in argon gas at the 4atm pressure and 140fs, 3.5GW peak power input laser. (b) Spectral broadening in argon gas at the 3.3atm pressure and 20fs, 4GW peak power input laser. The spectra of the input pulses are shown as dashed lines. (Reprinted with permission from [39])

As mentioned above, Nisoli's group used the dispersive compressor setup to control the accumulated dispersion of the optical components³⁹. There are many methods to control the phase of the spectrum. In the Waterloo lab, we are using the ultra broad band dispersion compensating mirror set (BBCOMP) to compensate the system dispersion. Eniko et al. (2003) used an Acousto Optic Programmable Dispersive Filters (AOPDF) compressor setup to balance the dispersion⁴⁰. This compressor setup is able to compensate the higher order dispersions of the optical system. Their experiment set up is shown in Figure 15. They used an inner diameter of 200 μ m hollow fibre (they did not mention the length of the fibre) filled with the

pressure of 1.5 atm argon gas to generate duration of 8fs and peak power of 9GW laser pulses.

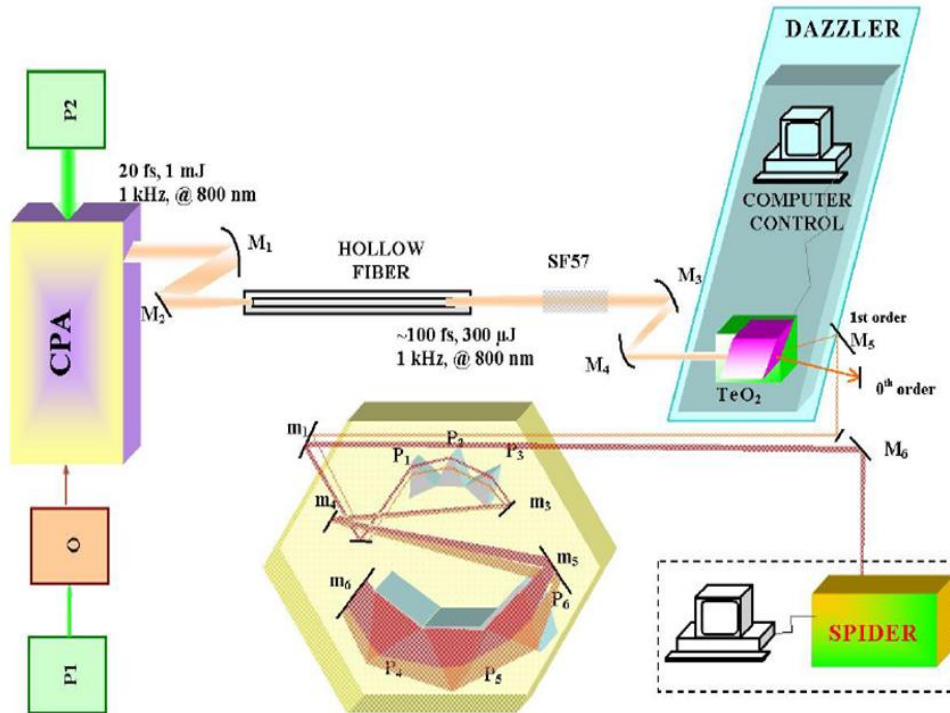


Figure 15 : Schematic of Eniko's experiment setup. P1 is the YVO4 pump laser for the oscillator. P2 is the Nd:YLF pump laser for the chirp pulse amplification stage (CPA) Laser pump laser. SF57 is a 5cm glass block. Compressor contains AOPDF (DAZZLER system) and a set of Brewster angle fused silica prisms. (Reprinted with permission from [40])

5.1 Achieving High Energy Pulses from a Hollow Fibre

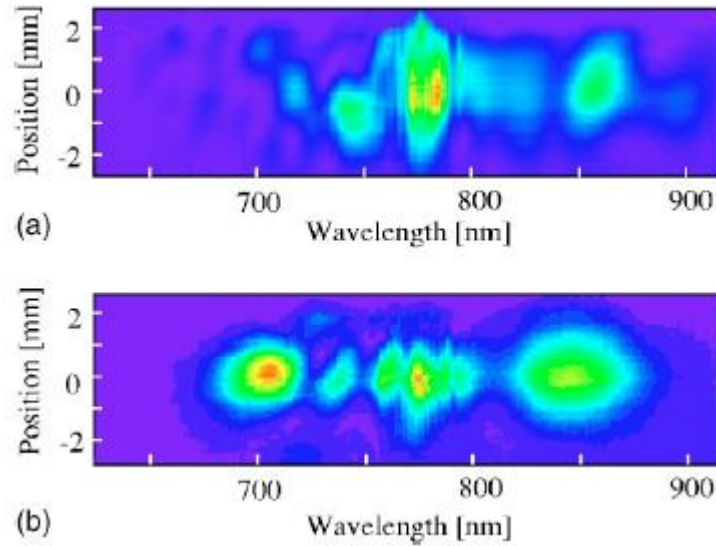


Figure 16 : (a) Laser pulses output spectral when hollow fibre is set in a constant pressure chamber. (b) Laser pulses output spectral when hollow fibre is placed in a pressure gradient chamber. (Reprinted with permission from [42])

Pressure distribution formula inside the hollow fibre is expressed as⁴²

$$p(x) = \sqrt{p_0^2 + \frac{x}{L}(p_L^2 + p_0^2)}$$

where p_0 is the gas pressure at the input side of the hollow fibre and P_L is the gas pressure at the output edge of the hollow fibre. L is the length of the hollow fibre.

Robinson et al. (2006) showed their comparison of the spectral broadening results between methods by using constant pressure chamber and differentially pumped chamber⁴¹. They used a length of 220cm, the inner diameter of 500 μ m argon gas filled hollow fibre with 8.5mJ, 40fs input pulses to generate 5.5mJ, 9.8fs output pulses.

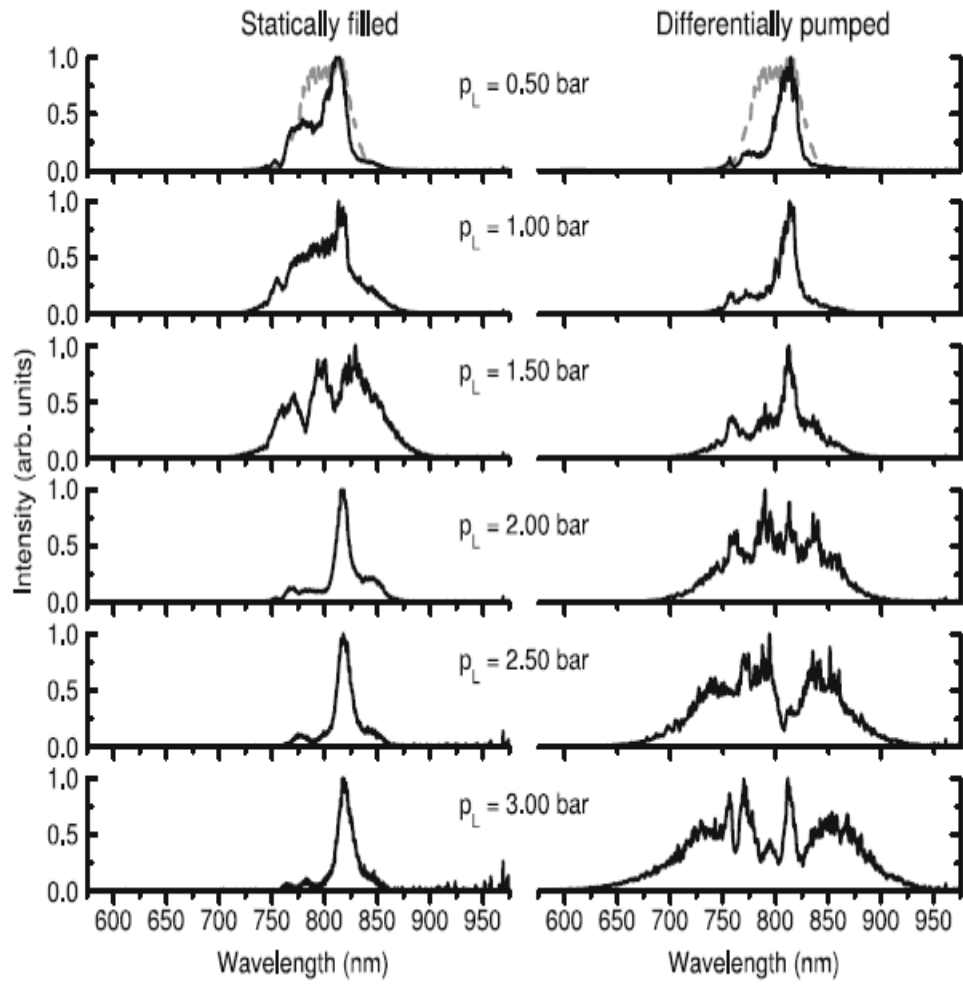


Figure 17 :Spectral broadening comparison between the statically filled chamber and the differentially pumped chamber. The grey dashed line represents the input resource pulse spectra. (Reprinted with permission from [Error! Bookmark not defined.])

Above figure 17 shows Robinson's results of the spectrum obtained from statically filled and differentially pumped chambers for different gas pressure. It is observed from the statically pumped spectrum, that the spectrum started to broaden and stretch above a gas pressure of $p=0.50$ bar; however, the spectrum researched the widest extent when the gas pressure was $p=1.5$ bar, and then contracted to even narrower bandwidth. The right figure shows the spectrum changing when the hollow

fibre was placed in a differentially pumped chamber. It is observed that the spectrum continually broadens with the increasing gas pressure. Compared with the statically pumped chamber, below 3 bar gas pressure, the spectrum in the differentially pumped chamber did not have the pressure limitation. As a result a much shorter pulse could be obtained under the high pressure differentially pumped system.

Akira et al. (2005) developed a pressure gradient technique to make it possible to generate high energy pulses with a duration of sub-10-fs.⁴² They used a hollow fibre with a length of a 220cm and a 250 μ m inner diameter. The hollow fibre chamber was separated into two parts; gas was sent to the output end of the fibre through the last chamber and pumped out at the input of the fibre in the front chamber; therefore, it would create a pressure gradient inside the hollow fibre. The gas pressure at the laser input side of the hollow fibre chamber is 0kPa and laser output side is 40kPa. A Ti: sapphire chirped pulse amplification system provided pulses of duration 40fs, with an energy of 8.5mJ and repetition rate of the 10Hz. After that, this laser was focused by a f=3m focus lens and then delivered to the hollow fibre chamber. Figure 18 (a) and (b) show their spectra comparison between input and output pulses. The duration of the short pulse was as short as 9.8fs when calculated by the into inverse Fourier transform o the broadened spectrum.

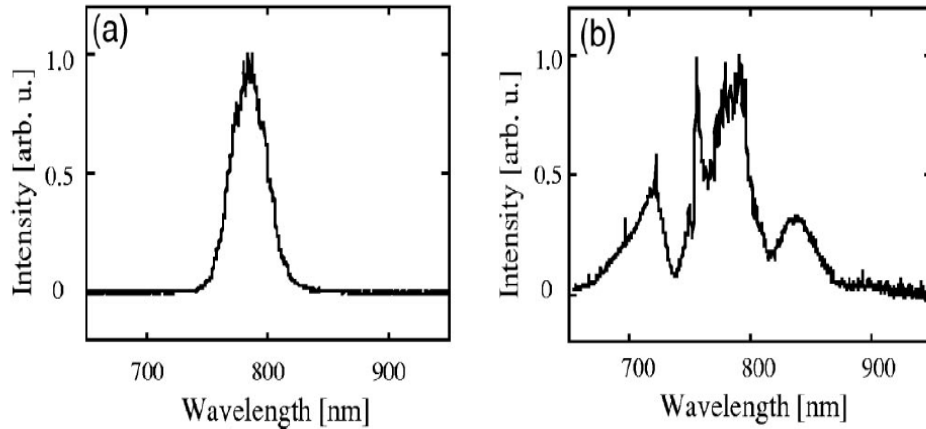


Figure 18 : Spectral broadening in argon gas. (a) Spectrum of the input laser pulse, the energy of the input pulse is 8.5mJ. (b) Spectral broadening in argon gas, the pulse energy is 6.5mJ. (Reprinted with permission from [42])

Samuel et al. (2010) also used the differentially pumped technique sending 12mJ input pulses of 27fs duration into a neon filled hollow fibre with a length of the 220cm and inner diameter of 500 μ m.⁴³ They tested their setup with different input pulse energies and different gas pressures on the exit side of the chamber. They obtained 5mJ 5fs short pulse by controlling the pressure of chamber exit side to be 0.18MPa with an input pulse energy of 9.5mJ.

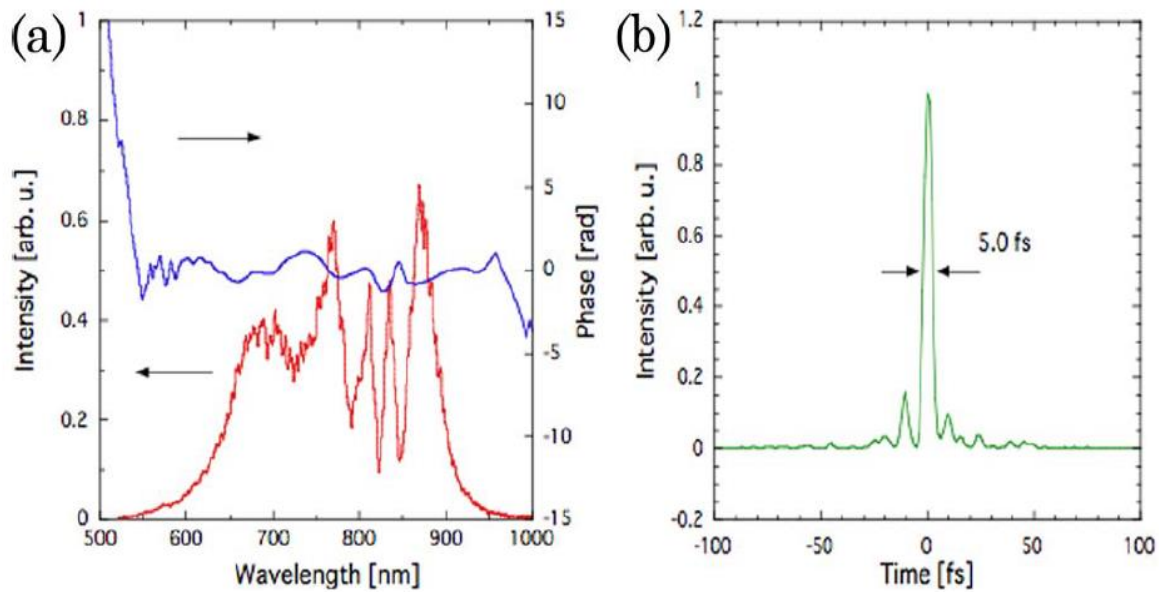


Figure 19 : Spectral broadening in neon gas, the pulse energy is 5.0mJ, and the pulse duration is 5fs by taking (a) into Fourier transform. (Reprinted with permission from [43])

In order to generate a broadened spectrum in this project we use a hollow fibre manufactured by FEMTOLASERS along with ultra broad band dispersion compensating mirror set (BBCOMP), from the same manufacturer⁴⁹. Figure 20 shows a spectrum generated by the FEMTOLASERS company, using the same parameters as the hollow fibre that is used in our lab, a length of 1m, an inner diameter of 250 μ m filled with 2 bar pressure of neon gas, to generate a pulse of duration 5.5fs. The input laser pulse had an energy of 0.8mJ and duration of sub-25fs.

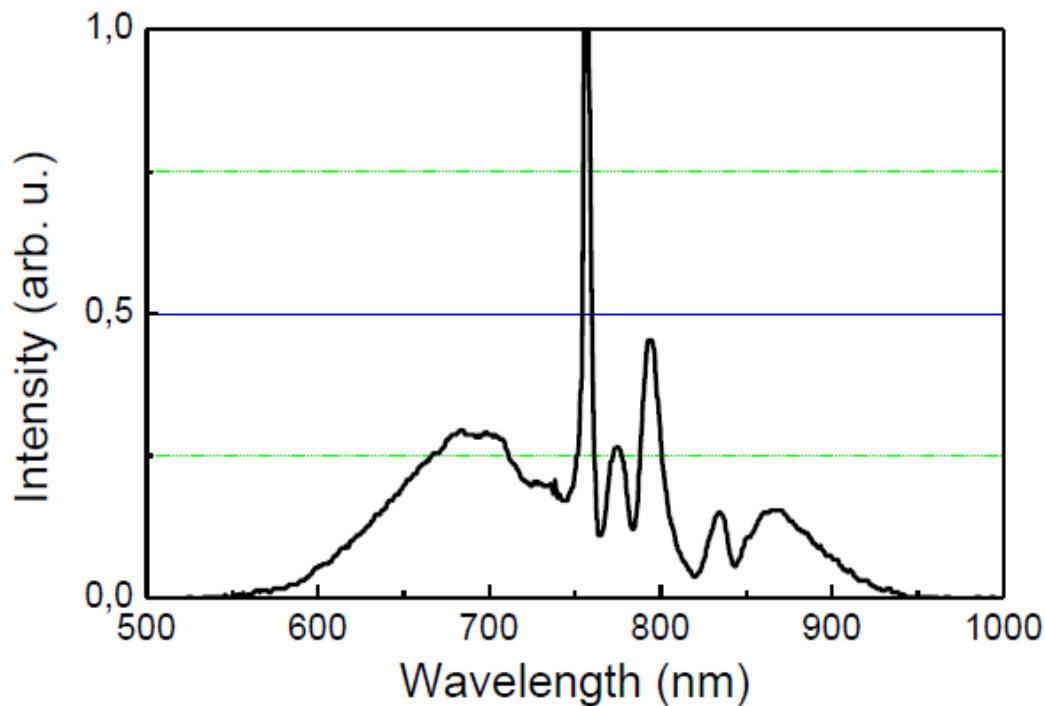


Figure 20 : Spectral broadening test results by the ultra broad band dispersion compensating mirror set (BBCOMP) manufacturer: FEMTOLASERS⁴⁹.

5.2 Evaluating the Few Cycle Pulse Duration Using Coulomb Explosion Imaging (CEI)

One of the earliest works which could be used to evaluate the laser pulse is L egar e et al. (2003)⁶². They used a wavelength of 800nm, a pulse duration of 40fs and energy of 250 J and repetition rate of 500Hz Ti: sapphire laser amplifier, and fibre with a length of 1m, and an inner diameter of 250 m filled with 1atm argon gas to generate 9fs laser pulses. The laser pulses then delivered to the Coulomb explosion chamber at the background pressure of 10^{-9} mbar. They make the D₂ gas into a molecule beam by expanding D₂ through a 100 m aperture and then a skimmed jet to produce a molecule beam of 40 m thickness. Therefore, the confocal parameter of the laser beam, which is 100 m, is larger than the molecule beam. The molecular

beam will only experience a slight change of the laser intensity along the laser beam. Their technology allows a molecule to be exposed to a rapidly increasing but near spatially uniform pulse intensity. They were able to measure the time difference between the first and the second electron moved from the atom by using what they refer to as a molecule clock. Then the kinetic energy is a measurement of the time delay between the first and second ionization. The kinetic energy of the deuteron molecule is shown in Figure 21.

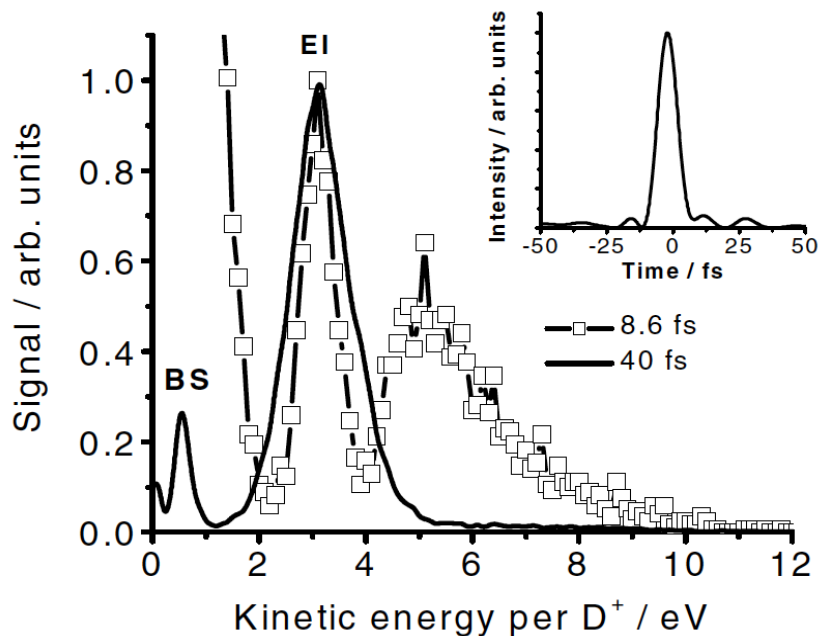


Figure 21: Deuteron molecule kinetic energy spectra obtained under 40fs (solid line) and 8.5fs (square) pulse. (Reprinted with permission from [62])

The peaks at 3eV is a signature of Enhanced Ionization for both 40fs and 8.3fs laser pulses, i.e. $D^+ + D \rightarrow D^+ + D^+$ (at close to $2xR_{eq}$), in which the total energy released is around 50% of the expected Coulomb explosion from equilibrium. The peak at 0.7eV for 40fs laser pulses represents $D^+ + D$ bond soften^{44,45} without future

ionization while the peak from 4eV-10eV only present for 8.5fs laser pulses that originates from double ionization close to equilibrium.

6. The Laser System

This chapter introduces the laser system that is used in the Waterloo lab. The 10fs, seed laser that is produced by the oscillator is delivered to the stretcher. The stretcher then introduces positive GVD which stretches the pulse duration to 100ps. After that, the laser enters the amplifier which increases the pulse energy to 7mJ and sends it to the compressor. The compressor provides negative GVD in order to compensate the accumulated positive GVD of the optical components and the stretcher; during this process some energy is lost into higher orders from the grating, so that a pulse of up to 4.35mJ and duration as short as 35fs is produced. The single shot autocorrelation system is also introduced in the last section of this chapter which can measure the pulse duration.

6.1 Oscillator

The Kerr-lens mode-locked (KLM) Ti: Sapphire oscillator (FEMTOLASER Scientific PRO) is used to seed the amplification process. The Oscillator contains a Compact Laser Head (CLH), and external chirped mirror dispersion components. Controls on the CLH are used to adjust the position of the Ti: Sapphire crystal and mirrors to achieve mode locking; the details will be discussed later. The oscillator is pumped by a Spectra Physics "Millennia S", YVO laser which produces 532 nm, 5W laser beam. The oscillator can produce a pulse of duration 10fs, and an average power of 300mW, at the repetition rate of 80MHz and wavelength centred at 800nm of which 50% is used to provide the seed laser to the amplifier.

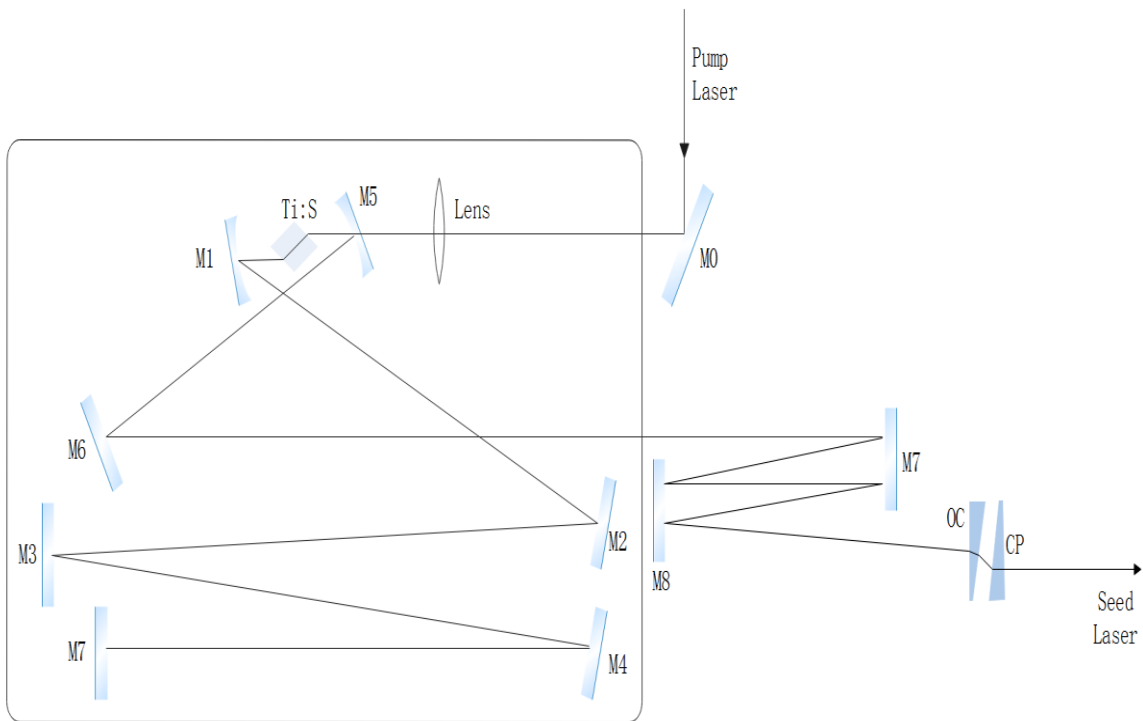
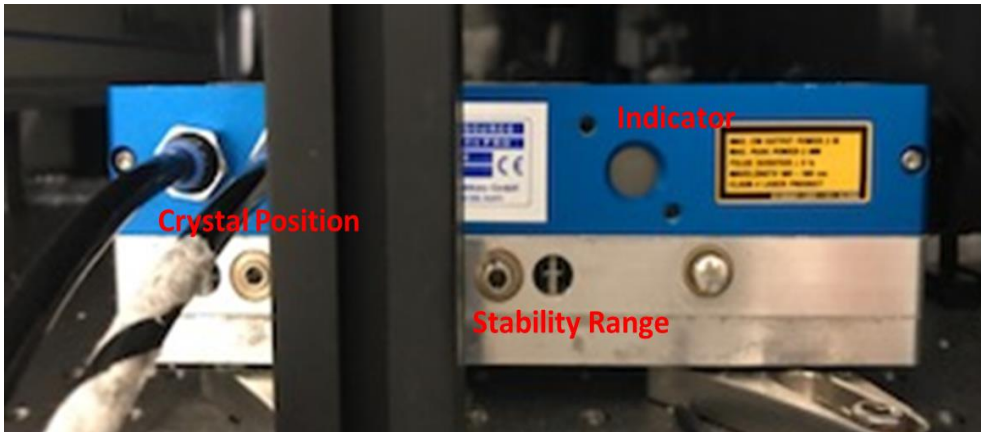


Figure 22 : Layout of the Compact Laser Head and its real picture in the Waterloo lab.

The layout of CLH is shown in Figure 22. For optimum self-mode-locked operation, the distance between the two curved focusing mirrors (M1 and M5 in Figure 22), also called the stability range, can be adjusted by the micrometre screwdriver (Stability Range hole in Figure 22). The position of the M7 can also be controlled by adjusting the ‘Crystal Position’ in Figure 22. The output coupler (OC in

Figure 22) can also be adjusted to improve pulse energy and improve mode locking stability.

6.2 Regenerative Amplifier

The Spectra-Physics Spitfire[®] Ace[™] amplifier system has been used in the Femtosecond Laser Lab of University of Waterloo since 2015. This amplifier system contains respectively three internal sub-assemblies, the optical pulse stretcher, Ti: Sapphire regenerative amplifier and optical pulse compressor. A Timing and Delay Generator (TDG) and a Temperature Control Unit (TCU) are two control consoles connect to the amplifier. The TDG is used to synchronize timing for trapping the seed pulse in the regenerative amplifier cavity and after the amplification, releasing the laser pulse to enter the compressor. The TCU is used to monitor the temperature and humidity of the crystal. The Empower 45 is an intracavity-doubled, diode-pumped Nd:YLF Laser system, which provides a nanosecond pulsed green beam of repetition rate between 500Hz to 10kHz, the laser delivers 28mJ per pulse at a wavelength at 527nm to excite the Ti: Sapphire crystal. The seed pulse is delivered to the stretcher in the amplifier, as indicated by the arrow in Figure 24: The multi-pass diffraction grating stretcher (Stretcher Grating in Figure 24) reduces the power in the amplifier crystal and prevents damage during amplification; by extending the pulse duration to 100ps. The bandwidth detector (BWD) monitors the intensity of light at each end of the spectrum to ensure that only a pulse is injected into the regen, to protect the amplifier from the accidental damage and also indicates the alignment of the seed beam. The stretched pulse is switched into the regenerative cavity by the extra-

cavity Pockles cell (PC1 in Figure 24), and then propagates back and forth in the amplifier to increase the energy of the pulse. The second intracavity Pockles cell (PC2 Figure 24) switches the pulse to the compressor (grey area in Figure 24) where energy is lost. The compressor grating compensates the accumulated positive GVD. Then a duration of 35fs, average energy up to 4.35mJ laser pulses is produced. The process to align and set up the amplifier is shown in Appendix H.

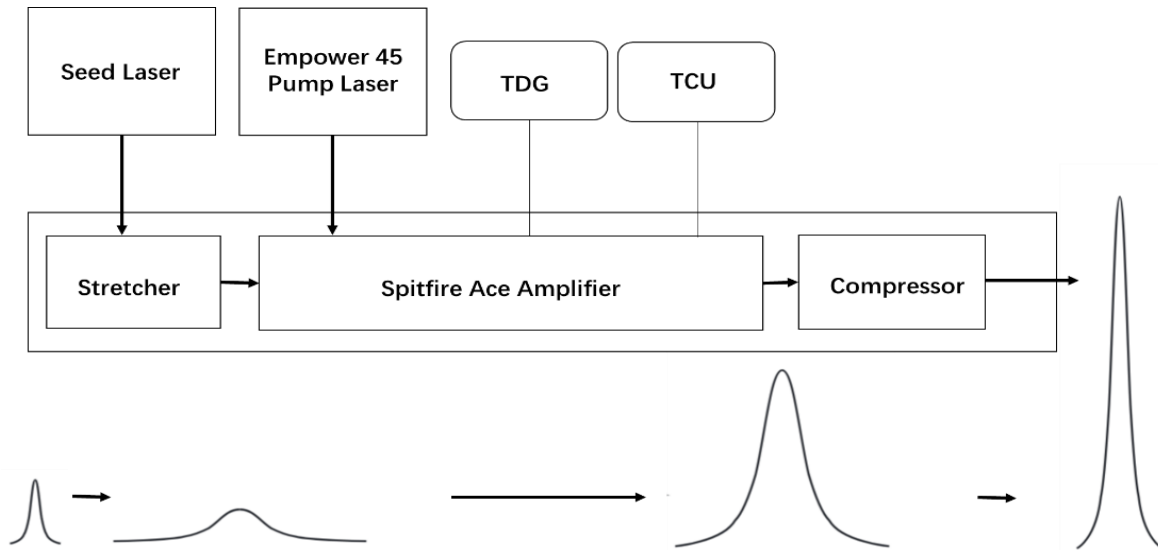


Figure 23: Principle of the laser system. The seed laser is produced by the oscillator and then delivered to the Spitfire Ace-35F regenerative amplifier system.

Below figures show the optical layout of the Spitfire Ace regenerative amplifier.

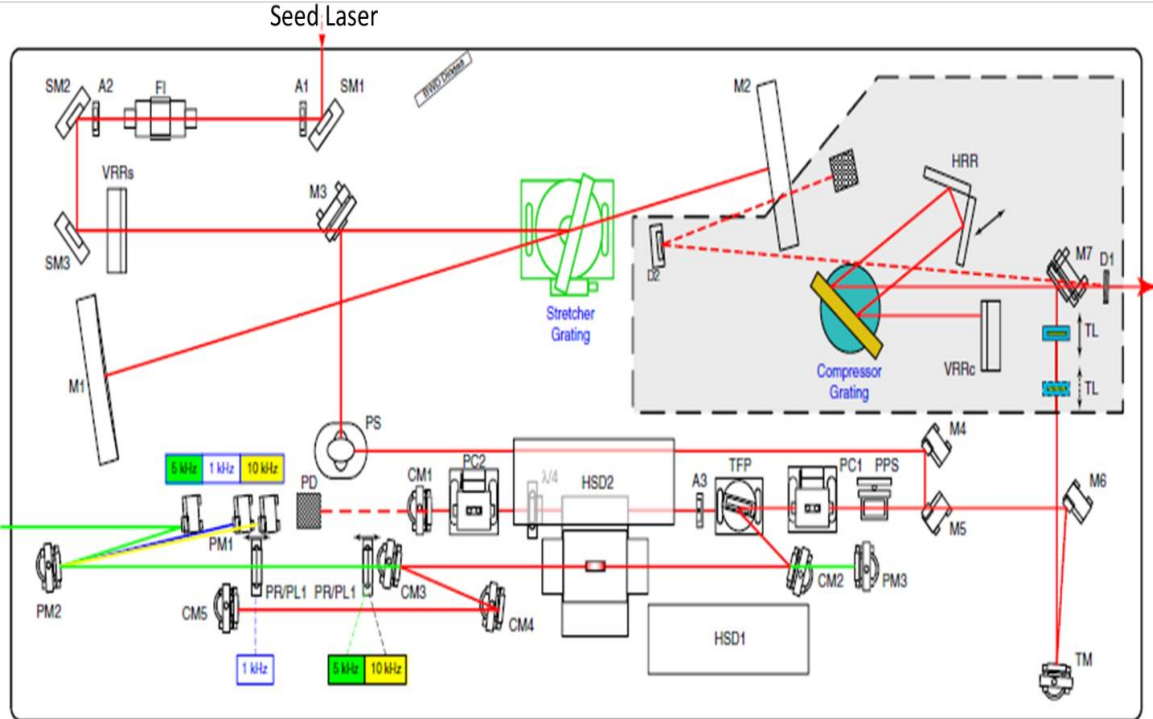


Figure 24: Spitfire Ace Regenerative amplifier optical layout. The grey part is the Compressor part.⁴⁶

6.3 Autocorrelator System

A single shot autocorrelator⁴⁷ is used to measure the duration of the ultrashort laser pulses. The experimental optical layout is shown in Figure 25. A beam splitter splits the laser pulse into two paths, and then two beams overlap in the nonlinear BBO crystal with a large incident angle. This process produces a range of time delay across the nonlinear crystal. A transverse distribution of ‘signal light’, which has twice the frequency of the input light is produced. The path delay τ between the two paths varies across the BBO crystal and is expressed as⁴⁸:

$$I_{sig}^{SHG}(t, \tau) \propto I(t)I(t - \tau) \quad (30)$$

The detector will measure the pulse intensity by the equation:

$$I(\tau) = \int_{-\infty}^{\infty} I(t)I(t - \tau)dt \quad (31)$$

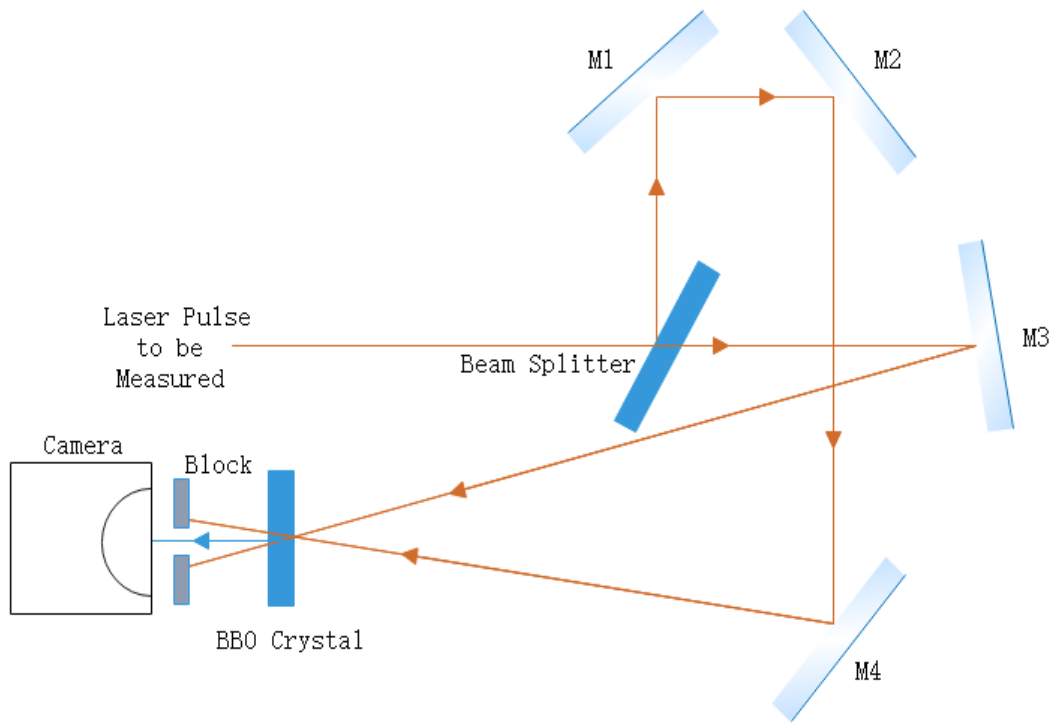


Figure 25: Optical layout of autocorrelation system.

7. Spectral Broadening by Hollow Fibre System

This chapter starts by introducing the experimental setup of the hollow fibre system, discussed in section 7.1, after that, modifications to the experimental setup are considered, to prevent damage to steering mirrors and eliminate nonlinear effects in the incident window. The control of output pulse energy by modifying polarization with a half-wave plate and reflecting from an uncoated Ge window is discussed in section 7.1.3. Then the optimization of the hollow fibre input pulse is discussed in terms of adjusting the regen compressor is discussed in section 7.3. The dispersion control by adjusting compressor setting and is also introduced. In this section, the dispersion of the hollow fibre system, and the beam path to the target chamber is simulated including chirped mirrors, in order to find the amount of fused silica to add to the beam in order to eliminate GVD, and thus achieve the incident laser pulse on target with the shortest pulse duration, limited only by high order dispersion. The potential to generate 9.76fs laser pulses at the power of 0.453W is shown in this last section.

7.1 Experiment Setup of Hollow Fibre System

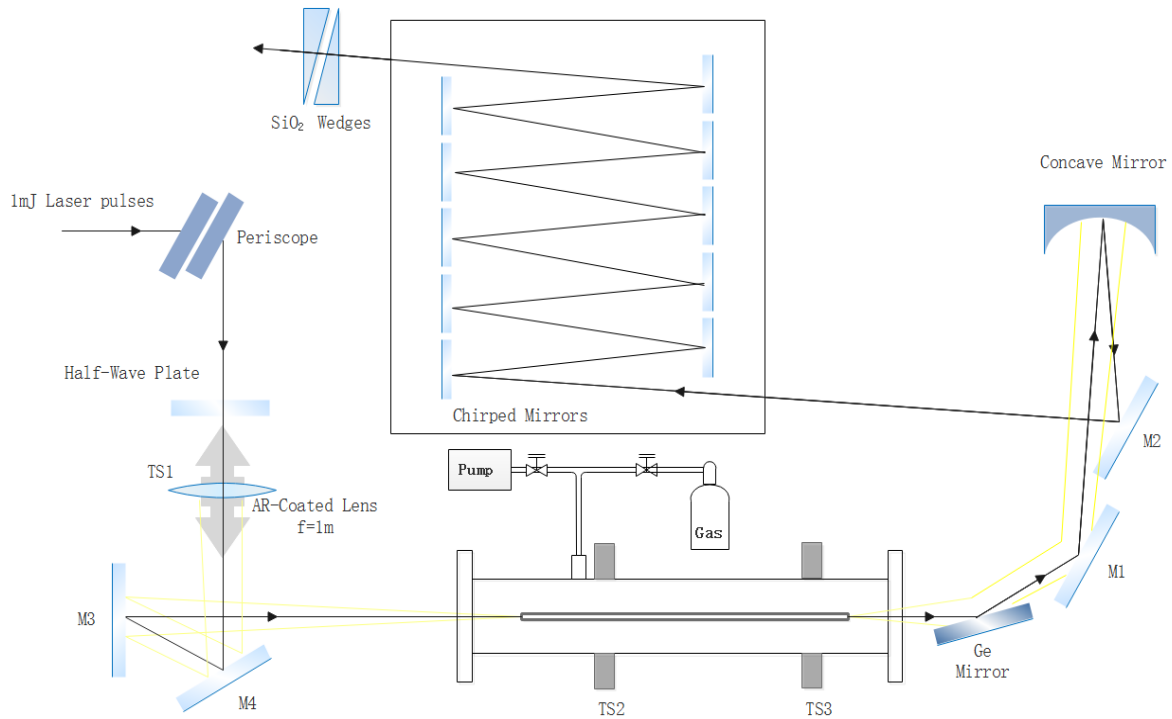


Figure 26: Layout of Hollow fibre system.

The hollow fibre system is used for achieving pulse shortening through the effect of self-phase-modulation. A FEMTOLASERS hollow silicon fibre with 1 m length and 250 μ m inner diameter is utilized in the lab to generate the short pulse. The hollow fibre, is positioned on a V-shaped aluminium base to hold it perfectly straight, and they are placed in a transparent vacuum chamber which can be filled with argon gas. The gas pressure is controlled to be between 0.35atm to 0.60atm. The Ti: sapphire laser system provides an input pulse with a minimum of 35 fs pulse duration and is limited to 1mJ of energy per pulse (the maximum recommended by the manufacturer) at 800nm. The beam is focused on the input side of the fibre using a f=1m lens. The distance from the lens to the input of the hollow fibre was carefully adjusted, by placing the lens on a rail (transit line TS1) to align the

beam efficiently into the fibre and avoid damage. The whole vacuum tube is held by two translation stages (TS2 and TS3) which can be adjusted horizontally and vertically. The alignment procedure developed to maximise the light transmission through the fibre is non-trivial and is provided in detail in 'Appendix F: Hollow fibre alignment steps'. A half-wave plate combined with a germanium plate to control the energy of the output laser pulse without changing the input energy. Low dispersion P-Ag mirrors (A1-112-P2) are used to set up this optical system. A $f=1\text{m}$ concave mirror is placed 1m away from the output end of the hollow fibre to re-collimate the diverging beam. After that, the beam is delivered to the ultra-broadband dispersive mirror compressor system (BBCOMP)⁴⁹. This system produces negative 500 fs^2 GVD, as shown in Figure 27, to counteract the positive GVD from all components from the input of the fibre to the input of the target chamber. Fused silica wedges, the thickness of which can be adjusted continuously, are set to control the superfluous GVD. The thickness of the wedge is 1mm at the thinnest part and 2mm at the fullest part; therefore, the setting for combined two wedges, shown in Figure 26, can provide positive GVD from 72.18 fs^2 to 144.36 fs^2 .

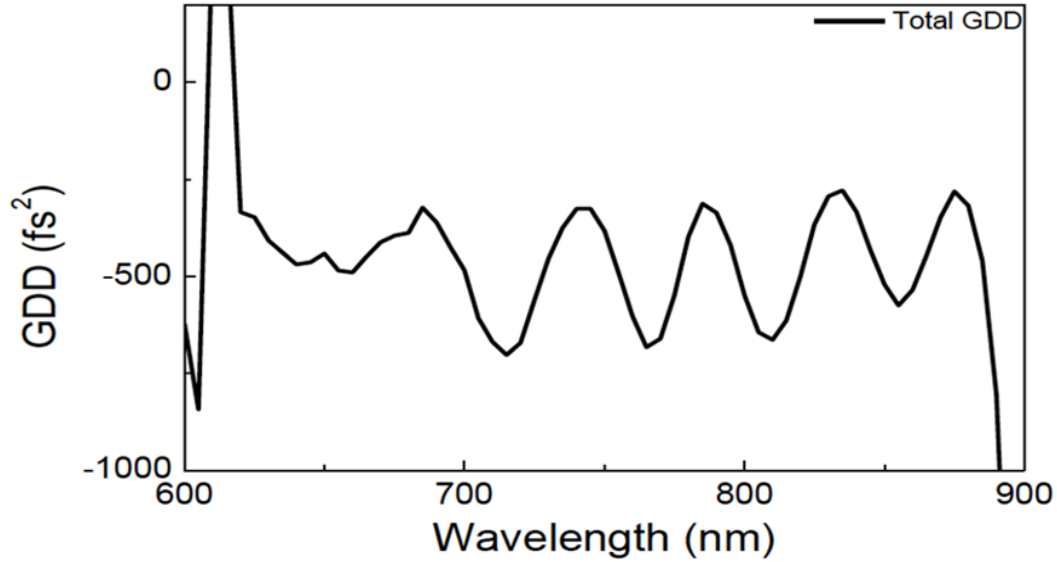


Figure 27: Plot of group delay dispersion versus wavelength for chirped mirror compressor. The system provides negative 500 GDD⁴⁹.

7.1.1 Beam Size After a Focus Lens

In this project, the laser beam is focused by a 1m focused lens and then propagate through a hollow fibre. The inner diameter of the fiber is 250 μm . To figure out the effect of the beam spot size of pulse generation. It is significant to calculate spot size of the laser beam that has been focused by a focus lens. The focused beam size should be smaller than 60% of the hollow fibre inner diameter. Equation to calculate spot diameter is

$$\text{Spot Diameter} = \frac{1.27 \times f \times \lambda}{D} \quad (32)$$

where f is the focused length, λ is the centre wavelength and D is the initial diameter of the laser beam. For the diameter of 1cm, wavelength of 800nm laser beam, focused by a 1m focused lens, the focused spot size is calculated as 101.6 μm .

7.1.2 Modification to The Incident Window

Once beam alignment was achieved into the hollow fibre, It was apparent that there was damage to the mirrors and focusing lens caused by back reflection from the silicon window at the input of the vacuum chamber, a new window mount was designed, shown in below Figure 28. This window was designed with a 45° to the table. This window was designed with a 45° angle to the table. The reason 45° was chosen is that the window was not at the Brewster angle (55.4 degrees), therefore, the rotation of the incident polarization angle would not affect the energy of the pulse incident on the fibre. This is important as the spectrum is dependent on the incident intensity, or energy and so changing the output energy can not involve changing the input energy. Instead, a half-wave plate (Newport, Part # 10RO-52-2, range 700nm-1000nm) is set in front of the tube and combined with a Germanium mirror which was set at Brewster angle (78.04°) after the hollow fibre chamber. The test results of this energy selector will be discussed in following section 7.1.2.

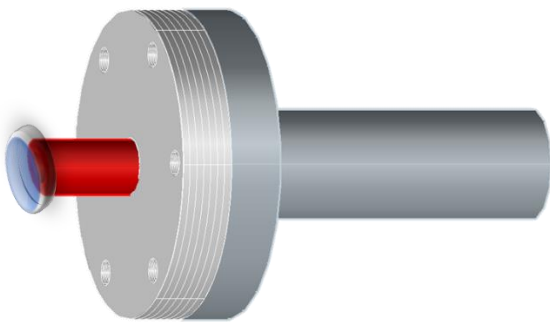


Figure 28: Design of the incident window amount.

7.1.3 Preliminary Output Results and Modification to The Position of The Hollow Fibre

Figure 29 shows the broadened spectrum that was obtained from the hollow fibre filled with 0.43atm argon gas, once the new window was installed, also shown is the shortest possible pulse length calculated using the Fourier transform. The spectrum in blue is compared to a reference spectrum from FEMTOLASERS49, shown in grey, produced using the current fibre but with a 20fs input pulse of 1mJ. Comparing the difference between the two spectra, the observation is that the blue spectrum has a broad spread (greater than 200nm FWAB) but with highly modulated features not present in the reference spectrum. The likely cause of the modulations is nonlinear processes present outside of the fibre with the most likely culprit the input window. The presence of an unwanted nonlinear phase shift can confirm this by calculating the B-integral.

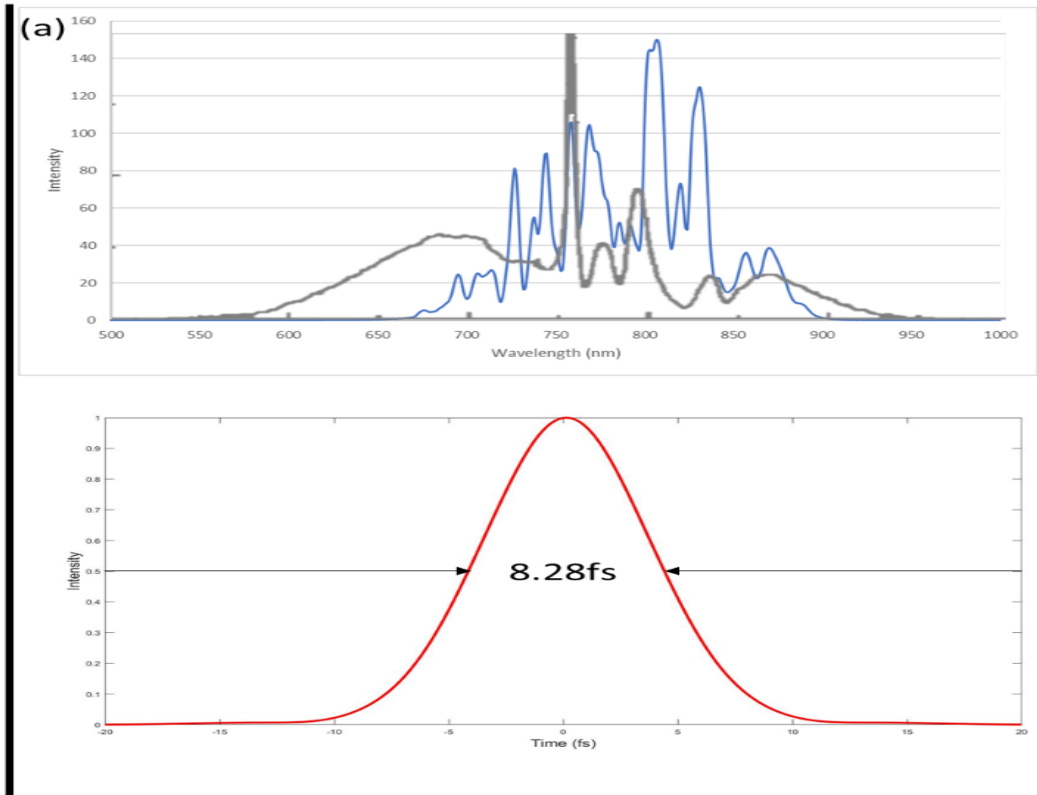


Figure 29 : Spectrum derived from a gas pressure $p=0.4\text{atm}$ and the calculated transform limited pulse duration 8.28fs. The light grey spectrum is the ideal spectral broadening test result provided by the manufacturer: FEMTOLASERS⁴⁹.

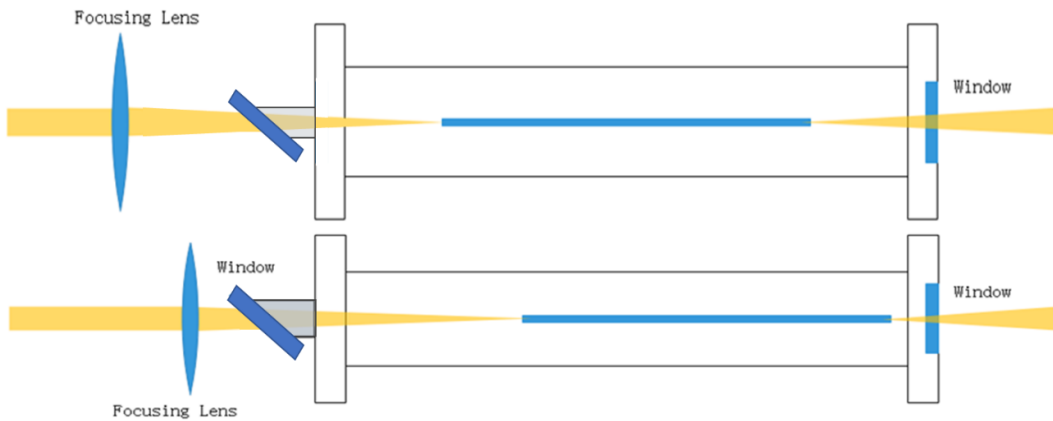


Figure 30: Configuration of the incident window and the comparison between old experimental setting and the new setting.

The equation for calculating the B-integral when the laser propagates through on an optical element of thickness t can be expressed as:

$$\varphi_{NL} = \frac{Pn_2t}{0.06w^2\lambda_0} \quad (33)$$

where $\lambda_0 = 800nm$ is the centre wavelength of laser. t is the thickness of the optical elements. w is the beam diameter when the laser propagate through the window. The nonlinear index of refraction n_2 of SiO_2 material is $3.0 \times 10^{-20}m^2/W$. P is the peak power expressed by equation

$$P = \frac{P_{ave}}{f\tau_p} \quad (34)$$

P_{ave} is the average pulse power measured as 1W, f equals 1kHz is the laser frequency. τ_p is pulse width of 35fs FWHM.

B-integral calculations for all optical transmission elements are shown below in table 6:

Optical Component	Thickness (mm)	Beam Diameter (mm)	Pulse Width (fs)	Power Average (mW)	Peak power (W)	B-Integral
Half-Wave Plate	1.00	10.00	35	1000	2.86E+10	0.02
Focus Lens	3.00	10.00	35	1000	2.86E+10	0.05
Input Window	1.00	6.00	35	1000	2.86E+10	0.05
Output Window	1.00	2.50	35	510	1.46E+10	0.15
Input Window (before)	1.00	3.00	35	1000	2.86E+10	0.20
Output Window (before)	1.00	3.50	35	510	1.46E+10	0.07

Table 6: Peak power and B-integral calculation of components in the hollow fibre system.

The group delay due to the nonlinear phase shift can be expressed as⁵⁰ :

$$\tau = \frac{d\phi}{d\omega} = \frac{B}{\Delta\omega} \quad (35)$$

where B is the B-integral value, and $\Delta\omega$ is the frequency at full width of half maximum. $\Delta\omega$ is much larger after the fibre induced spectra broadening, therefore; the output window effect may be much smaller as the pulse spectrum is wide and the pulse is at that point uncompressed. For the previous setting, as discussed in section 7.1.1, the distance from the input window to the fibre was short so that the beam size on the window was approximately 3mm giving the moderate value of B (0.2) but substantially higher than in any other element. In response to this the decision was made to move the front of the fibre further from the window giving an input diameter of 6mm. Table 6 shows that the B-integral value of the new designed input window is much smaller (0.05) than the old design.

7.1.4 Germanium Plate Calibration

Figure 31 , that, if a light is incident at the Brewster angle, the reflected beam will only contain s-polarized light, which means the polarization of the reflected beam is perpendicular to the plane of the incident. The formula to calculate the Brewster angle is

$$n = \tan(i) \quad (36)$$

n is the refractive index of the material, and i is the Brewster angle.

The refractive index of germanium plate⁵¹ at 800nm laser is 4.7096 so that Brewster's angle is calculated as 78.04°.

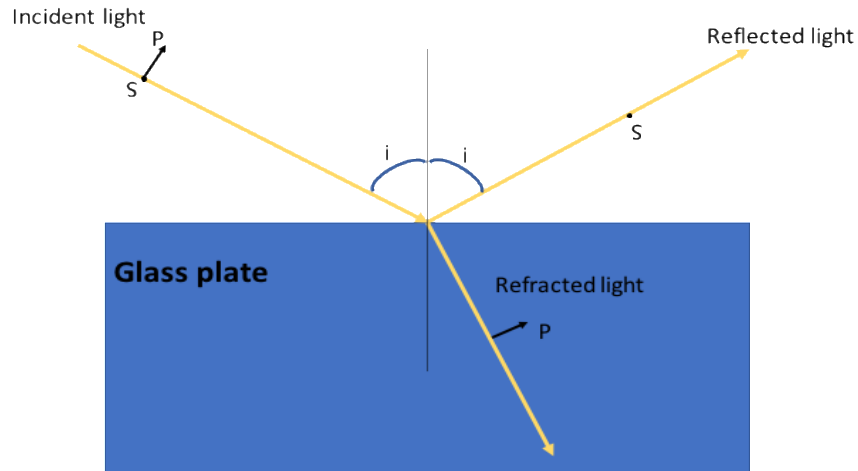


Figure 31 : Incident light propagates on a glass plate at Brewster's angle. The reflected light only has s-polarized wave and refracted light only has the p-polarized wave.

A 5mm thick, uncoated Ge window is used to in combination with a half-wave plate to control the output power and polarization of the short pulse beam. The transmission versus wavelength of the Ge window is reprinted from its manufacturer:

Throlabs' website.

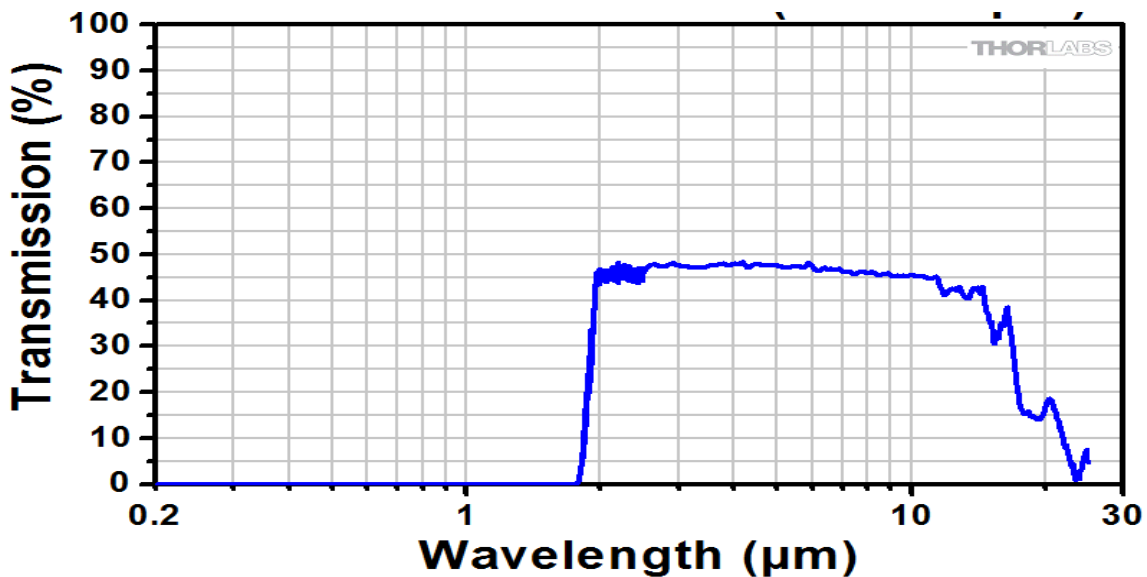


Figure 32 : Germanium window transmission versus wavelength. Transmission is zero if the wavelength below 1000nm.⁵²

The wavelength range of the beam output from the hollow fibre is 400nm to 1000um. From the above figure 32, it is evident that the percent transmission is nearly

zero at that range. Therefore, there is zero transmission loss on s-polarized beam. Ge plate is set at Brewster's angle and only allows the vertically polarized beam to be reflected. A half-wave plate is placed before the hollow fibre tube window. The beam output from the amplifier is horizontally polarized, it is then delivered to a polarization changing periscope to change the height after which it is vertically polarized. By rotating the half-wave plate the polarization of the laser beam is controlled keeping the incident energy on the fibre constant. After the fibre the germanium plate will only reflect vertically polarized light. When the output power approaches the maximum value, it means the Ge plate reflects all vertically polarized beam. However, the polarization direction should not affect the spectrum and the consequent pulse duration. To test out this setup, a power meter is set after the Ge plate to measure the laser power.

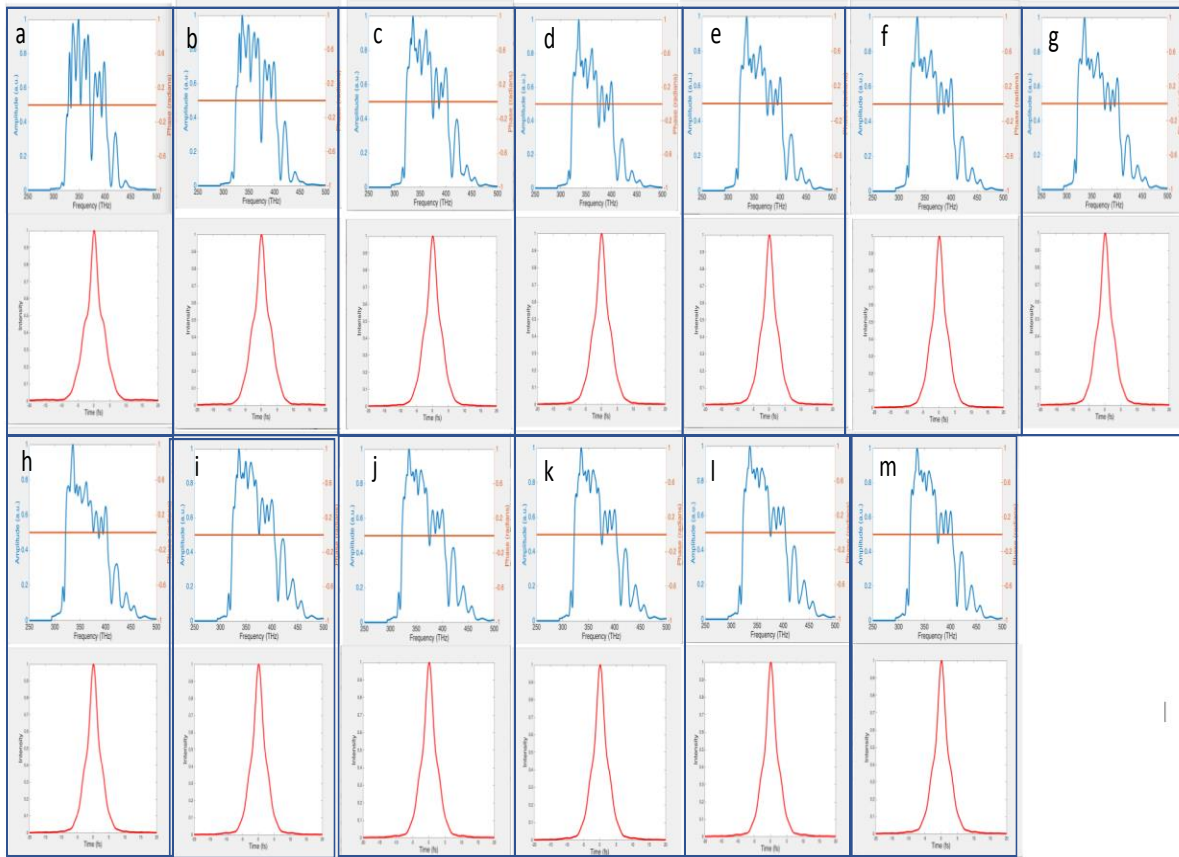


Figure 33: Spectrum and transform limited pulse durations recorded after the hollow fibre filled with argon at a pressure of $p=0.43$ atm and the input laser power of 1W, and output power after the Ge plate from (a) to (m) varied from 20mW to 280mW in steps of 20mW.

Above figure 33 shows the broadened output spectrum, with the red curves showing the calculated transform limited pulse duration. Input power is 1W, and output power is controlled by changing the polarization of the laser beam in steps of 20mW from 20mW at a to 280mW at m. It is observed that the spectral shapes and pulse shapes hardly change from the figure (a) to figure (m). This result proves that the modification of the polarization of the laser beam into the fibre system will not influence the intensity incident on the fibre and so the generated spectrum and or pulse duration. The setup is therefore an efficient method to control the power of the short pulse beam.

7.2 Beam Polarization Control

In the ultrashort pulse application, such as Coulomb Imagine, it is essential to control the direction of polarization entering the experimental chamber. As mentioned above, after the laser beam passes the germanium plate, the beam is vertically polarized. Another half-wave plate (Spectra Optics, range 600nm-900nm), was therefore, set after the wedges to change the beam polarization to be horizontally polarized if that is desired.

7.3 Dispersion Estimation

During the few-cycle pulse generation experiment, it is important to know the input pulse duration to the hollow fibre; therefore, running the autocorrelation system at the same time as the hollow fibre system is desirable. The autocorrelation system setup is discussed in the above chapter. It is expected that the dispersion from the amplifier to hollow fibre can be compensated by adjusting the setting of the value of the compressor. Therefore, it is crucial to obtain the dispersion from the output of the regenerative amplifier to the autocorrelator that we might know when the pulse is shortest at the fibre as this will not be when it is shortest on the AC, due to different accumulated GVD over that path length. The accumulated dispersion of AC system and hollow fibre system are calculated in section 7.3.1.

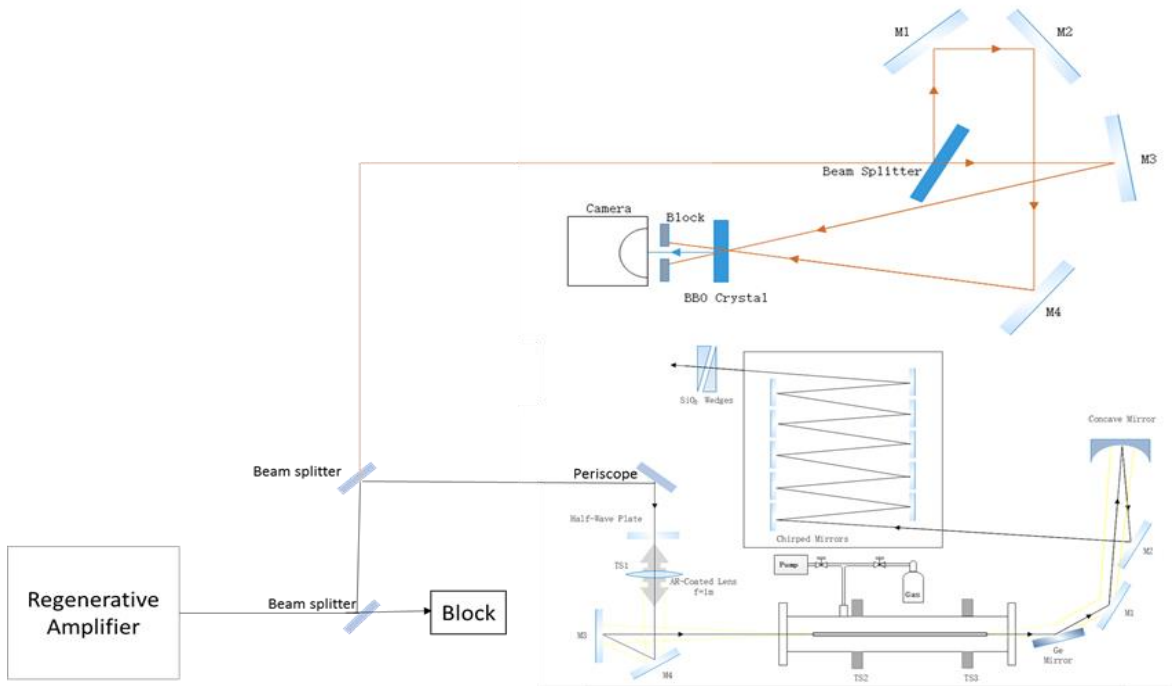


Figure 34: Optical layout of autocorrelation and hollow fibre system.

The control computer can adjust the compressor setting of Spectra-Physics Spitfire Ace amplifier primarily to compensate for differences in the number of round trips in the regenerative amplifier. The compressor inside the amplifier provides negative GVD and thus it is also possible to pre-compensate for the positive GVD created by other optical components after the laser as well as the GVD introduced by the stretcher. Autocorrelation is used to measure the pulse duration and thus to calibrate the GVD setting of the compressor. When the autocorrelation shows the shortest pulse length, it is said that the total GVD has been adjusted to be zero from the output of the amplifier to the AC.

7.3.1 Calculation of Accumulated Total Group Delay Dispersion

The dependence of the time delay of the composite signal suffered at each component of the frequency, on wavelength within the pulse is called group delay

dispersion (GDD). The general formula has been discussed in section 3.1. A MatLab program 'GDD sum' is written to calculate the sum of all group delay dispersion versus wavelength. Below figures show GDD versus wavelength over the range of 0nm to 1500nm. To calculate the dispersion from the amplifier to the input of the hollow fibre, shown in Figure 35, components include a 5mm focus lens and a thickness of 0.7mm input window. Laser beam path length starts from the amplifier to the output of the vacuum tube, passing through 2472.2mm, 1.0atm of air. Figure 36 includes extra dispersion from a thickness of 1mm output window and beam passing 1828.8mm, 0.4atm of argon gas.

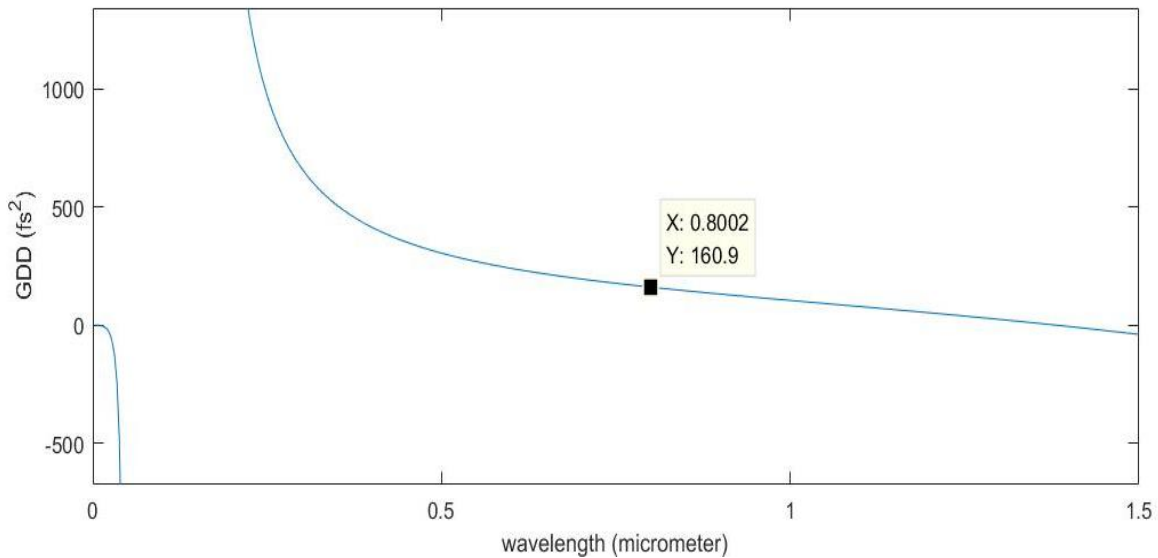


Figure 35: Group delay dispersion from the amplifier to the input of the hollow fibre versus wavelength. The dispersion at 800nm is 160.9 fs².

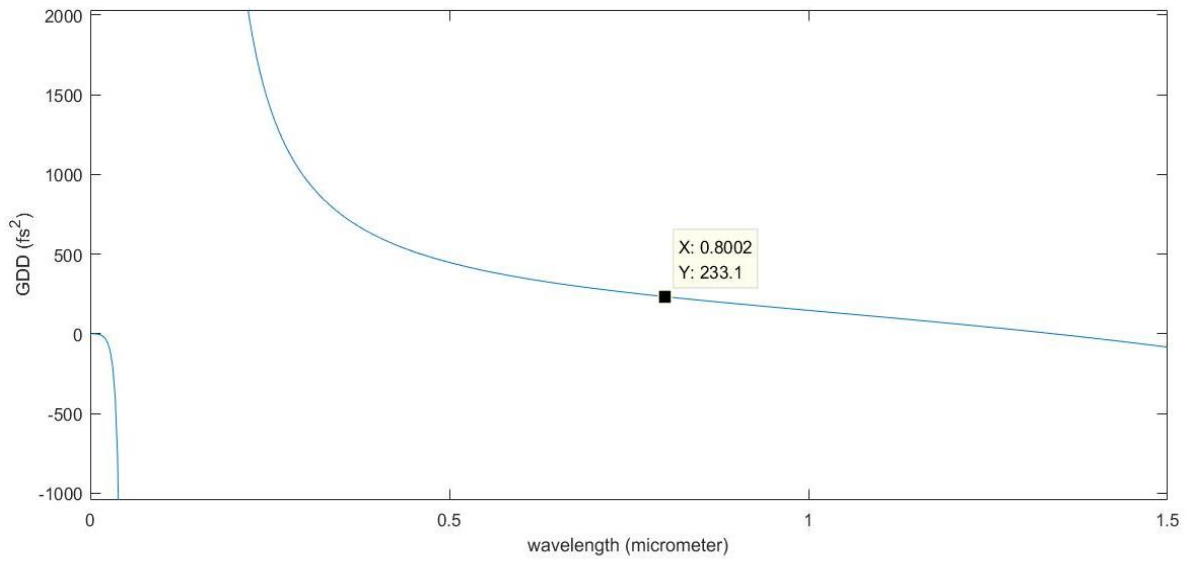


Figure 36: Group delay dispersion from the amplifier to the last window of the hollow fibre chamber versus wavelength. The dispersion at 800nm is 233.1 fs².

Figure 37 shows GDD versus wavelength at the range of 0nm to 1500nm.

The components include two of 1mm 50/50 beam splitters and a 0.25mm round continuously filter. Laser beam path length is calculated as 3855 mm.

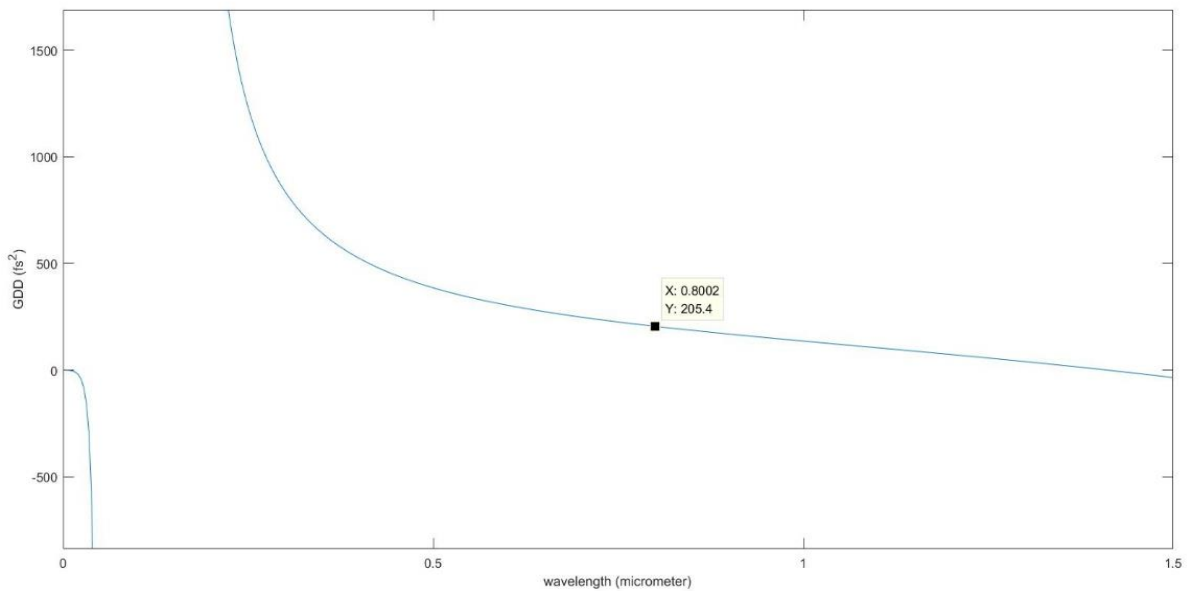


Figure 37: Group delay dispersion from the amplifier to autocorrelation BBO crystal versus wavelength. The dispersion at 800nm is 205.4 fs².

Below table 7 shows the accumulated GVD, TOD and FOD for autocorrelation system and each stage of the hollow fibre system. The net dispersions of autocorrelation system are zero, which means compressor provide -205.52 fs^2 of GVD, -132.25 fs^3 of TOD and 35.09 fs^4 of FOD for the laser beam out of the regenerative amplifier. Autocorrelation measures the pulse duration as the shortest value, 35fs, it is said that the total GVD has been adjusted to be zero from the output of the amplifier to the AC, the compressor setting value is around 6865. However, it does not mean the input laser pulse has the duration of 35fs because the dispersion from the out put of the amplifier to the input of the fibre is not same as the dispersion from the output of the amplifier to the AC. When the compressor set to 7300, the GVD was compensated to 0 from amplifier to the input window of the hollow fibre chamber and gave the shortest pulse to the hollow fibre.

Optical system	Accumulated GVD	Accumulated TOD	Accumulated FOD	Net GVD
Autocorrelation	205.52	132.25	-35.09	0.00
Regen. to Input Hollow Fibre	160.99	106.77	-31.47	-44.53
Regen. to Output Hollow Fibre	233.21	161.65	-54.35	27.69

Table 7: Accumulated dispersion for autocorrelation and hollow fibre system and calibrated GVD for the hollow and chirped mirror compressor system.

7.4 Impacts of Compressor setting on Generating Short Pulse

It is interesting to see how compressor setting influence the spectrum when the chamber filled with argon gas.

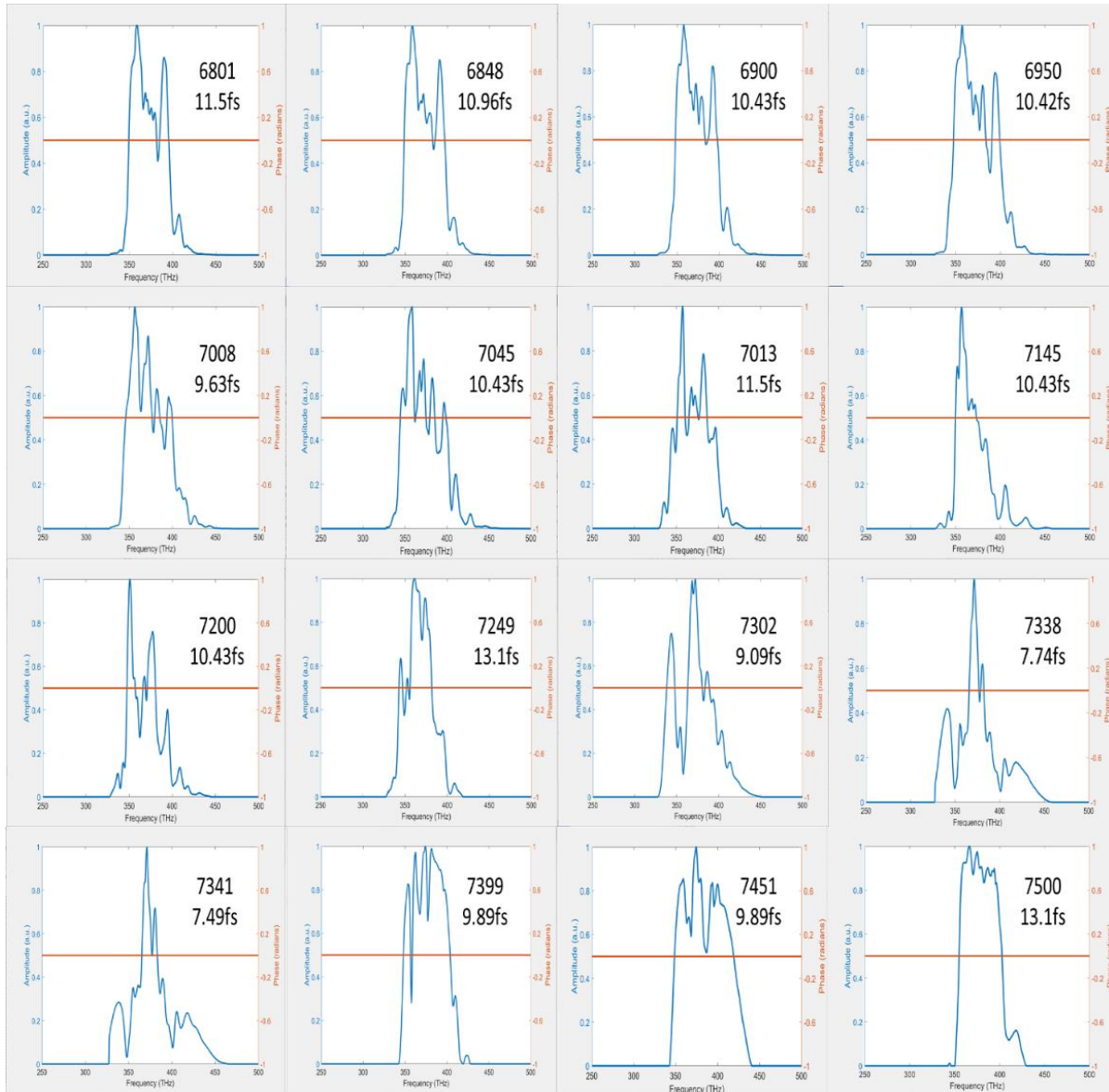


Figure 38: *Compaction of spectrum in different compressor setting and transform limited pulse duration.*

Figure 38 shows the spectra that were obtained for various compressor settings with the argon gas filled in the chamber. These spectra were recorded after the lens-hollow fibre position modification, and the hollow fibre chamber was filled with 0.43atm argon gas. It is observed that the width of the spectra widens and consequently, the duration of the transform limited pulse becomes shorter with increasing compressor setting value up to 7341. We deduce that this corresponds to

the compressor setting which reduces the GVD from the amplifier to the input of the hollow fibre to 0.

7.5 Experiment Result and Discussion

7.5.1 Impacts of Pressure on Generating Short Pulse

The hollow fibre system is filled with noble gas in order to generate few-cycle laser pulses through sepph phase modulation. Many research groups have published papers in which they generate short pulses by using different gas in a hollow fibre system. Eiichi et al. obtained a duration of 2.6fs by using a length of 37cm, an inner diameter of 140 μ m hollow fibre filled with 3.0atm argon gas⁵³. Robinson and group members generated a pulse with duration of 6.5fs in a neon-filled hollow fibre an argon gas pressure of 2.5 atm**Error! Bookmark not defined..** Nisoli et al. (1997) used krypton and argon gases to fill in hollow fibre to a pressure of 2atm to 3atm to generate pulse durations of 5.3fs and 4.5fs pulses³⁹. Nurhuda and Suda (2007) compared their spectra obtained at gas pressures from 1atm to 0.4atm ⁵⁴. In the Waterloo lab, the hollow fibre chamber was filled with argon gas, and the spectra that were obtained for different gas pressures are shown in Figure 39. The background has been reduced from the spectrum, the method shown in Appendix E.

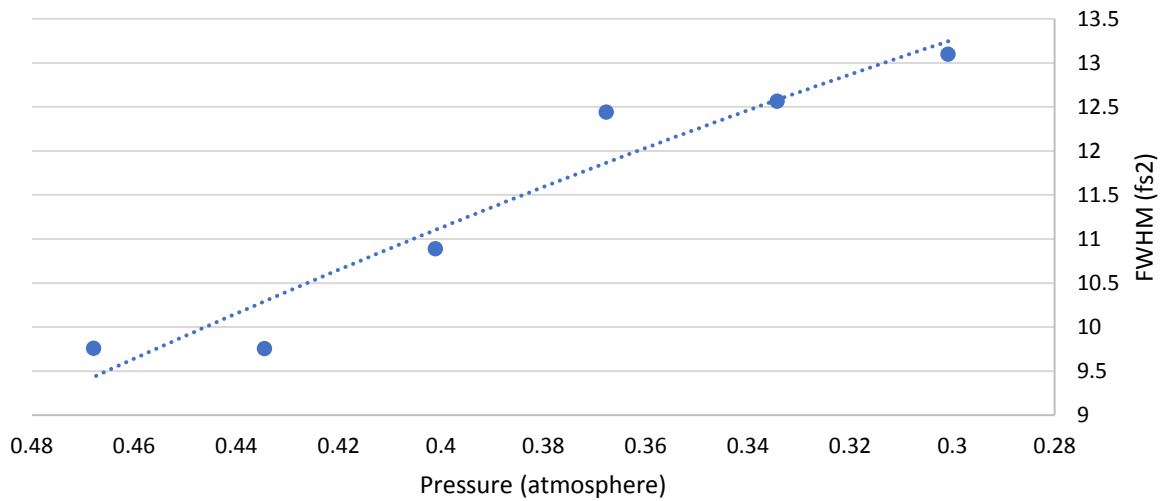
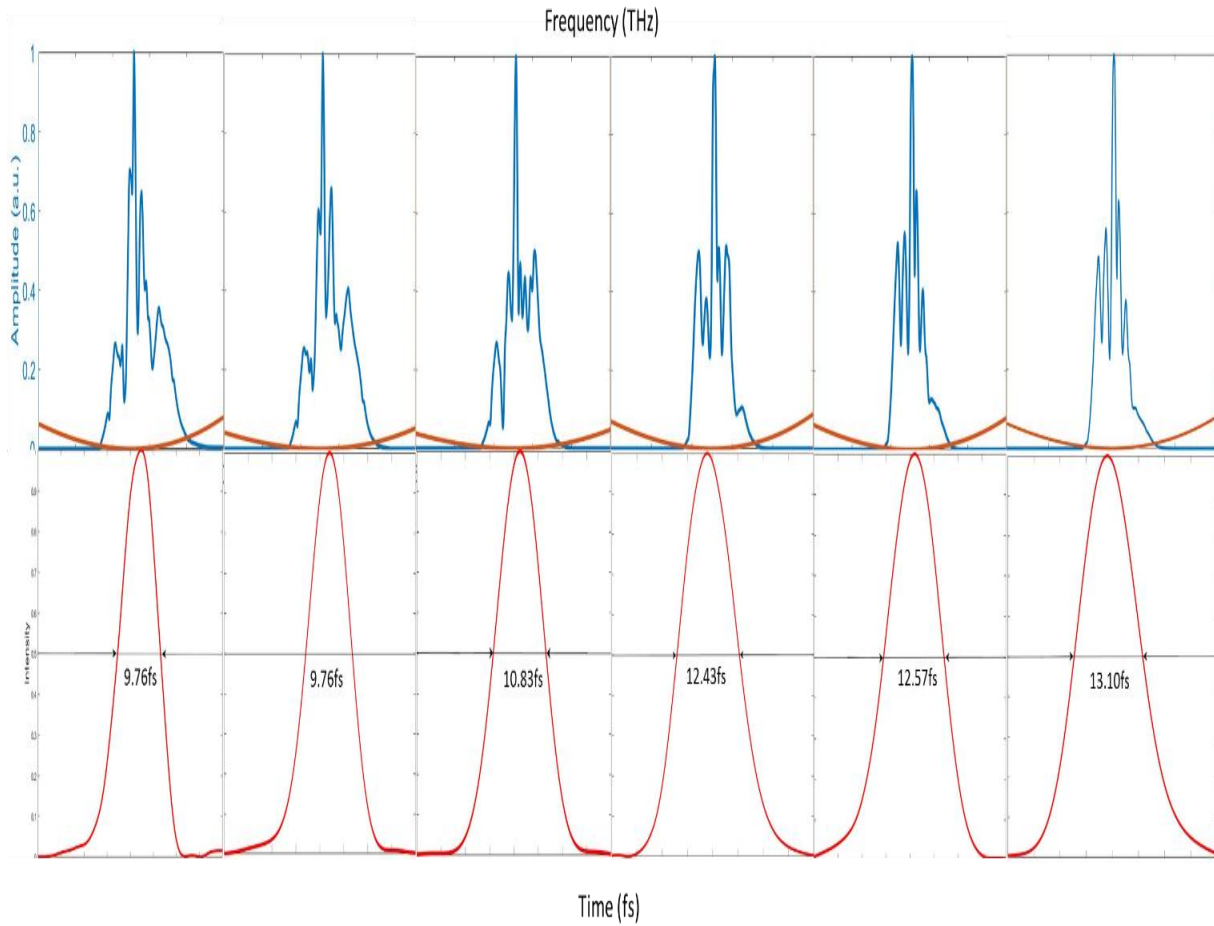


Figure 39 : Spectra and transform limited pulse obtained by varying the gas pressure from a): 0.468atm, b) 0.434atm, c) 0.401atm, d) 0.368atm, e)0.334atm, f) 0.301atm . The frequency range for each plot is from 250THz to 500THz. Below shows the transform limited pulse duration versus gas pressure. There is a trend (dotted line) of increasing pulse duration as decreasing gas pressure.

Figure 39 shows the broadened output spectrum, with the red curves showing the calculated transform limited pulse duration. From left to right the pulses duration that was measured at FWHM are separately 9.760 fs, 9.759 fs, 10.829 fs, 12.433 fs, 12.566 fs and 13.102 fs, and the gas pressure are separately 0.468atm, 0.434atm, 0.401atm, 0.368atm, 0.334atm, 0.301 atm. Based on these values, a plot of the relationship between pulse duration and gas pressure is presented in above figure. The different simulation of dispersion was added in pulse calculation, shown in table 8.

Pressure (atmosphere)	GVD (fs ²)	TOD(fs ³)	FOD(fs ⁴)
0.301	10.435	4.753	0.425
0.334	11.595	5.281	0.472
0.368	12.754	5.810	0.519
0.401	13.913	6.338	0.566
0.434	15.073	6.866	0.613
0.468	16.232	7.394	0.661

Table 8 : Dispersion calculation for argon gas at different pressure.

It is observed that the increasing gas pressure results in the decreasing pulse duration. An interesting observation can be found from the figure is that each spectrum broadens as ridges and peak, the highest peak in the spectrum tends to rise at a higher frequency as more decrease gas pressure. It is complicated to explain the reason; one possible conjecture is because the self-phase modulation occurred less when pressure is low. Also, the range of the wavelength starts to expand and swell at both edge sides as the increasing gas pressure. The little spike at the edge side will dilate to high intensity and finally merge with the forward peak. These results agree with the Nurhuda's (2007) observation⁵⁴; they also obtained the similar change tendency of spectrum broaden as increasing gas pressure. It is also worth to mention

that at the more significant pressure, the mode would form a higher order instant of the fundamental mode. It is because the nonlinear effect might occur if the gas pressure was high. The gas pressure should be control around 0.43 atm, at that time, both mode shape and the most simulation spectrum broadens would satisfied.

7.5.2 Generation of the Shortest Laser Pulse

The spectrum in Figure 40 was obtained when the argon gas pressure was 0.43atm, and the mode was observed as fundamental mode. Input laser power was 1.00W, and output power was 0.453W. It is observed from the Figure 40 that the duration of input pulse $\tau_0=35\text{fs}$, and calculated chirped pulse duration τ at FWHM is 7.49fs. The self-phase modulation and dispersion would both occur when the laser propagates through the hollow fibre. Discussion of the evaluation of self-phase modulation and gas dispersion as showed as follow. Govind proposed a method in 1995, is to evaluate the influence of those nonlinear effects⁵⁵. The nonlinear length L_{NL} assesses the impact of self-phase modulation, expressed as

$$L_{NL} = \frac{1}{\gamma P_0} \quad (37)$$

where P_0 is the input peak power and γ is the nonlinear coefficient, defined as

$$\gamma = \frac{n_2 \omega_0}{c A_{eff}} \quad (38)$$

$n_2 = 19.6 \times 10^{-23} \text{ s}^2/\text{m}/\text{atm}$ is the nonlinear refractive index of argon gas and the gas pressure is 0.43 atm, $\omega_0 = 1\text{kHz}$ is the laser central frequency, $c= 3 \times 10^8 \text{ m/s}$ is the speed of light and A_{eff} is the effective mode area, which is also the focus size of the 1 m focus lens, the diameter $d=1\text{mm}$ of the effective mode area is calculated by using equation (4). This area is less than the inner diameter of the hollow fibre.

The dispersion length L_D evaluates the impact of dispersion, expressed as

$$L_D = \frac{\tau_0^2}{|\beta_2|} \quad (39)$$

$\tau_0 = 35\text{fs}$ is the initial pulse duration and β_2 is the group delay dispersion in the hollow fibre.

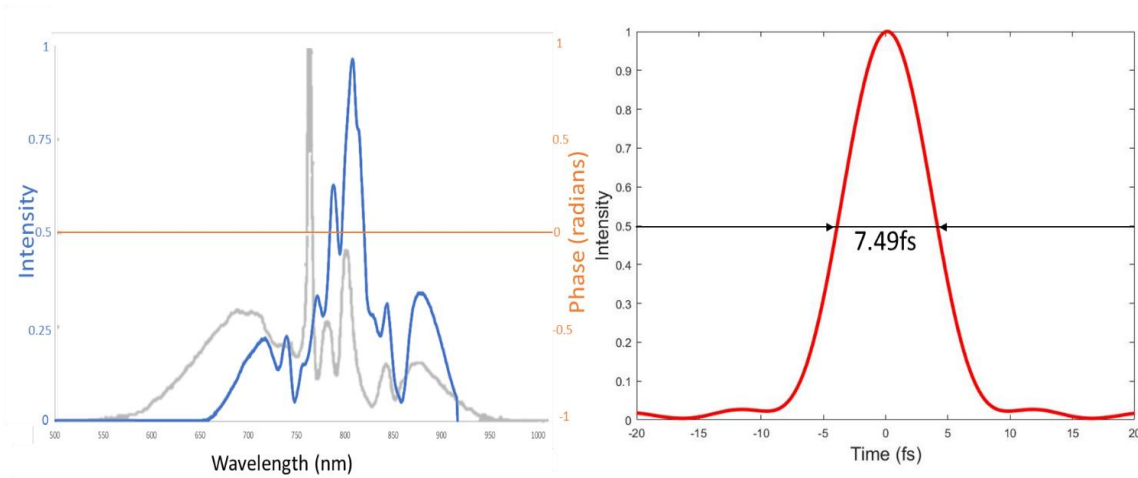


Figure 40: Spectrum and transform limited pulse durations. The input pulse duration is $\tau_0=35\text{fs}$. Chirped pulse duration τ at FWHM is 7.49 fs. The argon gas pressure $p=0.43\text{atm}$, and the mode was observed as fundamental mode. Input laser power was 1.00W, and output power was 0.453W. The light grey is the ideal spectral broadening test results by the ultra broad band dispersion compensating mirror set (BBCOMP) manufacturer: FEMTOLASERS⁴⁹.

The nonlinear length is calculated as $L_{NL}=0.002\text{m}$ and the dispersion length

$L_D= 47.44\text{m}$. The optimization of the length of the hollow fibre is expressed by

Tomlinson et al. (1984)⁵⁶ :

$$L_{opt} \approx \sqrt{6L_{NL}L_D} \quad (40)$$

For the above spectrum, the most appropriate thermal length of the hollow fibre is calculated as $L_{opt}=0.89\text{m}$. Compared with the 1 m length of hollow fibre used in the lab, the simulated length is similar but a little shorter than the real fibre.

This result indicates that the gas dispersion also plays a significant role in spectral broadening. The peak power would decrease as it propagates through the hollow fibre, this would result in the increase of the nonlinear length and, thus, the real optimized fiber

length could be longer. Nisoli et al. (1997) showed the slimier result and, they also did the calculation for the 140fs input pulse at peak power equals 3.5GW and the gas pressure at 4 bar³⁹. The result showed a much longer simulated fibre length at the longer duration of input laser pulse. A discussion is that when the resource pulse is short, the entry laser already has a wide range of the wavelength, it gives a more flexible range for spectral broaden when laser propagates through a hollow fibre, and the gas dispersion has a greater influence of shorter input laser pulse. The group delay dispersion and the higher order dispersion (TOD, FOD) from the amplifier to the input fibre were compensated to zero by the compressor. The group delay dispersion of the hollow fibre to the target chamber is compensated by chirped mirror sets and wedges. Table 9 shows the dispersion of optical components and gases from the hollow fibre tube to the target chamber. The total thickness of 5mm wedges can help to compensate the exceeding GDD to zero. However, there were still higher order dispersions TOF=255.26 and FOD=-42.74 that would affect the shape of the laser pulses.

Components	GVD (fs ² /mm)	TOD (fs ³ /mm)	FOD (fs ⁴ /mm)	Thickness (mm)	Numbers	GDD (fs ²)	Net TOD (fs ³)	Net FOD (fs ⁴)
Hollow Fibre Window	36.11	27.44	-11.44	1.00	4.00	144.44	109.76	-45.76
Half-Wave Plate	19.75	13.71	-5.03	1.00	1.00	19.75	13.71	-5.03
Air	0.02	0.01	0.00	6454.60	1.00	137.48	63.84	7.44
Argon	0.02	0.09	0.00	1828.80	0.43	14.92	67.95	0.61
Chirped Mirror	-500.00			1.00	1.00	-500.00		
Sum of the Dispersion						-183.41	255.26	-42.74

Table 9: Dispersion calculation from the hollow fibre chamber to the target chamber. The optical components include a 1mm hollow fibre output window, a 3mm window of the target chamber and a 1mm half-wave plate. The path length from the output window of the hollow fibre tube to the target chamber is 6454.60mm. The length of the argon filled hollow fibre tube is 1828.8mm. Chirped mirror system provides GDD of -500.

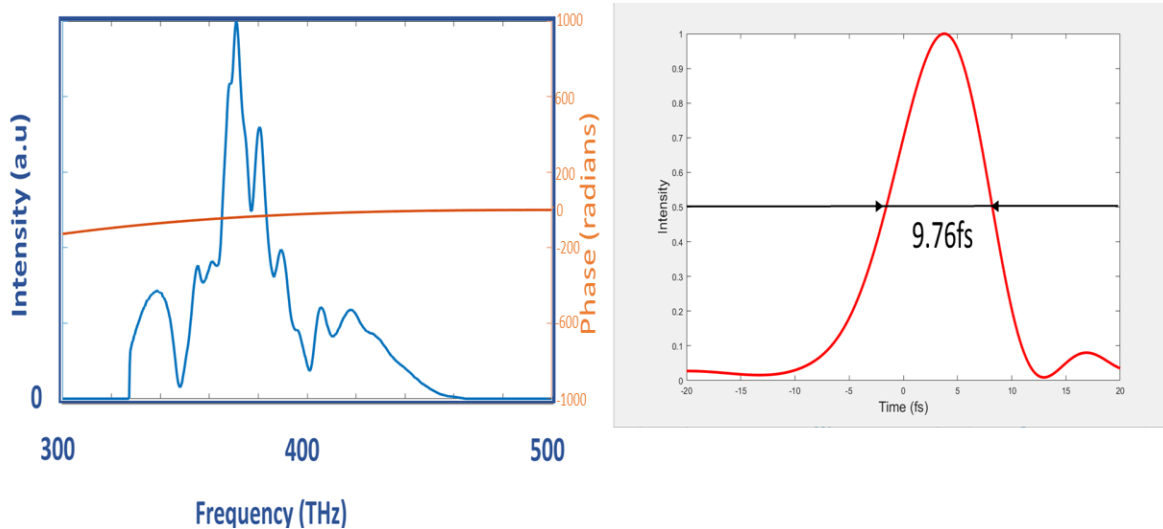


Figure 41: Original spectrum and pulse duration by taking spectrum into inverse Fourier Transform. Higher order dispersions $TOD=255.26\text{fs}^3$ and $FOD=-42.74\text{fs}^4$ were added to the PulseSim.m program to simulate the phase effect. The input pulse duration is $\tau_0=35\text{fs}$. Chirped pulse duration τ at FWHM is 9.76fs . The argon gas pressure $p=0.43\text{atm}$, and the mode was observed as fundamental mode. Input laser power was 1.00W , and output power was 0.453W .

The accumulated third order dispersion $TOD=255.26\text{fs}^3$ and the fourth order dispersion $FOD=-42.74\text{fs}^4$ were added to the phase and the pulse duration as shown in Figure 41. The duration of the pulse was affected and increased to 9.76fs . There is no method for now to compensate the third order dispersion and the fourth order dispersion. However, the influence of the higher order dispersions will not cause a severe effect on the pulse shape nor length by comparing with the pulse length $\tau=7.49\text{fs}$ in Figure 40.

8. Conclusion

The few-cycle laser pulses have much application due to the short time duration. Researchers have used the few-cycle pulses to study the molecules dynamic Coulomb explosion imaging^{57,58,59,60}. In the Waterloo lab, the few-cycle pulses that obtained from the hollow fibre system are expected to be used for the Coulomb explosion imaging experiment. Scientists are looking forward to recording the imaging when molecules are near to the equilibrium by using the short laser pulses. Figure 42 displays the (2,2,2) channel ($\text{CO}_2 \rightarrow \text{CO}_2^{6+} \rightarrow \text{C}^{2+} + \text{O}^{2+} + \text{C}^{2+}$) of carbon dioxide gas CO_2 energy released as a percentage of that expected from Coulomb explosion at the equilibrium geometry ($R_{\text{C-O}}=1.16\text{\AA}$) as a function of the final charge states⁶¹. The bond length will further stretched if the pulse length is longer. Figure 42 shows the CO_2 molecules near to the equilibrium state when irradiated with the 7fs laser pulses, where CO bond length $R_{\text{C-O}}=1.29\text{\AA}$ and percent of the Coulombic energy is nearly 90%.

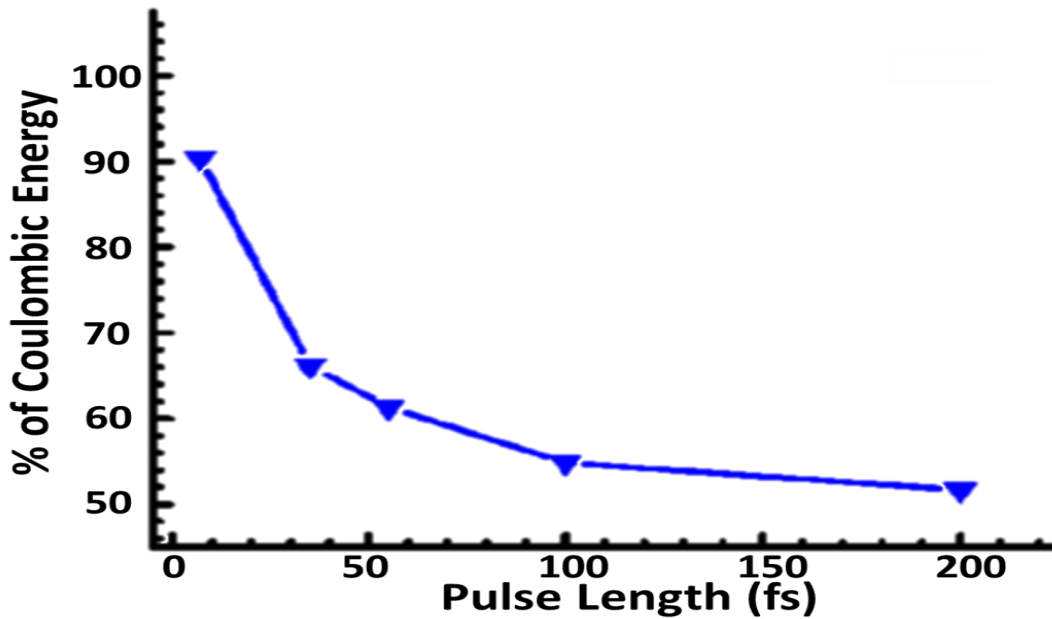


Figure 42 : (2,2,2) Channel of CO_2 energy released as a percentage of that expected from Coulomb explosion at the equilibrium geometry as a function of the final charge states. (Reprinted with permission from [61])

As discussed previously, the linear and nonlinear effects will influence the duration of the laser pulse which is incident on the molecule inside of the Coulomb explosion chamber. By simulation and analysis of the accumulated GVD, we can only give an approximate picture of the final pulse length inside the Coulomb explosion apparatus. However, it is desirable to measure the pulse at the molecular target, and this may be achieved at least partially by comparison with the published result of double ionization of the deuterium D_2 , the Coulomb explosion fragments $\text{D}^{++} \text{D}^+$ of which will have different kinetic energy at various pulse duration^{62,63}. It is expected to obtain the kinetic energy of D^+ around 5eV so that we can say that the hollow fibre system had achieved laser pulses that duration less than 10fs.

In conclusion, the duration of 9.76fs and energy of 0.453W laser pulses were successfully generated by the hollow fibre and chirped mirror compressor system.

This system is expected to provide the source laser to the Coulomb Explosion Imaging chamber in the Waterloo lab.

Reference

- 1 Keller, U. (2003). Recent developments in compact ultrafast lasers. *Nature*, 424(6950), 831-838.
- 2 Shur, M. (2005, September). Terahertz technology: devices and applications. In *Solid-State Device Research Conference, 2005. ESSDERC 2005. Proceedings of 35th European* (pp. 13-21). IEEE.
- 3 Fermann, M. E., & Hartl, I. (2009). Ultrafast fiber laser technology. *IEEE Journal of Selected Topics in Quantum Electronics*, 15(1), 191-206.
- 4 Whitaker, B. J. (Ed.). (2003). *Imaging in Molecular Dynamics: Technology and Applications*. Cambridge university press.
- 5 Hasegawa, H., Hishikawa, A., & Yamanouchi, K. (2001). Coincidence imaging of Coulomb explosion of CS₂ in intense laser fields. *Chemical physics letters*, 349(1), 57-63.
- 6 Valdmanis, J., & Fork, R. (1986). Design considerations for a femtosecond pulse laser balancing self phase modulation, group velocity dispersion, saturable absorption, and saturable gain. *IEEE journal of quantum electronics*, 22(1), 112-118.
- 7 Fork, R. L., Cruz, C. B., Becker, P. C., & Shank, C. V. (1987). Compression of optical pulses to six femtoseconds by using cubic phase compensation. *Optics letters*, 12(7), 483-485.
- 8 Strickland, D., & Mourou, G. (1985). Compression of amplified chirped optical pulses. *Optics communications*, 55(6), 447-449.
- 9 Backus, S., Peatross, J., Huang, C. P., Murnane, M. M., & Kapteyn, H. C. (1995). Ti: sapphire amplifier producing millijoule-level, 21-fs pulses at 1 kHz. *Optics letters*, 20(19), 2000-2002.
- 10 Dancus I, Popescu ST, Petris A. Single shot interferometric method for measuring the nonlinear refractive index. 2013;21(25):31303–31308.
- 11 Petrov D. Reflection Z-scan technique for the study of nonlinear refraction and absorption of a single interface and thin film. 1996;13(7):1491–1498.
- 12 Dancus, I., Vlad, V. I., Petris, A., Gaponik, N., Lesnyak, V., & Eychmüller, A. (2010). Saturated near-resonant refractive optical nonlinearity in CdTe quantum dots. *Optics letters*, 35(7), 1079-1081.

-
- 13 Börzsönyi, Á., Heiner, Z., Kovács, A. P., Kalashnikov, M. P., & Osvay, K. (2010). Measurement of pressure dependent nonlinear refractive index of inert gases. *Optics express*, 18(25), 25847-25854.
- 14 Asobe, M., Suzuki, K. I., Kanamori, T., & Kubodera, K. I. (1992). Nonlinear refractive index measurement in chalcogenide-glass fibers by self-phase modulation. *Applied physics letters*, 60(10), 1153-1154.
- 15 Perry, M. D., Ditmire, T., & Stuart, B. C. (1994). Self-phase modulation in chirped-pulse amplification. *Optics letters*, 19(24), 2149-2151.
- 16 Chuang Y H, Zheng L, Meyerhofer D D. Propagation of light pulses in a chirped-pulse-amplification laser[J]. *IEEE Journal of quantum electronics*, 1993, 29(1): 270-280.
- 17 Perry, M. D., Ditmire, T., & Stuart, B. C. (1994). Self-phase modulation in chirped-pulse amplification. *Optics letters*, 19(24), 2149-2151.
- 18 Konoplev, O. A., & Meyerhofer, D. D. (1998). Cancellation of B-integral accumulation for CPA lasers. *IEEE Journal of selected topics in quantum electronics*, 4(2), 459-469.
- 19 Fibich, G., & Gaeta, A. L. (2000). Critical power for self-focusing in bulk media and in hollow waveguides. *Optics letters*, 25(5), 335-337.
- 20 Polynkin, P., & Kolesik, M. (2013). Critical power for self-focusing in the case of ultrashort laser pulses. *Physical Review A*, 87(5), 053829.
- 21 Marburger, J. H. (1975). Self-focusing: theory. *Progress in Quantum Electronics*, 4, 35-110.
- 22 Diels, J. C., & Rudolph, W. (2006). *Ultrashort laser pulse phenomena*. Academic press.
- 23 Chen, G. F. R., Wang, T., Donnelly, C., & Tan, D. T. H. (2013). Second and third order dispersion generation using nonlinearly chirped silicon waveguide gratings. *Optics express*, 21(24), 29223-29230.
- 24 Bhar, G. C. (1976). Refractive index interpolation in phase-matching. *Applied optics*, 15(2), 305_1-307.
- 25 Sutton, L. E., & Stavroudis, O. N. (1961). Fitting refractive index data by least squares. *JOSA*, 51(8), 901-905.
- 26 Malitson, I. H. (1965). Interspecimen comparison of the refractive index of fused silica. *Josa*, 55(10), 1205-1209.

-
- 27 Daimon, M., & Masumura, A. (2002). High-accuracy measurements of the refractive index and its temperature coefficient of calcium fluoride in a wide wavelength range from 138 to 2326 nm. *Applied optics*, 41(25), 5275-5281.
- 28 Salzberg, C. D., & Villa, J. J. (1957). Infrared refractive indexes of silicon germanium and modified selenium glass. *JOSA*, 47(3), 244-246.
- 29 Dodge, M. J. (1984). Refractive properties of magnesium fluoride. *Applied Optics*, 23(12), 1980-1985.
- 30 Peck, Edson R., and Donald J. Fisher. "Dispersion of argon." *JOSA* 54.11 (1964): 1362-1364.
- 31 Peck, Edson R., and Kaye Reeder. "Dispersion of air." *JOSA* 62.8 (1972): 958-962.
- 32 Backus, S., Durfee III, C. G., Murnane, M. M., & Kapteyn, H. C. (1998). High power ultrafast lasers. *Review of scientific instruments*, 69(3), 1207-1223.
- 33 Gholami, A., Molin, D., & Sillard, P. (2009). Compensation of chromatic dispersion by modal dispersion in MMF-and VCSEL-based gigabit ethernet transmissions. *IEEE Photonics Technology Letters*, 21(10), 645-647.
- 34 Sato, Takumi, Yuichi Kozawa, and Shunichi Sato. "Transverse-mode selective laser operation by unicursal fast-scanning pumping." *Optics letters* 40.14 (2015): 3245-3248.
- 35 Kasap, S., Ruda, H., & Boucher, Y. (2002). *An illustrated dictionary of optoelectronics and photonics: important terms and effects. Concise Second Student Edition Version*, 1(1).
- 36 Marcatili, E. A., & Schmeltzer, R. A. (1964). Hollow metallic and dielectric waveguides for long distance optical transmission and lasers. *Bell Labs Technical Journal*, 43(4), 1783-1809.
- 37 Ghatak, A., & Thyagarajan, K. (1998). *An introduction to fiber optics*. Cambridge university press.
- 38 Nisoli, M., De Silvestri, S., & Svelto, O. (1996). Generation of high energy 10 fs pulses by a new pulse compression technique. *Applied Physics Letters*, 68(20), 2793-2795.
- 39 Nisoli, M., Stagira, S., De Silvestri, S., Svelto, O., Sartania, S., Cheng, Z., ... & Krausz, F. (1997). A novel-high energy pulse compression system: generation of multigigawatt sub-5-fs pulses. *Applied Physics B: Lasers and Optics*, 65(2), 189-196.

-
- 40 Seres, E., Herzog, R., Seres, J., Kaplan, D., & Spielmann, C. (2003). Generation of intense 8 fs laser pulses. *Optics express*, 11(3), 240-247.
- 41 Robinson, J. S., Haworth, C. A., Teng, H., Smith, R. A., Marangos, J. P., & Tisch, J. W. G. (2006). The generation of intense, transform-limited laser pulses with tunable duration from 6 to 30 fs in a differentially pumped hollow fibre. *Applied Physics B: Lasers and Optics*, 85(4), 525-529.
- 42 Suda, A., Hatayama, M., Nagasaka, K., & Midorikawa, K. (2005). Generation of sub-10-fs, 5-mJ-optical pulses using a hollow fiber with a pressure gradient. *Applied Physics Letters*, 86(11), 111116.
- 43 Bohman, S., Suda, A., Kanai, T., Yamaguchi, S., & Midorikawa, K. (2010). Generation of 5.0 fs, 5.0 mJ pulses at 1 kHz using hollow-fiber pulse compression. *Optics letters*, 35(11), 1887-1889.
- 44 Saenz, A. (2004). Molecular Hydrogen in Strong Laser Fields: Bond Softening, Enhanced Ionisation, and Coherent Control. *Physica Scripta*, 2004(T110), 126.
- 45 Bucksbaum, P. H., Zavriyev, A., Muller, H. G., & Schumacher, D. W. (1990). Softening of the H₂⁺ molecular bond in intense laser fields. *Physical review letters*, 64(16), 1883.
- 46 User's manual for Ti:Sapphire Regenerative Amplifier Systems, Spectra-Physics, Mountain View, CA, 2014.
- 47 Salin, F., Georges, P., Roger, G., & Brun, A. (1987). Single-shot measurement of a 52-fs pulse. *Applied optics*, 26(21), 4528-4531.
- 48 Prasad, P. N., & Williams, D. J. (1991). Introduction to nonlinear optical effects in molecules and polymers (Vol. 1). New York etc.: Wiley.
- 49 User's manual for Ultra Broadband Dispersive Mirror Compressor, FEMTO LASERS, FEMTO LASERS Produktions GmbH, S.N. BBCOMP 081/2005.
- 50 Boyd, R. W. (2003). *Nonlinear optics*. Academic press.
- 51 Aspnes, D. E., & Studna, A. A. (1983). Dielectric functions and optical parameters of si, ge, gap, gaas, gasb, inp, inas, and insb from 1.5 to 6.0 ev. *Physical review B*, 27(2), 985.
- 52 Thorlabs. "Uncoated Ge Window." Germanium Windows, Thorlabs Germanium Window Graph, 1999, www.thorlabs.com/newgrouppage9.cfm?objectgroup_id=3980&gclid=Cj0KCQjw5arM

BRDzARIsAAqmJex5hfgJdzVfBVWTRcLsdo7BdSwluEYTkV6Q6rKnuqkznMZANdrU1
24aAg89EALw_wcB.

53 Matsubara, E., Yamane, K., Sekikawa, T., & Yamashita, M. (2007). Generation of 2.6 fs optical pulses using induced-phase modulation in a gas-filled hollow fiber. *JOSA B*, 24(4), 985-989.

54 Nurhuda, M., Suda, A., Kaku, M., & Midorikawa, K. (2007). Optimization of hollow fiber pulse compression using pressure gradients. *Applied Physics B: Lasers and Optics*, 89(2), 209-215.

55 Agrawal, G. P. (2000). Nonlinear fiber optics. In *Nonlinear Science at the Dawn of the 21st Century* (pp. 195-211). Springer, Berlin, Heidelberg.

56 Tomlinson, W. J., Stolen, R. H., & Shank, C. V. (1984). Compression of optical pulses chirped by self-phase modulation in fibers. *JOSA B*, 1(2), 139-149.

57 Sattler, K., Mühlbach, J., Echt, O., Pfau, P., & Recknagel, E. (1981). Evidence for coulomb explosion of doubly charged microclusters. *Physical Review Letters*, 47(3), 160.

58 Chelkowski, S., Zuo, T., Atabek, O., & Bandrauk, A. D. (1995). Dissociation, ionization, and Coulomb explosion of H_2^+ in an intense laser field by numerical integration of the time-dependent Schrödinger equation. *Physical Review A*, 52(4), 2977.

59 Vager, Z., Naaman, R., & Kanter, E. P. (1989). Coulomb explosion imaging of small molecules. *Science*, 244(4903), 426-431.

60 Bocharova, I., Karimi, R., Penka, E. F., Brichta, J. P., Lassonde, P., Fu, X., ... & Légaré, F. (2011). Charge Resonance Enhanced Ionization of CO_2 Probed by Laser Coulomb Explosion Imaging. *Physical review letters*, 107(6), 063201.

61 Karimi, R. (2013). Fragmentation Dynamics of Triatomic Molecules in Femtosecond Laser Pulses Probed by Coulomb Explosion Imaging.

62 Légaré, F., Litvinyuk, I. V., Dooley, P. W., Quéré, F., Bandrauk, A. D., Villeneuve, D. M., & Corkum, P. B. (2003). Time-resolved double ionization with few cycle laser pulses. *Physical review letters*, 91(9), 093002.

63 Staudte, A., Cocke, C. L., Prior, M. H., Belkacem, A., Ray, C., Chong, H. W., ... & Saalman, U. (2002). Observation of a nearly isotropic, high-energy Coulomb explosion group in the fragmentation of D_2 by short laser pulses. *Physical Review A*, 65(2), 020703.

Appendix A: Future Improvement of Pressure Gradient Technique



Figure 43: A design for the pressure gradient chamber.

As discussed in section 5.1, a design for a pressure gradient chamber is shown in **Error! Reference source not found.** The tube is conceived as two separate chambers, gas flows in the second chamber and is pumped out at the first chamber. The gas pressure will have the lowest value at the laser input side and differentially increase along the fibre and have the highest pressure at the laser output side.

Appendix B: MATLAB fitting.m

```

clear;
tic;
i1=0.6961663;i2=0.0684043;i3=0.4079426;i4=0.1162414;i5=0.897479
4;i6=9.89616;%fused silica
%i1=0.48755108;i2=0.04338408;i3=0.39875031;i4=0.09461442;i5=2.3
120353;i6=23.793604;%MgF2
%i1=0.0000806051;i2=0.0248099;i3=132.274;i4=0.000174557;i5=39.3
29577;%air
%i1=0.000064432135;i2=0.028606021;i3=144;i4=0;i5=0;%argon
syms x;
y=(1+((i1*x^2)/(x^2-(i2)^2))+((i3*x^2)/(x^2-
(i4)^2))+((i5*x^2)/(x^2-(i6)^2)))^(1/2);
%y=1+i1+(i2/(i3-x^2))+i4/(i5-x^2);% air and argon
%y=(2.5388484-0.0066855865*x^2+0.015111456*x^(-2)-
0.00015247241*x^(-4)+0.0000408340116*x^(-6)-
0.0000024061785*x^(-8))^(1/2)%HOYYA glass
%y=(1+((0.6961663*x^2)/(x^2-
(0.0684043)^2))+((0.4079426*x^2)/(x^2-
(0.1162414)^2))+((0.8974794*x^2)/(x^2-(9.89616)^2)))^(1/2);
n=subs(y,'x','0.8')
%o=diff(y,x,1);
f1d=diff(y,x,2);
f2d=diff(y,x,3);
f3d=diff(y,x,4);
%pretty(f1d)
%o1=subs(o,'x','0.8'), dn/dx,matched with theoretical valve
a=subs(f1d,'x','0.8')*(1E12);
b=subs(f2d,'x','0.8')*(1E18);
c=subs(f3d,'x','0.8')*(1E24);
%x=0:0.1:1500;
GVD=(((800E-9)^3)*1*(a))/(2*3.1415926*((3E8)^2))*1E27%
36.16fs^2/mm
TOD=-(((800E-9)^4)*1*(3*a+(800E-
9)*b))/(4*(3.1415926^2)*((3E8)^3))*1E42%normal unit
27.45fs^3/mm
FOD=(((800E-9)^5)*1*((12*a+8*(800E-9)*b)+((800E-
9)^2)*c))/(8*(3.1415926^3)*((3E8)^4))*1E57 %-11.76

figure(1);
GVD=(((x*(10^-
6))^3)*1*(f1d*1E12))/(2*3.1415926*((3E8)^2))*1E27;
ezplot(GVD,[0,1.5]);
title('')

```

```

figure(2);
TOD=-(((x*(10^-6))^4)*1*(3*f1d*1E12+(800E-
9)*f2d*1E18))/(4*(3.1415926^2)*(3*10^8)^3))*1E42;
ezplot(TOD,[0,1.5]);
title('')

```

```

figure(3);
FOD=(((x*(10^-6))^5)*1*((12*f1d*1E12+8*(800E-
9)*f2d*1E18)+((800E-
9)^2)*f3d*1E24))/(8*(3.1415926^3)*(3E8)^4))*1E57;
ezplot(FOD,[0,1.5]);
title('')

```

Appendix C: MATLAB Code GDDSum.m

```
clear;
tic;
% glass material
i1=0.6961663;i2=0.0684043;i3=0.4079426;i4=0.1162414;i5=0.897479
4;i6=9.89616;
syms x;
y1=(1+((i1*x^2)/(x^2-(i2)^2))+((i3*x^2)/(x^2-
(i4)^2))+((i5*x^2)/(x^2-(i6)^2)))^(1/2);
% argon gas
a1=6.432135*10E-5;a2=2.8606021*10E-2;a3=144;a4=0;a5=0;
syms x;
y2=1+a1+(a2/(a3-x^-2));
%air
b1=8.06051*10E-5;b2=2.480990*10E-2;b3=132.274;b4=1.74557*10E-
4;b5=39.32957;
syms x;
y3=1+b1+(b2/(b3-x^(-2)))+(b4/(b5-x^(-2)));
%HoYA
y4=(2.5388484-0.0066855865*x^2+0.015111456*x^(-2)-
0.00015247241*x^(-4)+0.0000408340116*x^(-6)-
0.0000024061785*x^(-8))^(1/2)

n1=subs(y1,'x','0.8')
f1d=diff(y1,x,2);
n2=subs(y2,'x','0.8')
f1d2=diff(y2,x,2);
n3=subs(y3,'x','0.8')
f1d3=diff(y3,x,2);
n4=subs(y3,'x','0.8')
f1d4=diff(y4,x,2);

a11=subs(f1d,'x','0.8')*(1E12);
a22=subs(f1d2,'x','0.8')*(1E12);
a33=subs(f1d3,'x','0.8')*(1E12);
a44=subs(f1d4,'x','0.8')*(1E12);

GVD1=(((800E-9)^3)*1*(a11))/(2*3.1415926*((3E8)^2))*1E27%
36.16fs^2/mm
GVD2=(((800E-9)^3)*1*(a22))/(2*3.1415926*((3E8)^2))*1E26
GVD3=(((800E-9)^3)*1*(a33))/(2*3.1415926*((3E8)^2))*1E26
GVD4=(((800E-9)^3)*1*(a44))/(2*3.1415926*((3E8)^2))*1E27

figure(1);
```

```

GVD1=(((x*(10^-
6))^3)*1*(f1d*1E12))/(2*3.1415926*((3E8)^2))*1E27;
ezplot(GVD1,[0,1.5]);
title('')
figure(2);
GVD2=(((x*(10^-
6))^3)*1*(f1d2*1E12))/(2*3.1415926*((3E8)^2))*1E26;
ezplot(GVD2,[0,1.5]);
title('')
figure(3);
GVD3=(((x*(10^-
6))^3)*1*(f1d3*1E12))/(2*3.1415926*((3E8)^2))*1E26;
ezplot(GVD3,[0,1.5]);
title('')
figure(4);
GVD4=(((x*(10^-
6))^3)*1*(f1d4*1E12))/(2*3.1415926*((3E8)^2))*1E27;
ezplot(GVD4,[0,1.5]);
title('')
figure(4);
t1=1.25 %glass thickness, focus lens 3mm, window 1mm
t2=0% argon gas at 0.4 atm, tube length 1828.8mm
t3=3429%air pass from regen to H.F.2472.2mm ,toA.C 3429
t4=0 %HoYA A.C.
Sum=GVD1*t1+GVD2*t2+GVD3*t3+GVD4*t4;
ezplot(Sum,[0,1.5]);
title('')

```

Appendix D: Instructions and MATLAB Code

PluseSim.m

Instructions:

1. 'PluseSim.m' program must be copied to the file where the data were.
2. Copy and past the data file name to line 63 fName='XXXXX.dat'.
3. The dispersion can be added by entering a value to 'line 119' up to 'line 121'.

Code:

```
clear;
tic

%-----
%-----

%Inline functions
%Defining inline functions used to fit the simulated pulses???
%-----
%-----

fit_4      = inline('p(1).*x.^-4 + p(2).*x.^-3 + p(3).*x.^-2 +
p(4).*x.^-1 + p(5)', 'p(1)', 'p(2)', 'p(3)', 'p(4)', 'p(5)', 'x');
d2_fit_4   = inline('20.*p(1).*x.^-6 + 12.*p(2).*x.^-5 +
6.*p(3).*x.^-4 + 2.*p(4).*x.^-
3', 'p(1)', 'p(2)', 'p(3)', 'p(4)', 'x');
trend_fit  = inline('p(1).*x.^3 + p(2).*x.^2 + p(3).*x +
p(4)', 'p(1)', 'p(2)', 'p(3)', 'p(4)', 'x');
Gauss      = inline('exp(-1*((C_AngFreq-
Ang_Freq_Spec).^2)/(2.*sigma_square))');
%Inline definition of gaussian function
Lorentzian =
inline('(1./pi.*0.5.*FWHM_pulse)./((Ang_Freq_Spec-C_AngFreq).^2
+ (0.5.*FWHM_pulse).^2)'); %Inline definition of lorentzian
function
%-----
%-----
%-----
%-----

%-----
```

```

-----
%Constants
%Defining constants used for the simulations
%-----
-----
c = 3E5;                %speed of light, units structured to
produce frequencies in THz

fac =10;                %multiplier to domain length during
Fourier Transform

Freq_Range =748;       %a larger frequency range gives a
greater resolution in t-space following Fourier transform,
alternatively the pre-transformed data
                        %can be padded with leading and
trailing zeros.

fres =0.01;            %the real frequency mode resolution is
c/(2*L) where L is the length of the laser cavity. For a 100MHz
system, the cavity is 1.5m long so the
                        %mode spacing is 100MHz, or 0.00000001
Hz resolution is listed in THz smaller fres values will allow
for greater temporal range after FT is
                        %performed therefore for large GVD
values a small fres number is necessary for short pulses a
small fres number is not necessary.
%-----
-----
%-----
-----

%-----
-----

%Spectral Domain
%Defining and creating constants, arrays and other parameters
used o describe the spectral domain of the pulse.
%-----
-----

centerwave =
800;
%central wavelength of pulse
centerfreq =
c./centerwave;
%central frequency of pulse in TeraHertz
Frequencies = (centerfreq-

```

```

(Freq_Range/2):fres:(centerfreq+(Freq_Range/2));      %range of
frequencies used
Wave =
c./Frequencies;
  %Range of Wavelengths used
mode = 1:length(Frequencies);
total_modes =
length(mode);
%Total number of modes to be considered
center_mode = total_modes/2;
C_AngFreq =
(2*pi*centerfreq);
%Angular frequency of the central wavelength
Ang_Freq_Spec =
(2.*pi.*Frequencies);
%spectrum of angular frequencies
Freq_diff_ang = Ang_Freq_Spec -
C_AngFreq;                                     %used in Taylor
expansions
%-----
%-----
%-----

%-----
%-----
%-----

%Simulation of pulse
%There are three options for simulating the pulse, Gaussian,
Lorentzian or reading a collected spectrum from a file.
%The method used to generate the pulse is determined by the
string toDo. If reading from a file, the filename should be
%indicated by the variable fName.
%-----
%-----
toDo='File';
                                     %toDo can equal 'Gaussian',
'Lorentzian', or 'File'
fName='2016 April 12 - 1W 15 psi Argon Comp
7259.dat';
%Filename for file mode

if toDo=='File'
    disp(fName)

    [Wave_read spectra_read] =

```

```

textread(fName, '%f, %f', 'headerlines', 4);

    SpecAmpWave =
interpl(c./Wave_read, spectra_read, Frequencies, 'linear', 0);
    SpecAmpWave = SpecAmpWave./max(SpecAmpWave);

    %Jacobian Transformation of Spectral Amplitude To Frequency
Space, Necessary for spectra read from a file
    SpecAmpFreq = Wave.^2./c.*SpecAmpWave;
    SpecAmpFreq = SpecAmpFreq./max(SpecAmpFreq);
    %SpecAmpWave = SpecAmpFreq./(Wave.^2./c);
    %SpecAmpWave = SpecAmpWave./max(SpecAmpWave);

elseif toDo=='Lorentzian'
    toPrint='Pulse simulated using Lorentzian function';
    disp(toPrint)

FWHM_pulse_Wave=50;
                                %FWHM of the generated pulse
    FWHM_pulse = (2*pi*c/(centerwave-FWHM_pulse_Wave/2))-
(2*pi*c/(centerwave+FWHM_pulse_Wave/2)); %Computes the FWHM
of the pulse in units of Angular Frequency
    sigma_square = (FWHM_pulse./2.355).^2;
    SpecAmpFreq(mode) =
Lorentzian(C_AngFreq, Ang_Freq_Spec(mode), FWHM_pulse);

elseif toDo=='Gaussian'
    toPrint='Pulse simulated using Gaussian function';
    disp(toPrint)

FWHM_pulse_Wave=50;
                                %FWHM of the generated pulse
    FWHM_pulse = (2*pi*c/(centerwave-FWHM_pulse_Wave/2))-
(2*pi*c/(centerwave+FWHM_pulse_Wave/2)); %Computes the FWHM
of the pulse in units of Angular Frequency
    sigma_square = (FWHM_pulse./2.355).^2;

    SpecAmpFreq(mode) =
Gauss(C_AngFreq, Ang_Freq_Spec(mode), sigma_square);

else
    toPrint='Incorrect option input for pulse simulation.
Simulating pulse using a gaussian function';
    disp(toPrint)

```

```

FWHM_pulse_Wave=50;
                                %FWHM of the generated pulse
FWHM_pulse = (2*pi*c/(centerwave-FWHM_pulse_Wave/2))-
(2*pi*c/(centerwave+FWHM_pulse_Wave/2)); %Computes the FWHM
of the pulse in units of Angular Frequency
sigma_square = (FWHM_pulse./2.355).^2;

SpecAmpFreq(mode) =
Gauss(C_AngFreq,Ang_Freq_Spec(mode),sigma_square);
end
%-----
%-----
%-----
%-----

%-----
%-----
%Simulation of pulse stretching
%Phase shift of the pulse is calculated using a Taylor
expansion of the phase about the central frequency of the
pulse.
%This expansion is done up to seventh order.
%-----
%-----

GD =
0; %Group
Dispersion
GVD =
0; %Group
velocity dispersion.
TOD =
0; %Third
order term
FOD =
0; %Fourth
order term
QOD =
0; %Fifth
order term
SXOD =
0; %Sixth
order term
SepXOD =
0; %Seventh

```



```

pix_time = pix_time - pix_time(round(length(pix_time)/2));
t_space = pix_time(2)-pix_time(1);
Int_E_Field = E_Field.*conj(E_Field);
Int_E_Field = Int_E_Field/max(Int_E_Field);
%-----
%-----
%-----

%-----

%Figures
%-----
%-----

%Unstretched Pulse
figure(1);
[AX1,H1,H2] =
plotyy(c./Wave,SpecAmpFreq,c./Wave,phase,'plot','plot');xlim(AX
1(1),[250 500]);xlim(AX1(2),[250 500]);
set(get(AX1(1),'Ylabel'),'String','Amplitude
(a.u.)','FontSize',18);
set(get(AX1(2),'Ylabel'),'String','Phase
(radians)','FontSize',18);
set(get(AX1(1),'Xlabel'),'String','Frequency
(THz)','FontSize',18);

set(H1,'LineWidth',3);
set(H2,'LineWidth',3);

ylimits = get(AX1(1),'YLim');
yinc = (ylimits(2)-ylimits(1))/5;
set(AX1(1),'YTick',[ylimits(1):yinc:ylimits(2)],'FontSize',16)
ylimits2 = get(AX1(2),'YLim');
yinc2 = (ylimits2(2)-ylimits2(1))/5;
set(AX1(2),'YTick',[ylimits2(1):yinc2:ylimits2(2)],'FontSize',1
6)

%E-Field plot
figure(2);
figure(2);plot(pix_time,plotE_Field,'LineWidth',2);
figure(2);xlabel('Time (fs)','FontSize',16),ylabel('Amplitude
(a.u.)','FontSize',16);
figure(2);xlim([-50 50]);ylim([-1 1]);
A = gca;
set(A,'FontSize',16);
xlimits = get(A,'xLim');

```

```

xinc = (xlims(2)-xlims(1))/4;
set(A, 'XTick', [xlims(1):xinc:xlims(2)])

%Intensity Plot
%gausFit = fit(pix_time,Int_E_Field,'gauss1');
figure(5);
%plot(gausFit,pix_time,Int_E_Field,'-r','LineWidth',3);
plot(pix_time,Int_E_Field,'-r','LineWidth',3);
xlabel('Time (fs)','FontSize',16);
ylabel('Intensity','FontSize',16);
xlim([-20 20]);

%Phase plot. Supressed because phase is plotted on initial plot
figure(4);
plot(c./Wave,phase);
xlim([250 500]);
xlabel('Frequency (THz)');
ylabel('Phase (radians)');

%GVD Plot. Supressed because didn't provide any useful
information.
figure(3);
plot(c./Wave,GVD_plot);
xlim([250 500]);
xlabel('Frequency (THz)');
ylabel('GVD (fs^2)');

%-----
%-----
%-----
%-----

toc

```

Appendix E

1. Instructions for Using Spectrum Correction Program

A Hypertext Preprocessor (PHP) program 'Wave Spectrum Correction' was written to subtract background from the spectra collected during this project. The algorithm and code were devised in collaboration with Wei Du, of the department of Computer Engineering in the University of Waterloo. The program is declared to be free and open for every researcher. a website for the program has been created so that it is convenient to use.

The link is

<http://rtims.us-east-1.elasticbeanstalk.com/filter.html>

This program will not save any original or corrected data; therefore, it is safe all researchers.

1. Open the link, click 'Choose file'.
2. Choose the data file 'XXXX.dat' to upload to the program.
3. Enter the 'Filter value' that you want to be modified.
4. The program will automatically download the modified file to your laptop.
5. The file you obtained is 'XXXX.txt' file, to make sure it will favourably run in the MatLab program 'PulseSim.m', you need to change suffix 'txt' to 'dat'.
6. Now it is possible to run the corrected data in 'PulseSim.m'.

2. Application of Spectrum Correction Program

The spectrometer that has been used in the lab to collect spectral information can only obtain a spectrum over the range from 300nm to 936nm. However, spectral broadening gives some signal for wavelengths longer than 936nm. It results in a sharp cut off at the low-frequency side. It is worth to mention that the spectral intensity higher than 935nm is less than 0.5% percent of the entire spectrum. Additionally, the background light level will contribute a tiny amount to the spectrum. It is reasonable to ignore the cut off and subtract the background at this level.

A Hypertext Preprocessor (PHP) program 'Wave Spectrum Correction' was written to help to subtract the background value. All the spectra shown in experimental results part (section 7.4) have been processed in this manner.

Figure 47 shows the comparison between unmodified and modified spectra and the shortest possible pulse length calculated using the Fourier transform.

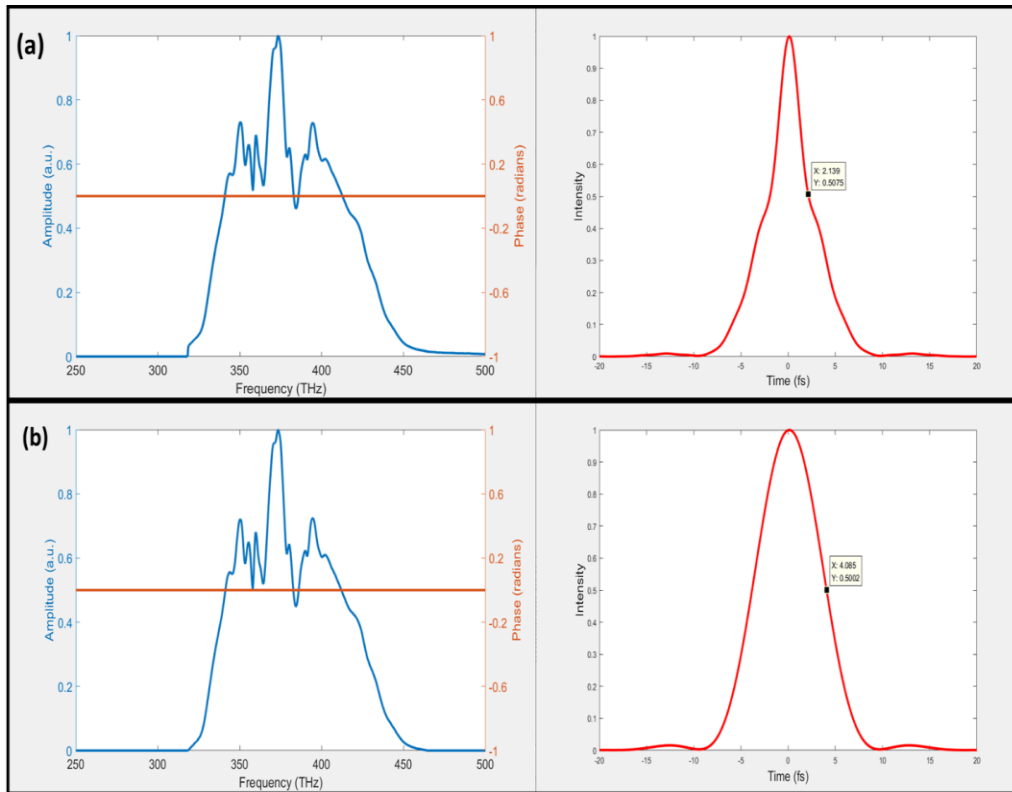


Figure 44 : (a) Original spectrum and pulse duration by taking the inverse Fourier Transform. Pulse duration at FWHM is 4.278fs. (b) Spectrum after background subtraction and pulse duration by taking the inverse Fourier Transform. Pulse duration at FWHM is 8.170fs.

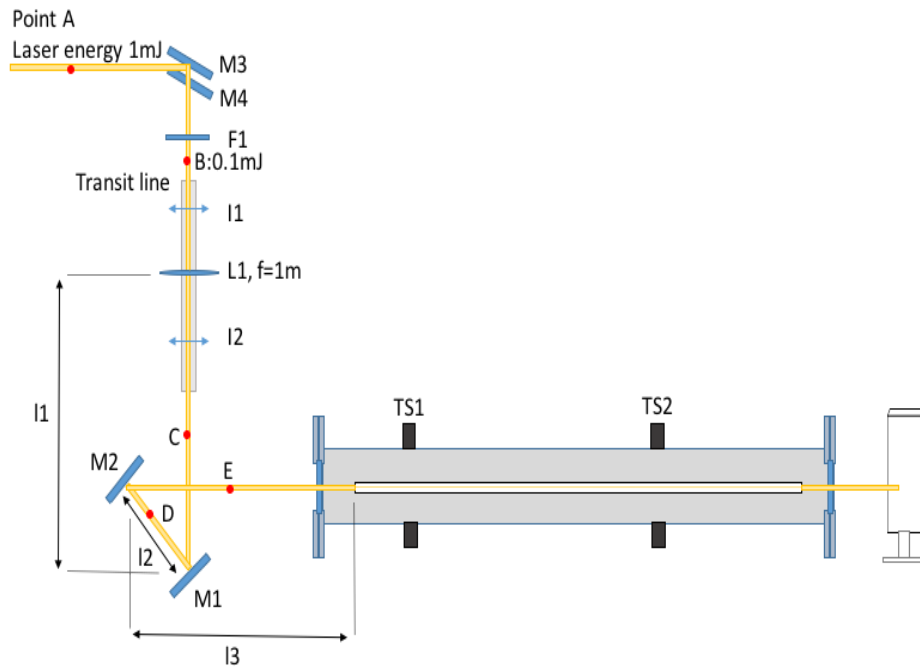
Figure 47 shows data which was obtained after the hollow fibre chamber, It can be observed that the spectrum shape has nearly no change except all spectral intensities decrease by the background value after processing with 'Spectrum correction program'. However, although this background comprises only less than 0.5% of the intensity of the whole spectrum, it does affect the pulse shape. From (a) it can be seen that the result of an un-subtracted background is an unreal pulse duration as low as 4.278fs. After processing the false temporal spike is removed. The reason for the difference is the influence of the wide background on the inverse

Fourier Transform. The Fourier Transform equation and the inverse equation can be expressed as⁶⁴ :

$$\mathcal{F}[f_t(t)] = \frac{1}{\sqrt{2}} \int f_t(t) e^{-i\omega t} dt \quad (41)$$

$$f_t(t) = \mathcal{F}^{-1}[f_\omega(\omega)] = \frac{1}{\sqrt{2\pi}} \int f_\omega(\omega) e^{+i\omega t} d\omega \quad (42)$$

Appendix F: Hollow Fibre Alignment Steps



F1: Mounted continuously variable neutral density filter

I1: 1st alignment iris

L1: AR-Coated lens

I2: 2nd alignment iris

M1: mirror 1

M2: mirror 2

M3: mirror 3

M4: mirror 4 (M3 and M3)

AT1: 1st translation stage

AT2: 2ndtranslation stage

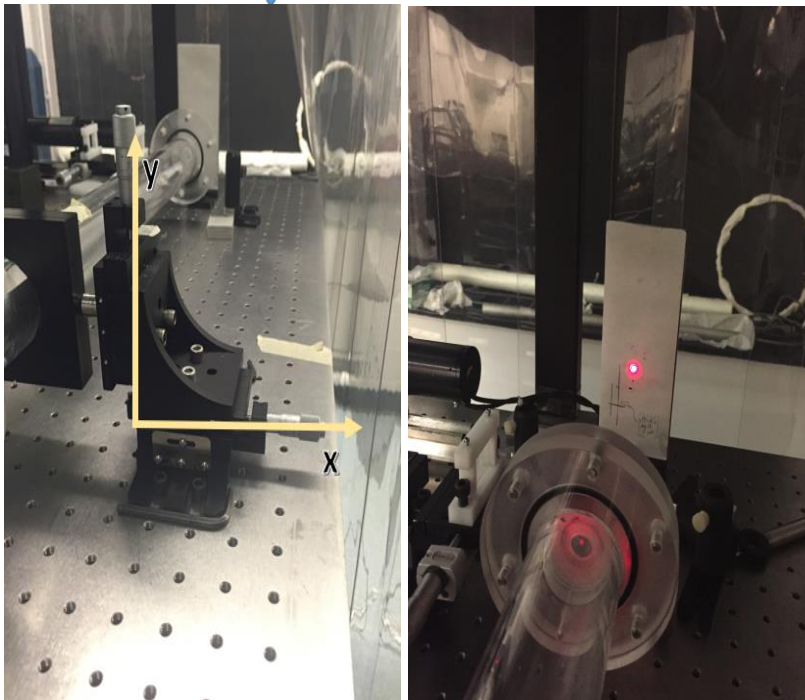
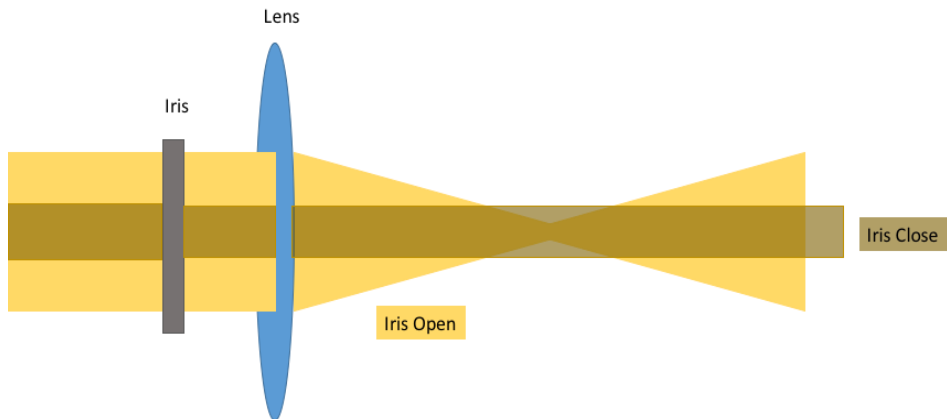
Before the alignment, make sure $l1+l2+l3 \approx 1m$. The function of M3 and M4 is to reduce the beam height, and change the polarisation of the laser. The height of the beam should be the same as that between the centre of the view port and the table.

1. Use a block panel, put it in front of the vacuum tube (after point E). Use power meter, measure beam power at point A (around 1mJ).
2. Remove L1, use M3, M4, I1 and I2 align the beam, make sure it is parallel to the table, then put L1 back.

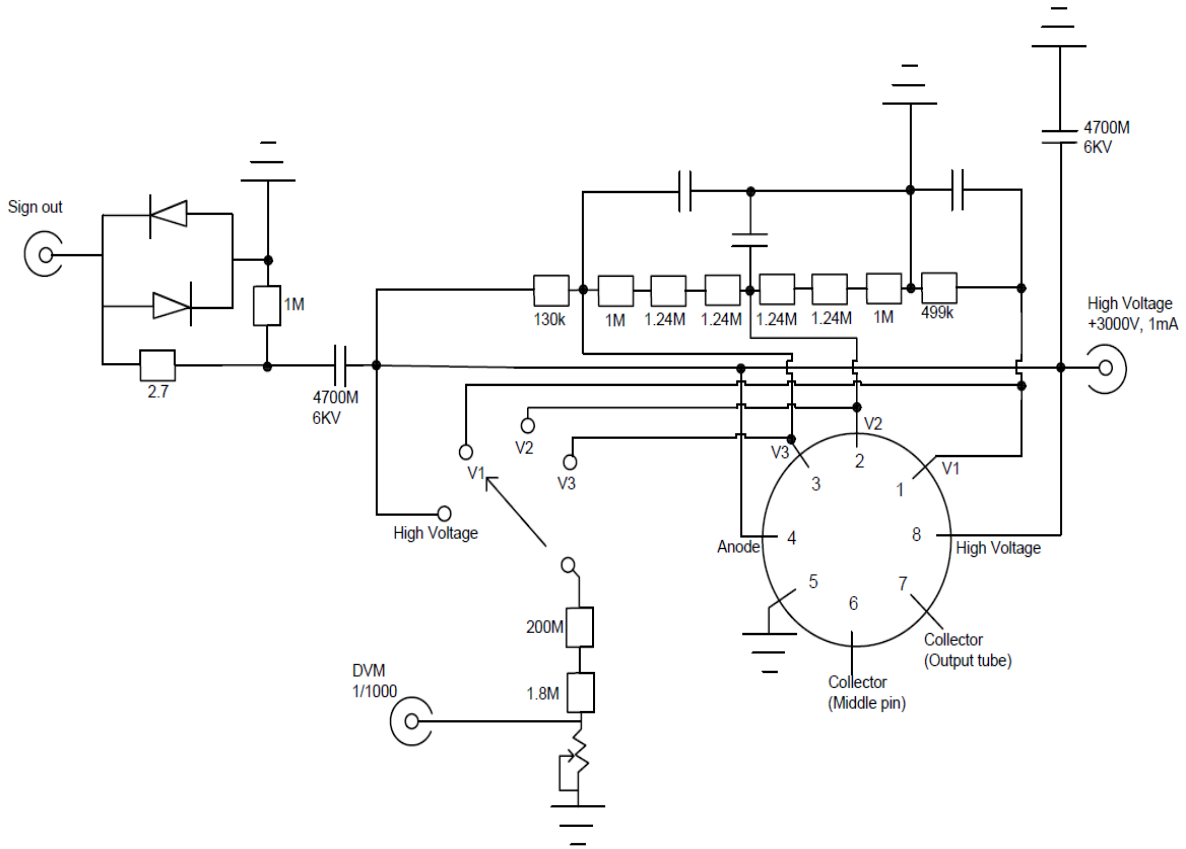
3. Put power meter at point B and put a beam dump behind the filter, rotate neutral density filter, let beam power decrease to 0.1mJ (decrease power by controlling the pump current if do not have a filter). In order to ensure there is no more energy loss, also measure power at point C, D and E (0.1mJ).
4. Close I1, remove block panel to the end of the vacuum tube.
5. Put I1 in front of the hollow fibre input window and I2 behind the output window, then remove the whole tube to the side, make sure it will not block the laser beam.
6. Adjust M1 and M2 to align the beam parallel to the edge of the table and horizontal. Put Irises I1 and I1 back in their original position and the hollow fibre tube back in place.
7. Set the 1st and the 2nd translation stages' 'y' direction to 5mm and 'x' direction to 3mm. Now the centre of the hollow fibre is around 1 cm lower than the height of the beam.
8. Switch 'y' direction knob of the 1st translation stage and then the 2nd translation stage to the same height of the beam.
9. Slightly adjust 'x' and 'y' direction knob of the 1st translation to let beam go through the hollow fibre. Now an ugly beam or a sandwiched-like beam spot (it is easy to find if beam alignment is good enough) can be observed on the block plane.
10. Open I1 and I2, now the focus point at the beginning of the hollow fibre becomes smaller.(see below figure)
11. Carefully adjust TS1 and TS2, try to make the spot more rounded and more

uniform, with fewer rings around (T11 will be much more sensitive than TS2).

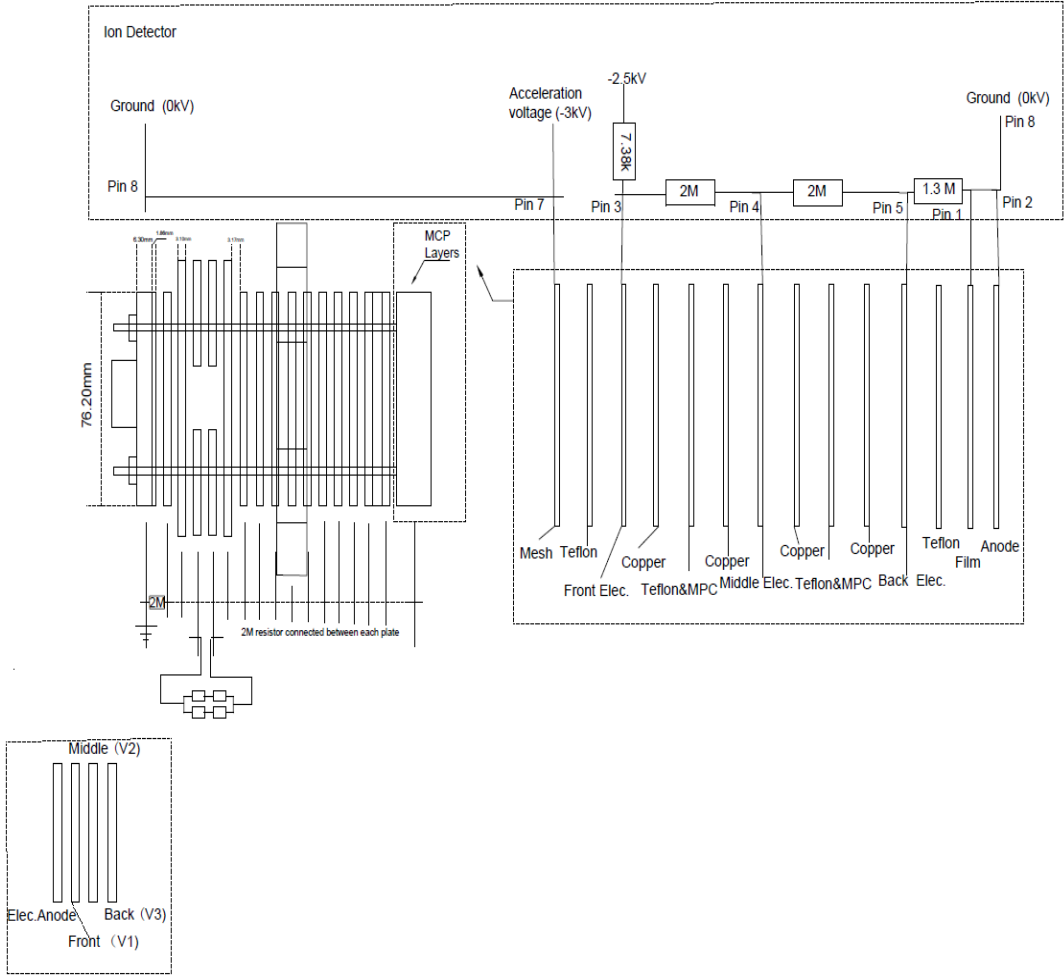
12. Use the power meter, measure the beam power into the hollow fibre and after the hollow fibre and then obtain the transmission.
13. Move L1 forward and backwards to get the largest transmission rate.
14. When the best transmission fraction rate has been achieved (50% would be right) gradually increase the energy using F1 and recheck the transmission, then the filter can be carefully removed.



Appendix G: Circuit Diagram of Electron Detector



Appendix H: Circuit Diagram of Time of Flight



Appendix I: Setup the Regenerative Amplifier

Startup Regenerative Amplifier:



Figure 45 : Real experimental setups of amplifier control boxes in the Waterloo lab. The top picture is the Spitfire Ace software 'main' control panel. The spectrum shows the build up when the current is 18.4 A, and timing setting: CH1: 83.25ns, CH2: 103.25ns, CH3:249.25ns. The output pulse has the duration of 35fs and power of 4.35W.

1. Turn on the Oscillator and ensure that it is outputting sufficient power while mode-locking (roughly 380-400 mW at the oscillator output and roughly 130-145 mW at the regen input).
2. Normally the TCU, TDG, Empower 45 power supply Push-Button Closures (light yellow button shown in **Error! Reference source not found.**) should always stay ON. If they are not ON, then turn them on from bottom to top: Empower 45 power supply → TDG → TCU.
3. Turn the Empower 45 power supply key switch to the ON position.
4. Turn the TDG key change to the ON position. The 'High voltage' indicator should become green.
5. Normally the Spitfire Ace software on the computer should stay open, if the software was not open, then open the Spitfire Ace software on the regen computer. Press the "Connect to system" button that appears. A progress bar should appear, and the program should connect to the system.
6. In the "Main" window, the "Pockels cell Repetition Rate" should be set to 1000, the "Rep Rate Divider" should be set to 1.
7. Once the software has connected, ensure that the BWD display "PD1" and "PD2" indicators are lit. These indicate seed alignment. If both indicators are lit, but the "Reset BWD" button is yellow, press the "Reset BWD" button to reset (it will turn grey and say BWD OK).
8. The Empower pre-set current should be set to 13A, which is a completely safe starting current.
9. On the 'Regen' control panel, check timing setting: CH1: 83.25, CH2: 103.25, CH3:249.25.
10. Click and hold the green EMPOWER ON/OFF button on the 'main' control panel about 3 seconds until the system turns on.

11. On the TCU control box, the “Communications” and “Humidity” indicators should be green, and now the “Temperature” indicator should be flashing yellow, wait until it turns to green. This process will take 5 mins.
12. Press the “Regen On/Off” switch to turn the regen on.
13. You may now turn the Empower current from the ‘pre-set’ 13A up to 18.4 A to get the maximum output power of 4.35W
14. You can the motor controls on the Regen tab display to optimize the compressor length to produce the shortest duration pulses.
15. Introduction of TDG, TCU and compressor is shown after the shut-down procedure.

Shut-down the Regenerative Amplifier

1. Chose the shutter of the regenerative amplifier (the indicator on the top of the entrance door should extinguish).
2. Set the current back to the safe value: 13A.
3. Click REGEN ON/OFF on the main control panel to turn off the regen.
4. Click EMPOWER ON/OFF on the main control panel to shut down the Empower.
5. Turn the TDG key switch to the OFF position. The ‘High voltage’ indicator should turn dark.
6. Turn the Empower 45 power supply key switch to the OFF position.
7. Leave the TCU, TDG, Empower 45 power supper Push-Button Closures (light yellow button is shown in Figure 50) stay ON.

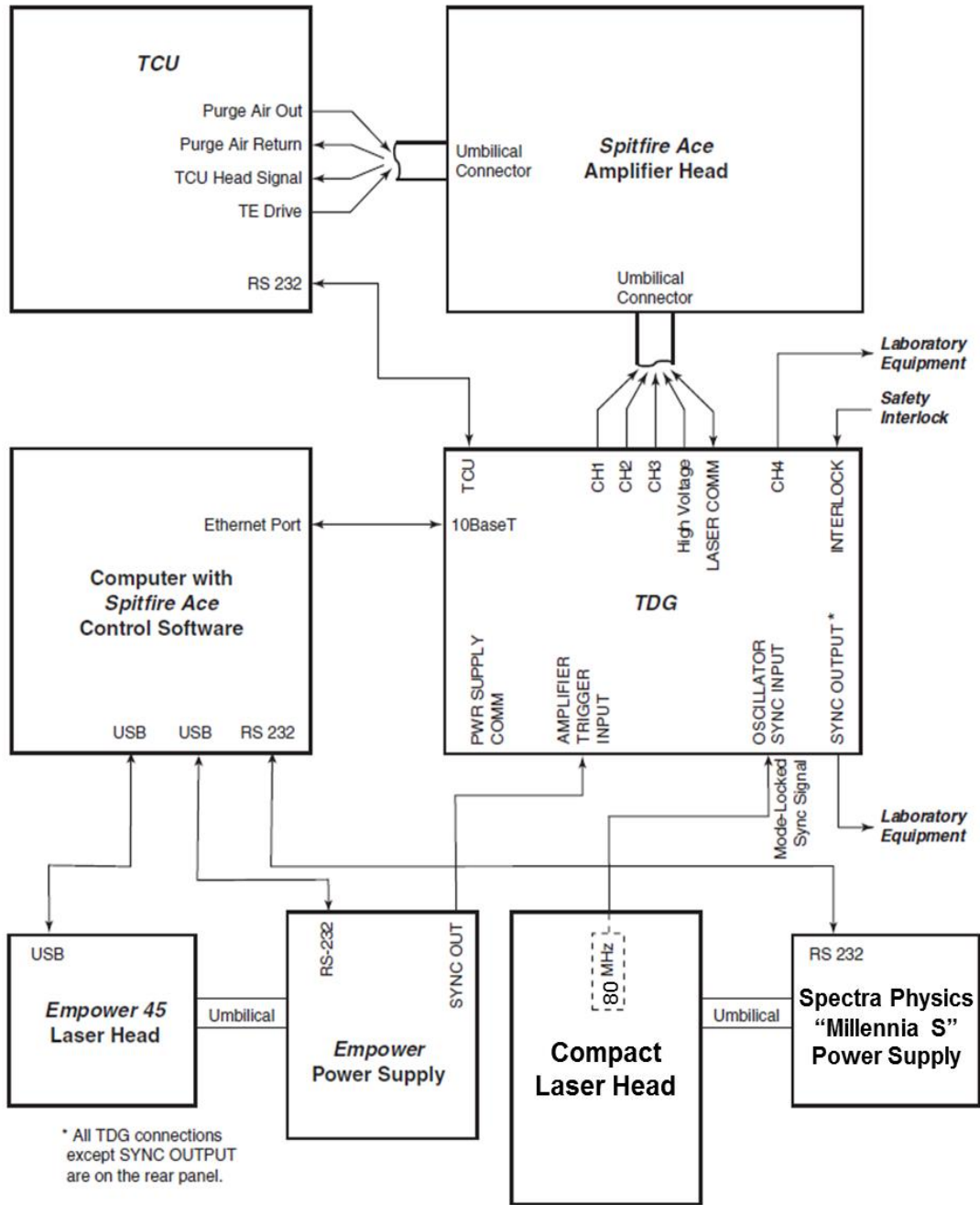


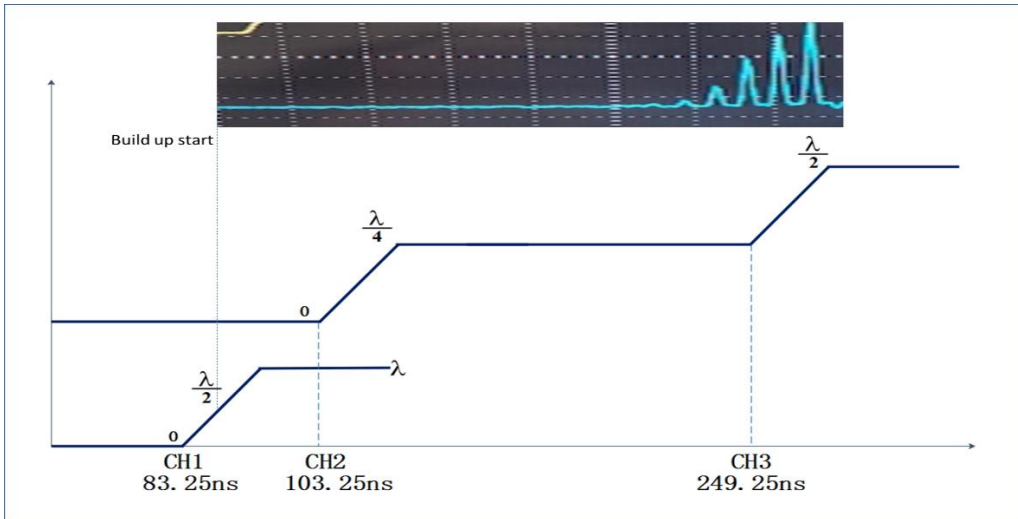
Figure 46 : Layout of connection between controllers of laser system⁴⁶.

Temperature Control Unit (TCU)

Temperature control is used to remove the heat from the Ti: sapphire crystal. The crystal temperature should be cooled to about -12°C , and the humidity should be below 1%. Those values will be indicated on the screen of control software.

Timing and Delay Generator (TDG)

The time and delay generator contains the power supply to the Pockels cells, and it indicates the BWD signals (mentioned in Chapter 6.2). The control software can control the timing parameters. The setting for the 'Pockels cell repetition rate' should be 1000, and the setting for 'Rep rate divider' should be 1. There are three channels on the control panel to adjust the time delay. CH₁ is used to monitor the extra-cavity Pockels cell (PC1 in Figure 24), it controls the timing when PC1 flips from doing 'nothing' → 1/2 plate → 'nothing' in order to create a window during which one seed pulse is allowed into the regen. CH₂ and CH₃ are used to adjust the intracavity Pockels cell (PC2 in Figure 24). CH₂ controls the timing when PC2 flip from 'nothing' to 1/4 plate in order to trap the pulse. CH₃ controls timing when PC2 flip from 1/4 plate to 1/2 plate to eject the pulse to the compressor. Of These three settings Ch1 and Ch2 normally do not need to be changed unless the alignment of the seed and pump have taken place, but Ch3 is changed regularly as it can control the number of round trips in the regen, and these must be controlled to limit energy build up in the cavity for high pump power (low Ch3) and allowed to increase for low pump current in order to aid seed alignment.



The Spitfire Ace Compressor

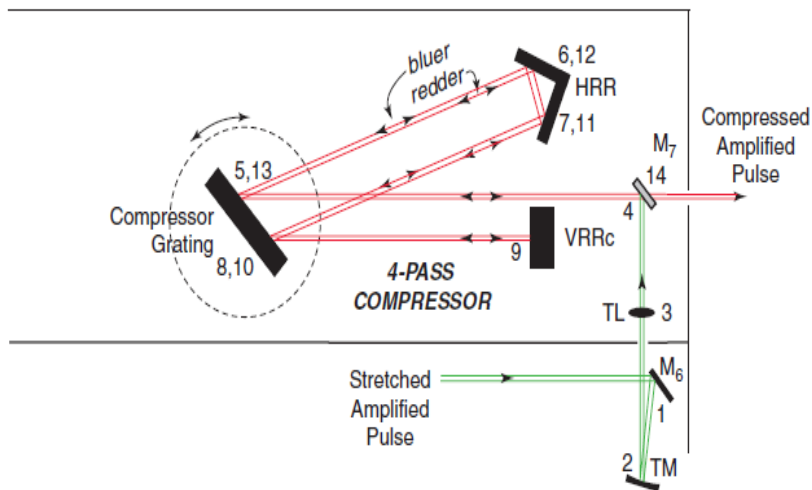


Figure 47 : The beam path in the compressor.⁴⁶

The motor position control in the software panel is used to adjust the length of the optical path in the compressor, which can be actually achieved by moving the horizontal retroreflector (HRR) in the compressor, the setting value can be observed in the panel as 'motor position'.

64 Haykin, S. (1979). Introduction. In *Nonlinear Methods of Spectral Analysis*(pp. 1-8). Springer Berlin Heidelberg.